A Facility for Transient Testing of Mobile Air Conditioning Systems

J. E. Rubio-Quero, W. E. Dunn and N. R. Miller

ACRC TR-80 July 1995

For additional information:

Air Conditioning and Refrigeration Center
University of Illinois
Mechanical & Industrial Engineering Dept.
1206 West Green Street
Urbana, IL 61801

(217) 333-3115

Prepared as part of ACRC Project 51
Design and Control of Mobile Air-conditioning Systems
W. E. Dunn and N. R. Miller, Principal Investigators

The Air Conditioning and Refrigeration Center was founded in 1988 with a grant from the estate of Richard W. Kritzer, the founder of Peerless of America Inc. A State of Illinois Technology Challenge Grant helped build the laboratory facilities. The ACRC receives continuing support from the Richard W. Kritzer Endowment and the National Science Foundation. The following organizations have also become sponsors of the Center.

Acustar Division of Chrysler
Amana Refrigeration, Inc.
Brazeway, Inc.
Carrier Corporation
Caterpillar, Inc.
Delphi Harrison Thermal Systems
E. I. du Pont de Nemours & Co.
Eaton Corporation
Electric Power Research Institute
Ford Motor Company
Frigidaire Company
General Electric Company
Lennox International, Inc.
Modine Manufacturing Co.
Peerless of America, Inc.
U. S. Army CERL
U. S. Environmental Protection Agency
Whirlpool Corporation

For additional information:

Air Conditioning & Refrigeration Center
Mechanical & Industrial Engineering Dept.
University of Illinois
1206 West Green Street
Urbana IL 61801

217 333 3115

A FACILITY FOR TRANSIENT TESTING OF MOBILE AIR CONDITIONING SYSTEMS

Jose Ernesto Rubio-Quero, M.S.
Department of Mechanical and Industrial Engineering
University of Illinois at Urbana-Champaign, 1995
W.E. Dunn, Advisor

A majority of the design and component selection processes for mobile air conditioning systems are based on results obtained from steady-state analyses. Although valuable, these steady-state tests do not accurately simulate the operation of mobile air conditioners. To allow transient testing of mobile air conditioning systems for use in model development and component selection, a heavily instrumented test facility was built. The test facility can accept any prototype or production mobile air conditioning systems. The current setup contains up-to-date components from a Ford 1994 Crown Victoria R-134a air conditioning system. The design and construction of the Crown Victoria test sections, as well as several improvements made to the test facility, are discussed in detail.

The test facility can achieve condenser and evaporator air-side versus refrigerant-side energy balances within 5% — quite good considering the large range of operating conditions tested. Also included in this report is a collection of preliminary transient results. These results display the versatility of the test stand and the ability to collect quality transient data. Future reports from this project will contain additional transient results and analyses.

TABLE OF CONTENTS

LIST OF TABLES

LIST OF FIGURES

NOMENCLATURE

English Symbols

A	amperage or area
A_{micro}	micro motion output amperage
C	venturi discharge coefficient
C_v	specific heat at constant volume
C_p	specific heat at constant pressure
d	diameter
E_{bal}	energy balance
F_a	thermal expansion factor (of metals), dimensionless
h	enthalpy
h_{air}	enthalpy of air
h_{R134a}	enthalpy of R-134a
h_{ref}	enthalpy of refrigerant
m	slope
$\dot{m}$	mass flow rate
$\dot{m}_{air}$	air mass flow rate
$\dot{m}_{micro}$	Micro Motion mass flow rate
$\dot{m}_{ref}$	refrigerant mass flow rate
P	pressure
P_{atm}	atmospheric pressure
$\dot{q}_{air}$	air-side heat transfer rate
$\dot{q}_{ref}$	refrigerant-side heat transfer rate
RH	relative humidity

T	temperature
T_{bath}	bath temperature
TRH	temperature at relative humidity sensor
V	voltage
V_{5V}	5 volt power supply voltage
V_{in}	input voltage
V_{offset}	transducer offset voltage
V_{out}	output voltage
V_{Tbath}	equivalent bath voltage
V_{tmstr}	thermistor voltage
x	quality

Greek Symbols

α	thermal expansion factor of material
β	venturi diameter ratio
ΔP	pressure differential
ω	humidity ratio
ρ	density
σ	standard deviation

1. INTRODUCTION

Currently, the majority of the design and component-selection processes for mobile air conditioning systems are based on results obtained from steady-state analyses. While valuable, these steady-state tests do not accurately simulate the operating conditions of mobile air conditioners. Because the most typical control schemes for mobile air conditioners involve thermostatic expansion valves and/or compressor clutch cycling, mobile air conditioners operate most often under transient conditions. For this reason, research into the transient characteristics and behavior of mobile air conditioners can be valuable and can lead to improved performance and better component selection. Transient testing can also be used to develop better, more efficient techniques for controlling mobile air conditioning systems.

1.1 Objectives

To study the transient behavior of mobile air conditioning systems, a heavily instrumented test facility, originally designed by Weston (1995), is used to gather research quality data. Air conditioning components from a Ford 1994 Crown Victoria automobile are used to collect steady-state and transient data. However, before reliable transient data can be collected, the test stand must be validated by verifying the accuracy of the instrumentation and the component-level energy balances. A great deal of the work presented in this report was undertaken with the goal of achieving the best possible condenser and evaporator energy balances. Once steady-state energy balances are verified, the test stand can be used to collect reliable transient data for computer model development. A computer model, in conjunction with transient data, can then be used to explore alternative control techniques that will lead to better component selection and more efficient air conditioner operation.

2. DESIGN AND CONSTRUCTION OF EXPERIMENTAL FACILITY

2.1 Introduction

In this chapter, two major efforts are discussed in detail. The first effort involves improvements to the mobile air conditioning test facility described in the report by Weston (1995). Heavily instrumented, this facility was designed by Weston to gather research quality data for model development. During shake-down testing, however, several deficiencies were found; namely, (a) inaccurate mass flow rates from refrigerant-line venturi flow meters, (b) large scatter in air-side flow rate measurements, and (c) deficiencies in air-side temperature measurements.

The second effort involves installing and testing a new Ford 1994 Crown Victoria air conditioning system. This system can accommodate testing of reciprocating swashplate and scroll compressors without exchanging any components other than the compressor. Additionally, it is a robust system that allows testing of the great number of transient operating conditions required for model development.

2.2 Improvements to Test Facility

The following text discusses modifications made to the test stand to correct the three problems noted above.

2.2.1 Refrigerant-side Venturi Flow Rate Measurements

In our test stand, venturi flow meters are used to measure refrigerant-side flow rates in the discharge line (after compressor and before condenser) and in the liquid line (after condenser and before throttling device). Previous tests identified large discrepancies between mass flow rates determined from the venturi flow meters and a very accurate, corriolis-effect meter (Micro Motion Model D25). Through extensive analysis, it was concluded that the Setra pressure transducers used to measure the pressure drop across the venturi were not working properly. The transducer output voltage—directly related to the pressure differential—varied greatly despite there

being no pressure difference applied to the transducer. The large drift in output voltage was attributed to the amplifier in the Setra transducers.

To correct the problem, new transducers without an amplifier were selected and purchased from Sensotec, Inc. The new transducers are: (a) 0-0.5 psid (Serial No. 437090) for the liquid-line venturi, and (b) 0-1 psid (Serial No. 411077) for the discharge-line venturi. Calibration curves for the two new pressure transducers are shown in Figure 2.1. An additional 0-1 psid (Serial No. 427337) pressure transducer was purchased as a spare.

2.2.2 Air-side Flow Rate Measurements

As stated earlier, instantaneous air-side mass flow rate readings were highly scattered although the air blowers were operating at constant speed. We determined that the scatter was caused by nonuniform flow entering the air-side venturis. To correct this problem, honeycomb flow straighteners, as shown in Figure 2.2, were installed in the duct upstream of the venturis. The flow straighteners proved sufficient for reducing the scatter in the air flow rate data. It is important to note that the air-side venturis, as all venturis, must be calibrated before reliable air flow rate measurements can be obtained.

2.2.3 Air-side Temperature Measurements

Arguably, the most critical improvement we made to the test facility was in the air-side temperature measurements. Previously, air temperature measurements were obtained by placing a nine-point thermocouple grid at the inlet and outlet of the heat exchanger. The nine-point thermocouple grid is sufficient for measuring the inlet air temperature, as it is essentially uniform. For this reason, a nine-point inlet thermocouple grid is again used in the new design. As one might expect, however, the heat exchanger outlet temperature profile is far from uniform. A nine-point thermocouple grid at the heat exchanger is not dense enough to accurately define the average outlet temperature. For this reason, new outlet temperature

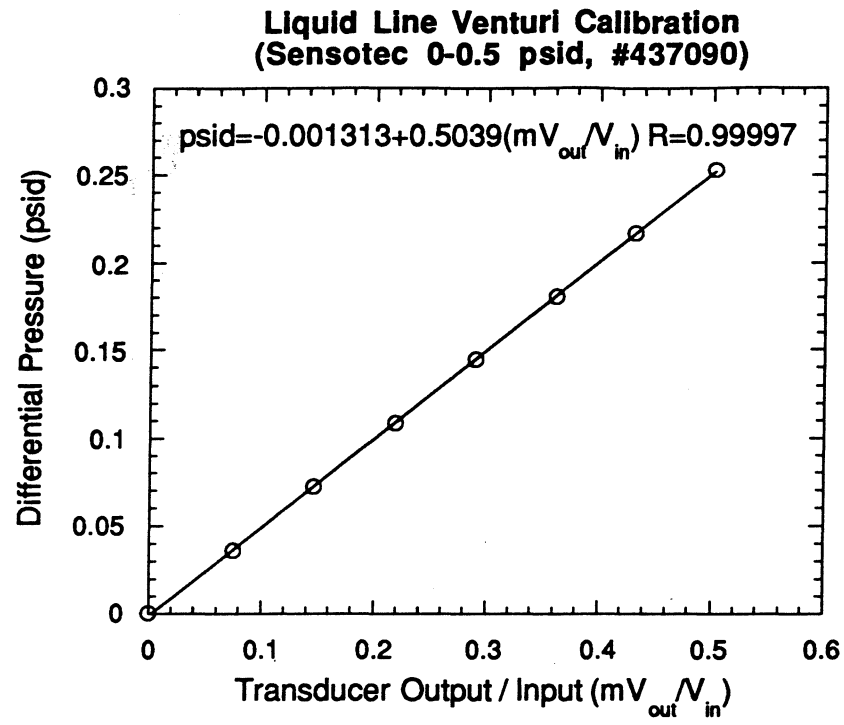

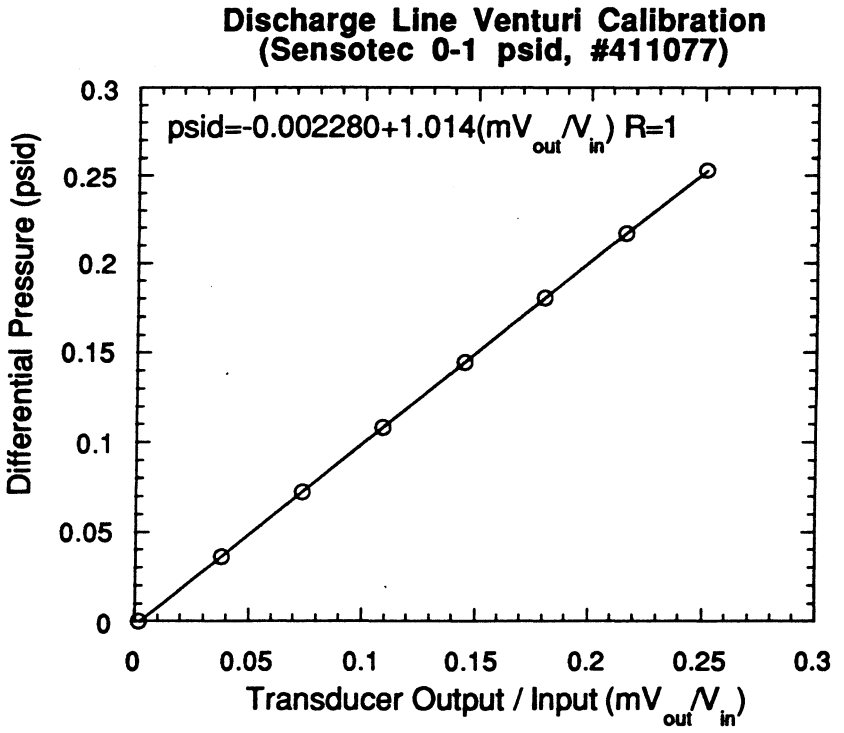

Figure 2.1: Refrigerant-side venturi pressure transducer calibration curves.

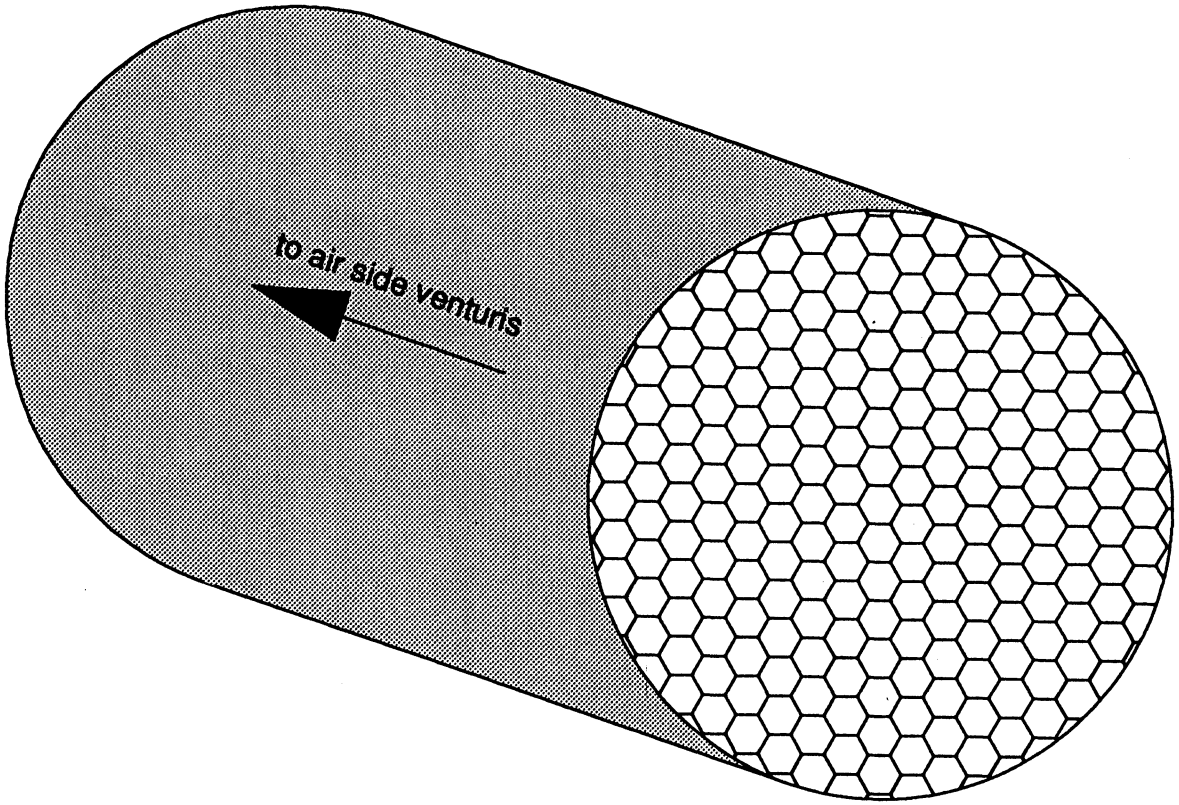

Figure 2.2: Air-side venturi flow straightener.

measurement sections were designed. The design and construction of the sections used to measure the average outlet temperature are later discussed in detail.

2.3 Ford 1994 Crown Victoria Component Description

The following section describes the components used to collect experimental data for this report. All components were obtained from Ford Motor Company, owing to their active participation in the Air Conditioning and Refrigeration Center (ACRC). The components are all standard on a 1994 Ford Crown Victoria R-134a air conditioning system. A summary of the components used in the test stand is given in Table 2.1.

Table 2.1: 1994 Ford Crown Victoria Component Summary

Component	Description	Model & Part No.
compressor	swashplate, fixed displacement	FS-10 19703
condenser	aluminum cross flow tube & fin	19712
throttling device	orifice tube type	19D990-AA (brown)
evaporator	alloy cross flow plate & fin	19A559
accumulator	aluminum with desiccant	19C836

2.3.1 Compressor

The role of a compressor in an air conditioning system is to raise the pressure of the refrigerant and provide the necessary mass flow rate. The A/C compressor used in the test facility is a fixed displacement swashplate compressor (Ford type FS-10). In our test stand, the compressor is driven by a belt attached to the compressor drive motor. The magnetic clutch on the compressor can be engaged and disengaged by applying approximately 12 volts to the clutch leads. With the clutch engaged, compression is produced by five double-acting cylinders positioned axially around the compressor shaft. Cool, low pressure refrigerant enters the

compressor through a 5/8-in. diameter tube on the attached manifold. The refrigerant exits the compressor through a 1/2-in. tube on the manifold.

2.3.2 Condenser

As hot refrigerant enters the condenser it is cooled as it transfers energy to the air flowing across the face of the condenser. This transfer of energy causes the refrigerant temperature to decrease and the state to change from vapor to liquid. The Ford 1994 Crown Victoria condenser is a painted aluminum "tube and fin" cross flow heat exchanger. Refrigerant enters near the top of the condenser into a header and passes across the entire condenser face twice before returning to the header and exiting near the bottom of the condenser, as shown in Figure 2.3. The condenser cross-section measures approximately 30 in. wide by 19 in. tall.

2.3.3 Throttling Device

A throttling device takes high pressure liquid refrigerant exiting the condenser and drops its pressure rapidly. The rapid pressure drop converts the liquid refrigerant to a two-phase mixture, thereby achieving the refrigeration effect. The Ford 1994 Crown Victoria air conditioner uses an orifice tube contained inside aluminum tubing as a throttling device. Figure 2.4 shows a typical orifice tube. The standard 1994 Crown Victoria system uses an orange color-coded orifice tube with a nominal diameter of 0.057 inches. When the Ford system was first installed, it was difficult to obtain subcooled liquid refrigerant at the condenser outlet while maintaining superheated vapor at the exit of the evaporator. Not being able to obtain subcooled liquid and superheated vapor clearly presented a problem, as they are both required to obtain accurate enthalpies at the condenser and evaporator outlets, respectively. To eliminate this problem, a brown orifice tube with a nominal diameter of 0.048 in. was installed. The smaller diameter orifice tube, with its greater resistance to flow, reduced the mass flow rate and made is easier to achieve both subcooled liquid at the condenser outlet and superheated vapor at the evaporator outlet.

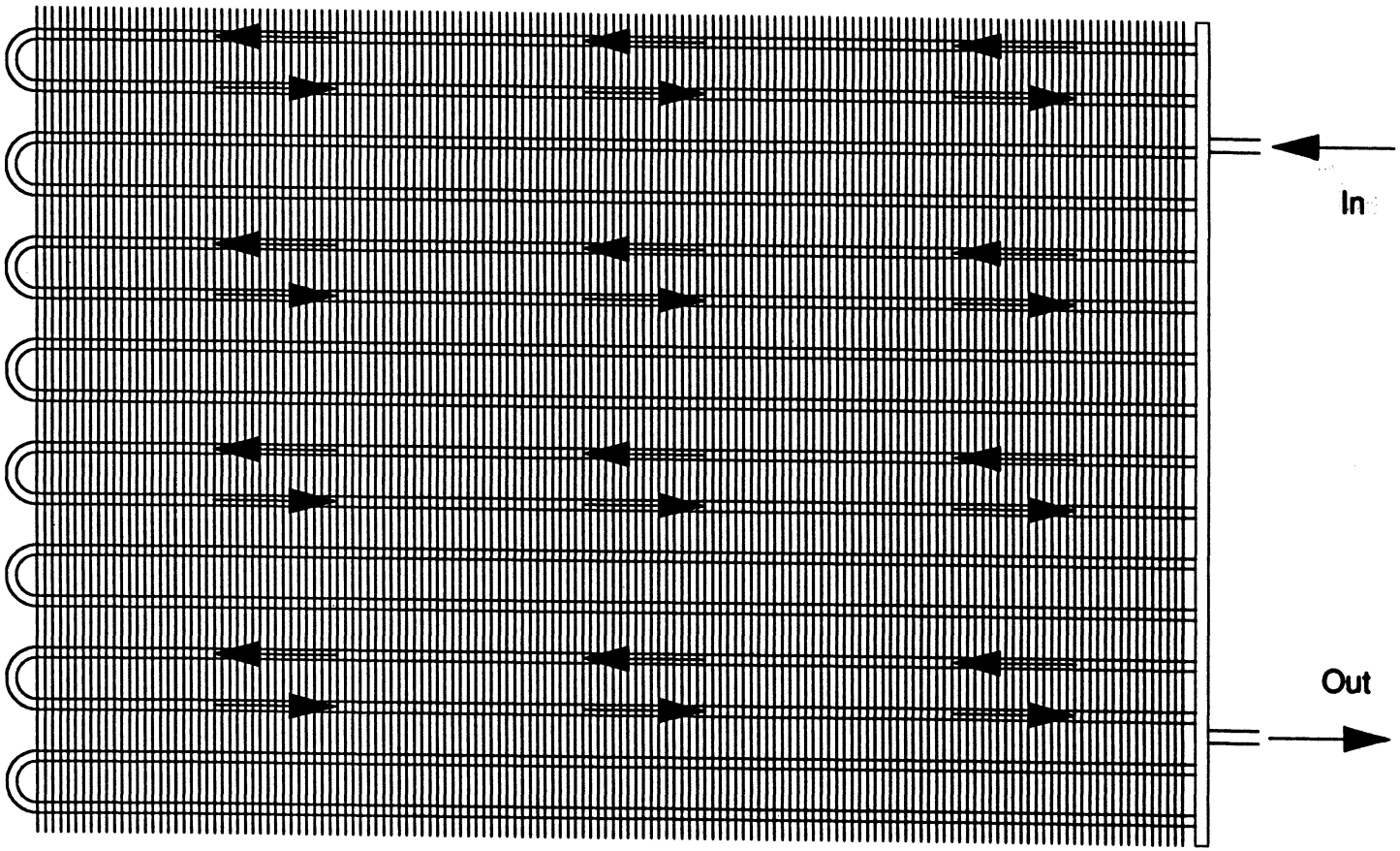

Figure 2.3: Ford condenser refrigerant flow schematic (looking upstream).

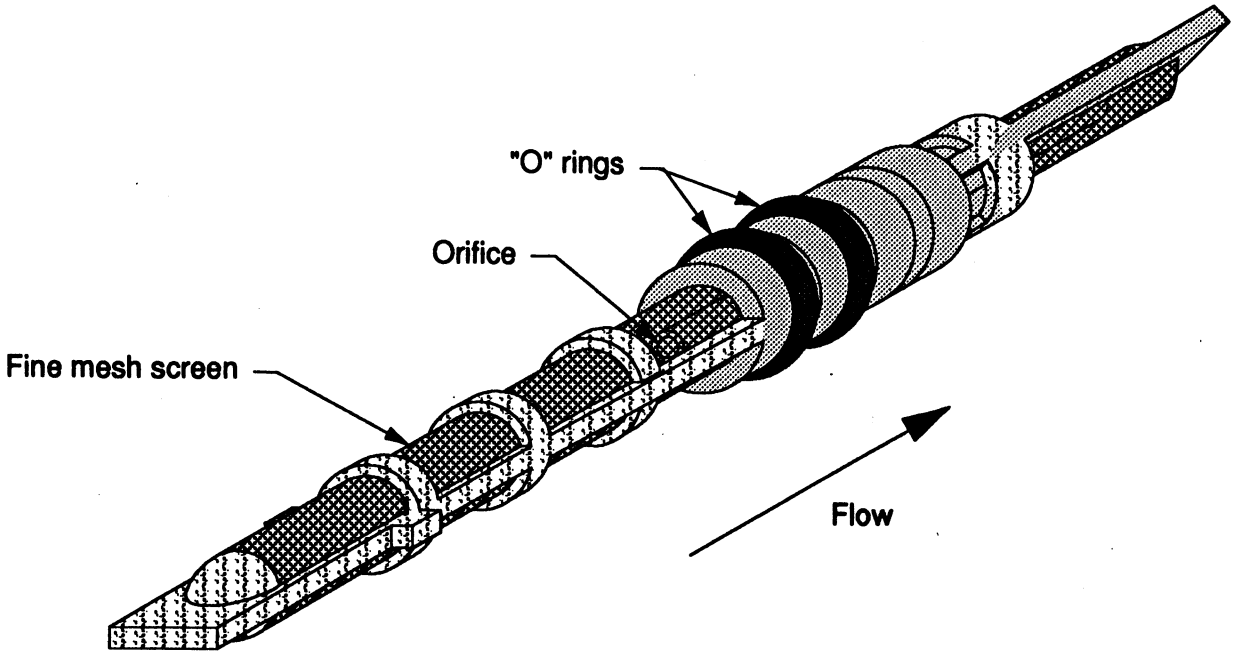

Figure 2.4: Orifice tube. (Weston, 1995)

2.3.4 Evaporator

One can say the evaporator plays the most important role in an air conditioning system, since it is what delivers cool, dehumidified air. As cold, two-phase refrigerant enters the evaporator, it is heated by air flowing across the face of the heat exchanger. The refrigerant is heated, and the air cooled, as energy is transferred from the air to the refrigerant. The 1994 Crown Victoria evaporator is made of an alloy material and, similar to the condenser, operates in a cross flow configuration. Two-phase refrigerant enters the evaporator at the bottom, passes through a bulk of thin, flat plates three times, as shown in Figure 2.5, and exits superheated at the top of the heat exchanger. The evaporator cross-section is approximately 8-1/4 in. wide and 9 in. tall.

2.3.5 Accumulator

After leaving the evaporator, the refrigerant enters the accumulator. The accumulator serves three major purposes. The first is to prevent two-phase refrigerant exiting the evaporator from entering the compressor. Air conditioning compressors are only intended to handle vapor and can be damaged if two-phase refrigerant is allowed to enter for extended periods of time. The second purpose of the accumulator is to protect the compressor from solid contaminants that may be entrained in the refrigerant flow. Two desiccant bags are housed inside the accumulator to absorb moisture in the refrigerant system. Absorbing moisture is the last major purpose of the accumulator. Figure 2.6 shows the Ford 1994 Crown Victoria accumulator. The accumulator is approximately 3-1/2 in. in diameter and 8 in. tall.

2.4 Condenser Air Loop Design and Construction

The condenser air loop contains all the equipment and components that provide and measure air to the condenser. A diagram of the condenser air loop is shown in Figure 2.7. Because the condenser inlet air is obtained from the room, the condenser inlet air temperature cannot be controlled and is determined by the

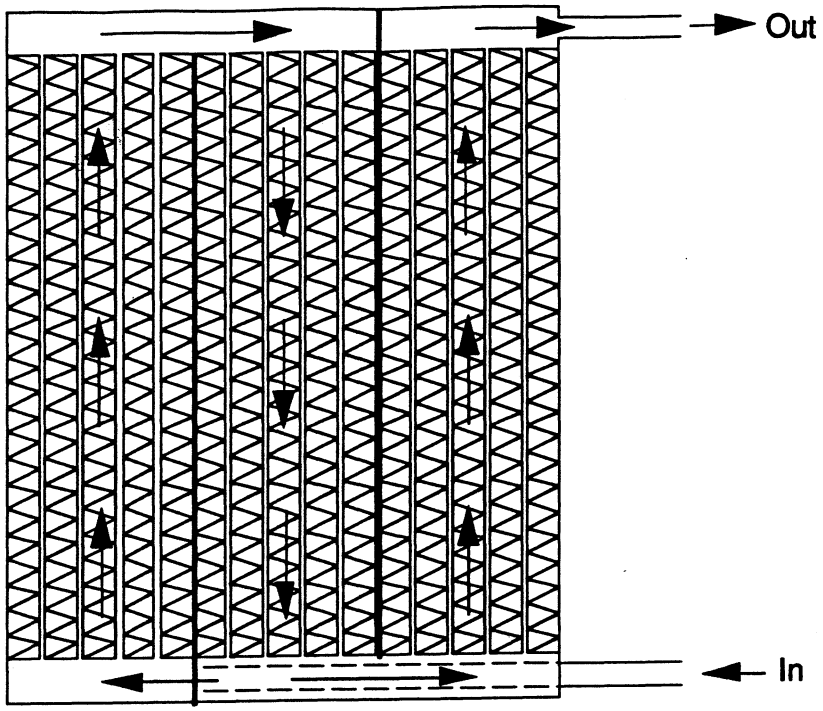

Figure 2.5: Ford evaporator refrigerant flow schematic (looking upstream).

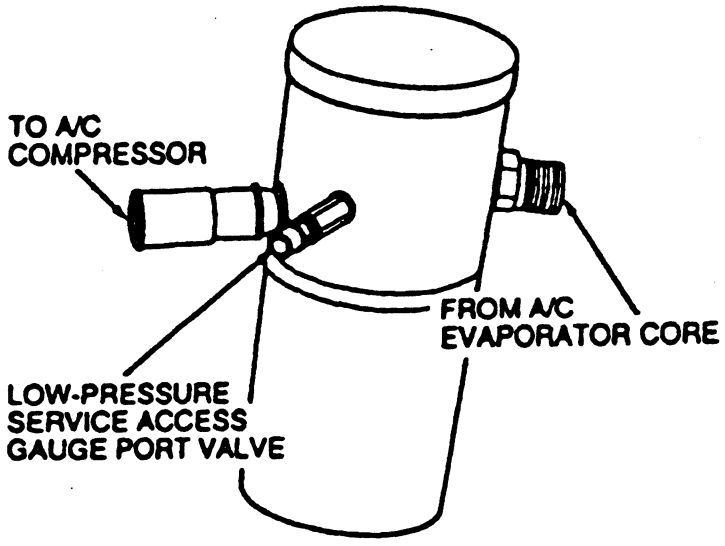

Figure 2.6: Ford accumulator/drier.

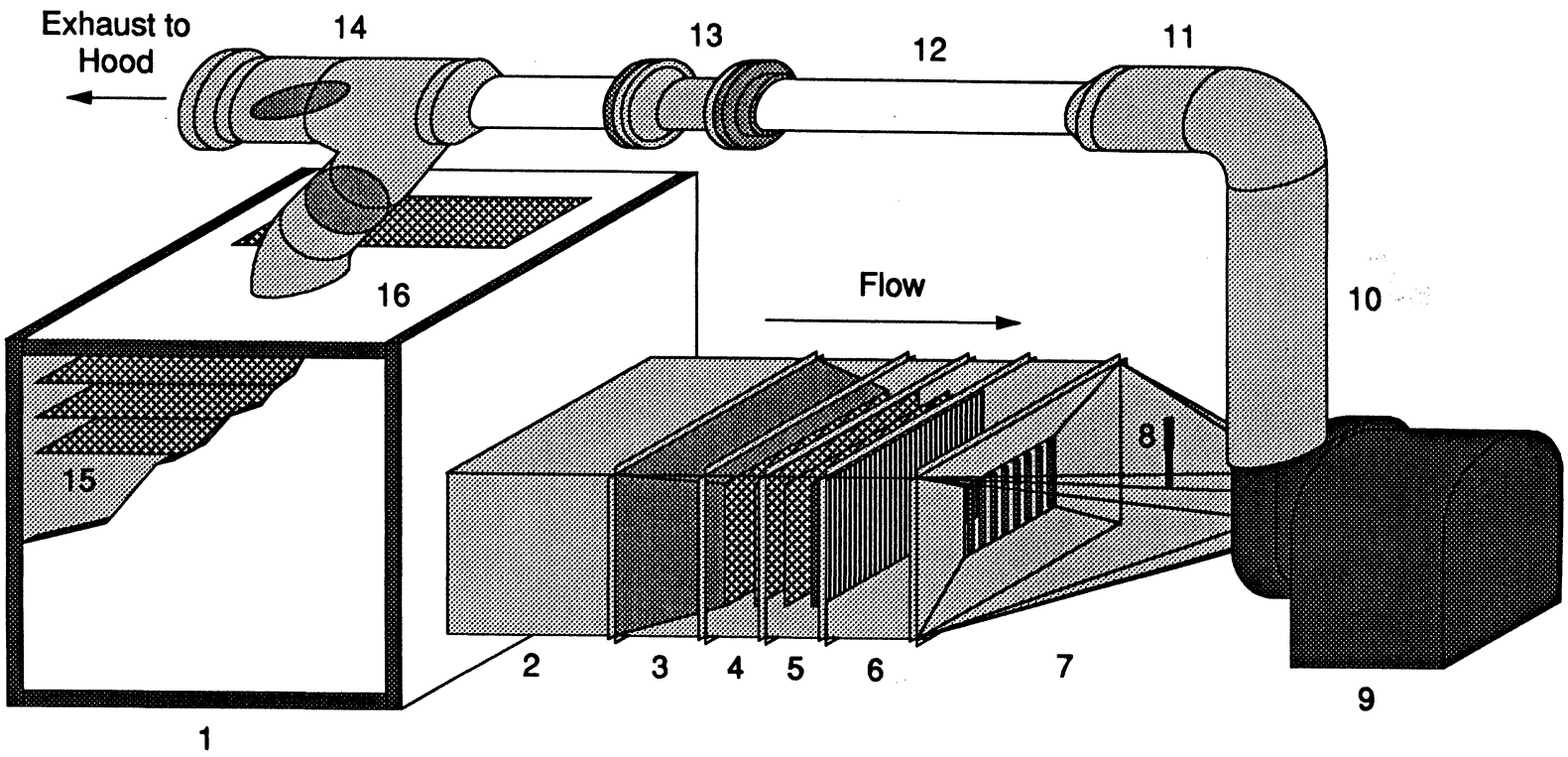

1. Plenum
2. Entrance Section
3. Reducer Section
4. Inlet Measurement Section
5. Condenser Section
6. Outlet Measurement Section
7. Rectangular-to-Round Transition
8. Humidity Sensor
9. Blower
10. 10" Sheet Metal Pipe
11. Flow Straightener
12. 6" PVC Pipe
13. Venturi Flow Tube
14. 10" Recirculation Section
15. Plenum Screens
16. Air Intake Port

Figure 2.7: Condenser air loop. (modified from Weston, 1995)

ambient room conditions. This section describes the work required to install the new Ford 1994 Crown Victoria air conditioning system condenser. For discussion relating to other aspects of the condenser air loop, including a detailed description of the condenser air loop instrumentation, the reader should refer to the report by Weston (1995).

To install the 1994 Ford Crown Victoria condenser, only the following test sections needed to be constructed: (a) reducer section, (b) measurement section, and (c) condenser section. Additionally, a new test section located after the condenser was built to correct inaccuracies in the condenser outlet temperature measurements. Figure 2.8 shows the rectangular duct pieces used in the condenser air loop. The reader should refer to Figures 2.7 and 2.8 frequently in the following discussion.

2.4.1 Converging Section

With previous condensers, a converging section was needed to reduce the size of the galvanized sheet metal duct from the standard 31 in. wide by 21 in. tall to the size of the condenser. The Ford Crown Victoria condenser, however, does not need a reducing section because its cross-section is only a few inches smaller than the galvanized sheet metal duct pieces used to hold the condenser in place. For this reason, the galvanized sheet metal duct that typically houses the reducer section is empty.

2.4.2 Inlet Measurement Section

The condenser inlet measurement section is contained inside a 31 in. by 21 in. by 8 in. (L × H × W) galvanized sheet metal duct and houses instrumentation for measuring the air-side temperature entering the condenser. As can be seen in Figure 2.9, the inlet measurement section is divided into two subsections—the first containing two flow conditioning fine-mesh screens, and the second containing a nine-point inlet thermocouple grid.

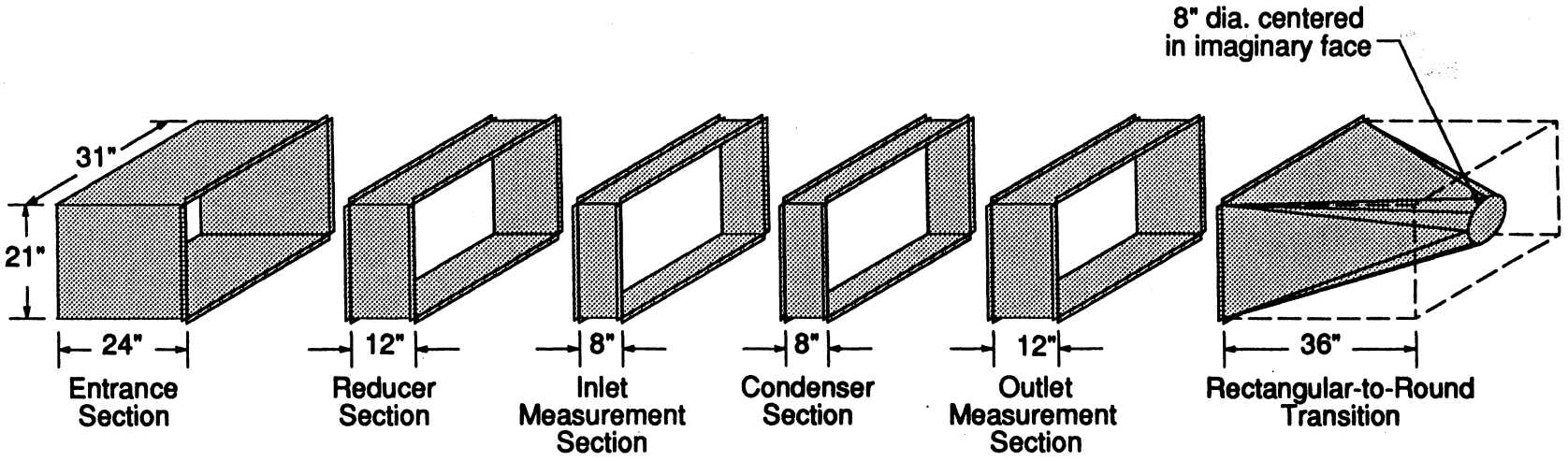

Figure 2.8: Condenser air loop duct pieces. (modified from Weston, 1995)

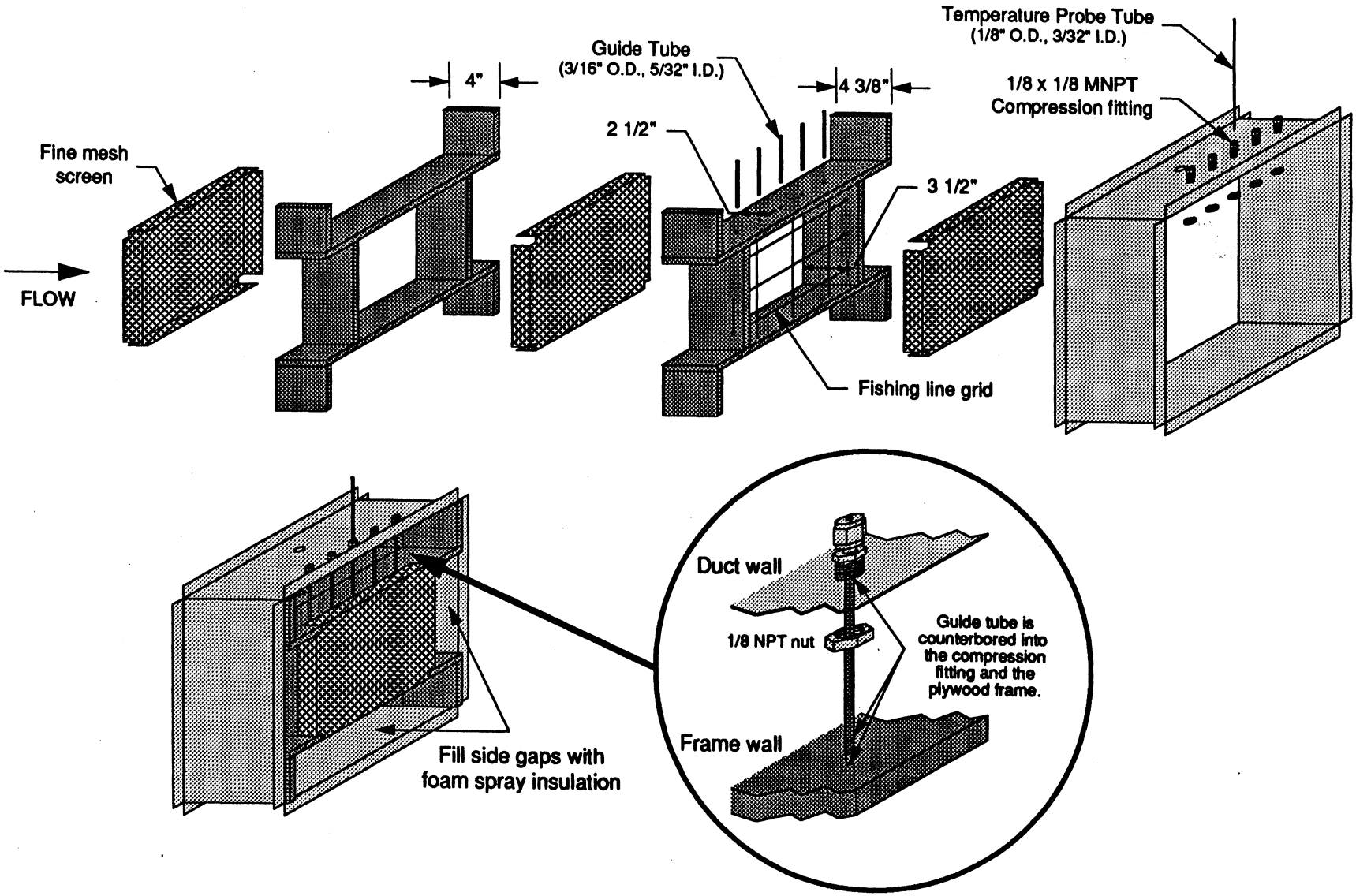

Figure 2.9: Condenser inlet measurement section. (modified Weston, 1995)

The flow conditioning subsection is constructed of 1/2-in. plywood and covered with aluminum foil tape (McMaster-Carr No. 76145A23 & 76145A24) to provide additional insulation. The plywood frame is 18-13/16 in. tall by 27-13/16 in. wide—the exact outside dimensions of the condenser. To ensure a uniform velocity profile entering the thermocouple grid and the heat exchanger, two fine-mesh screens are attached to the inlet and outlet of the plywood frame.

Located directly downstream of the flow conditioning subsection is the inlet temperature measurement subsection. This subsection contains the nine-point thermocouple grid as well as seven access ports that allow measurement of the inlet temperature independently of the grid. Because the inlet air has passed through two fine-mesh screens at this point, the flow can be assumed to be uniform. All nine thermocouples and access ports are equally spaced and numbered as shown in Figure 2.10. The thermocouples on the inlet grid are held together by fishing wire looped through holes drilled in the plywood frame. Yet another fine-mesh screen is located downstream of the thermocouple grid.

2.4.3 Condenser Section

As one might assume, the condenser section houses the Ford 1994 Crown Victoria condenser. A 1/2-in. plywood frame, covered with aluminum foil tape, is used to secure the condenser inside the 31 in. by 21 in. by 8 in. galvanized sheet metal duct. A diagram of the condenser section is shown in Figure 2.11. Two holes, cut out of the sheet metal duct, allow the condenser refrigerant tubing to be connected to the rest of the refrigerant loop. The condenser section, as with the inlet measurement section, has seven access ports spaced 4 in. apart that allow direct measurement of the condenser outlet temperature independently of the outlet thermocouple grid. The outlet thermocouple grid will be discussed in section 2.4.4.

Condenser section assembly was achieved by placing the wood frame inside the sheet metal duct, sliding the condenser into the wood frame, and securing the two remaining frame pieces with nails and aluminum foil tape.

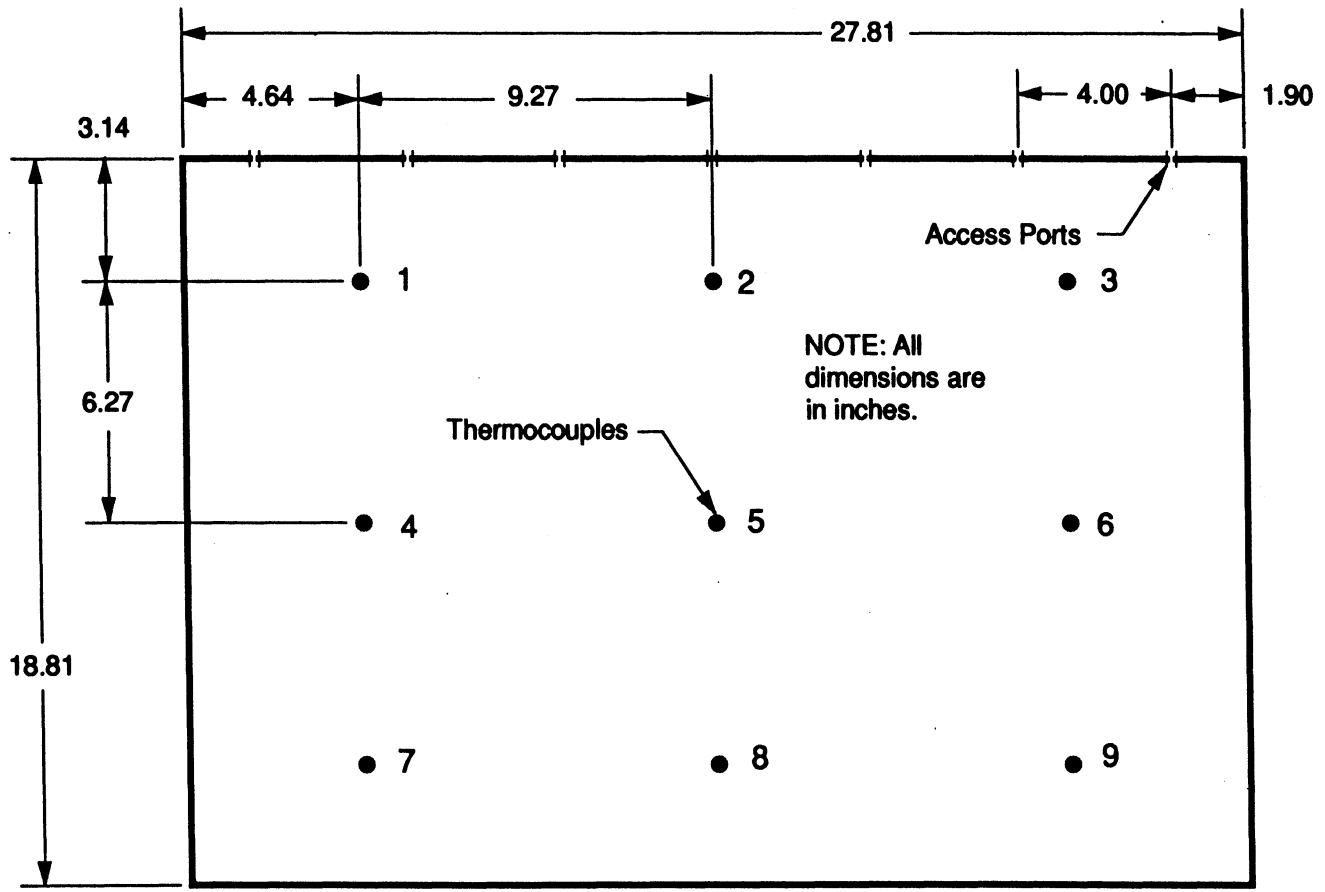

Figure 2.10: Condenser inlet temperature grid and access port numbering and spacing (looking upstream).

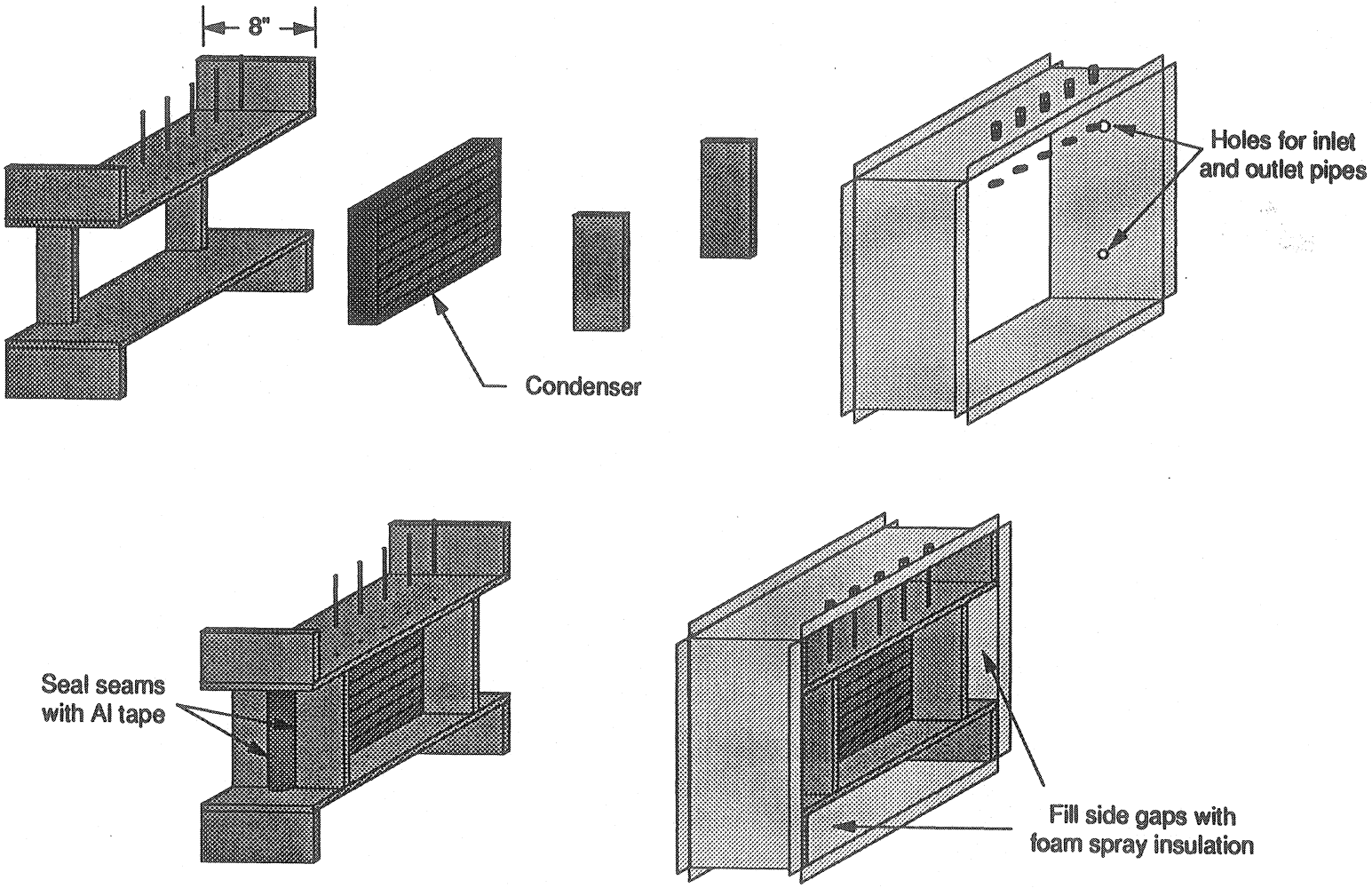

Figure 2.11: Condenser section. (modified from Weston, 1995)

2.4.4 Outlet Temperature Measurement Section

The outlet temperature measurement section contains the air-side outlet thermocouple grid. As previously stated, the outlet temperature profile is nonuniform, requiring a finer thermocouple grid than the nine-point grid used at the inlet of the condenser. In addition to a finer grid, the flow is contracted upstream of the outlet grid and cylinders are located directly before the thermocouples. The cylinders are used to generate eddies across the thermocouples and provide additional temperature averaging. Using the cylinders for temperature averaging is a novel technique that was selected after careful design and analysis based on our prior experience with wind tunnels. For the cylinders to perform properly, the Reynolds number of the air passing by the cylinders, with respect to the cylinder diameter, must be greater than 500 and the thermocouples must be approximately two diameters downstream of the cylinders. To obtain a Reynolds number greater than 500 at the cylinders and to remove flow inhomogeneities (required for accurate temperature average), the flow area is contracted to approximately 25% of the heat exchanger face area by a 1/4-in. plywood converging section. Figure 2.12 shows a drawing of the entire outlet measurement section. The reader should refer to this drawing frequently throughout this discussion.

Using the method mentioned above, 40 thermocouples are located behind eight 3/4-in. diameter cylinders and spaced two diameters (1-1/2 in.) apart. A schematic showing thermocouple numbering and spacing is provided in Figure 2.13.

Selected because it can be easily cut, 1-in. thick foam insulation is used to secure the eight cylinders. Holes approximately 1 in. deep, drilled into the side of the foam insulation, hold the wood cylinders in place. Another sheet of 1-in. thick foam insulation is located after the cylinder section. This section provides the required 2 diameter spacing between the cylinders and thermocouples. The second foam piece also provides a foundation for the wire mesh used to hold the 40 thermocouples with small wire ties. All 40 thermocouples are connected in parallel at an external junction box. A single thermocouple lead is used to measure the

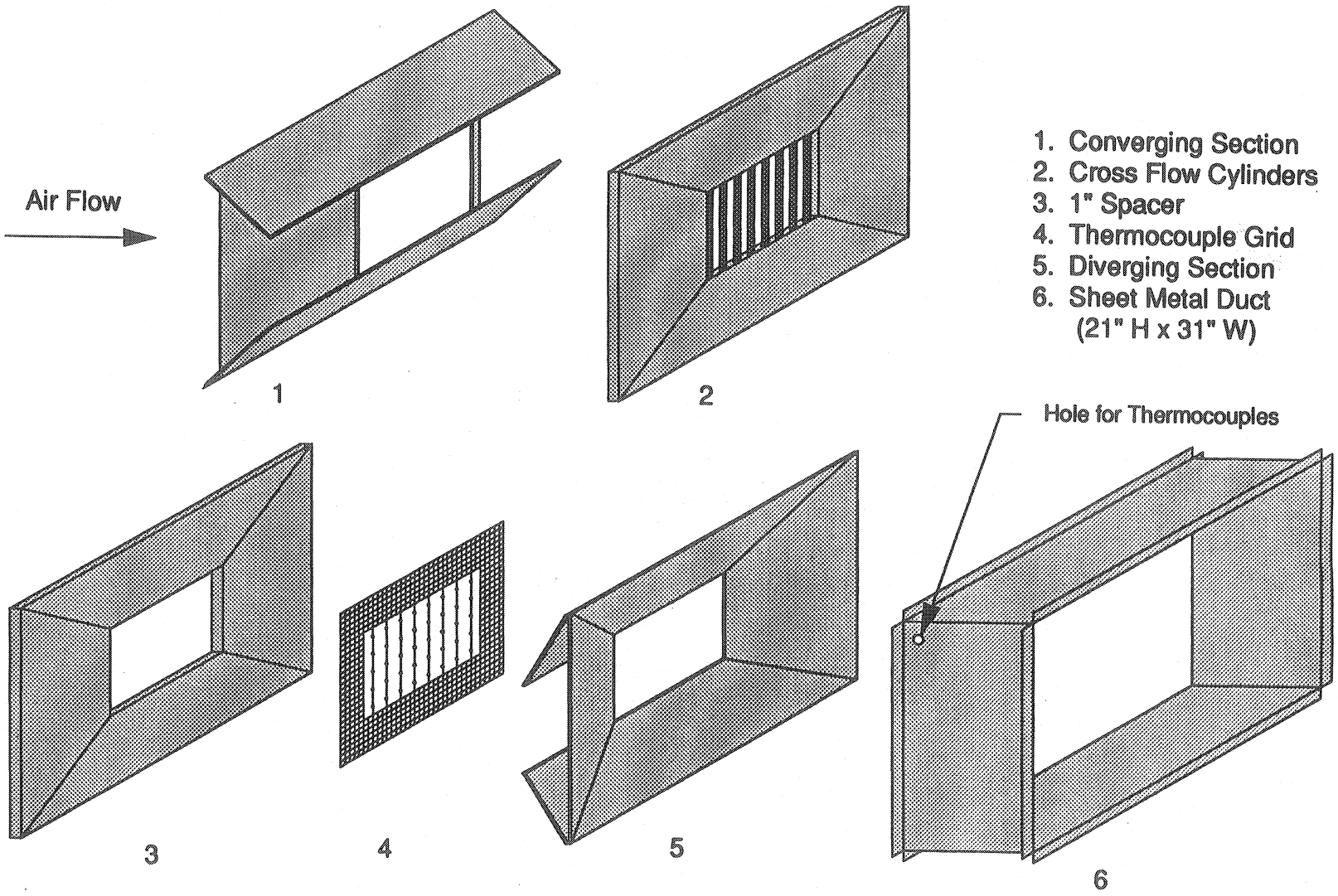

Figure 2.12: Condenser outlet measurement section (disassembled).

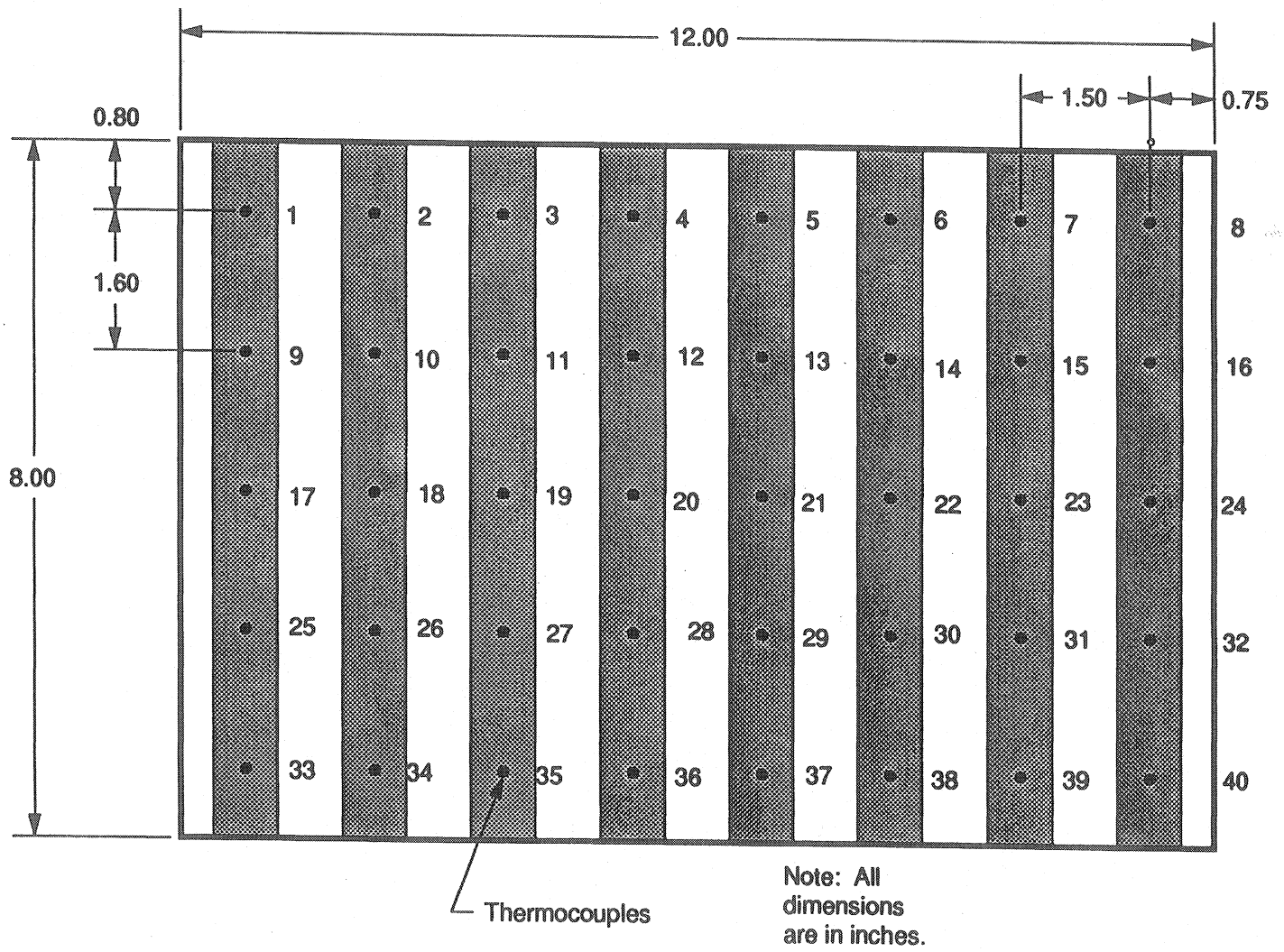

Figure 2.13: Condenser outlet temperature grid numbering and spacing (looking upstream).

thermocouple voltage of the entire parallel grid. The resulting measured thermocouple voltage is the arithmetic mean of the 40 independent thermocouples.

Downstream of the thermocouple grid is a 1/4-in. plywood diverging section. This section allows the flow to be expanded back to the size of the original galvanized sheet metal duct. All the separate pieces that constitute the condenser outlet measurement section are sealed and secured to each other with aluminum foil tape and putty, as shown in Figure 2.14.

The condenser loop air humidity is measured using a Vaisala Model HMP35A humidity sensor located on the rectangular-to-round transition piece downstream of the condenser outlet thermocouple grid, as shown in Figure 2.7. Since the humidity ratio of air cannot be changed by heat addition, humidity is only measured after the condenser. For this reason, the humidity entering the condenser is assumed to be the same as that at the condenser exit. It is important to note that, while the air temperature changes across the condenser, the amount of water in the air does not.

2.4.5 Condenser Ductwork Assembly

Once all condenser sections were constructed they were assembled together. The first step in accomplishing this was to join and seal the inside plywood-framed ductwork with aluminum foil tape and putty. It is extremely important that the ductwork not leak, as leaks will destroy the system calorimetry. The second step was to connect the flanges on the inlet measurement and condenser sections using small nuts and bolts. Foam insulation was then sprayed to fill the empty space between the galvanized sheet metal duct and the wooden frame. When applying the foam insulation, it is best to only spray several inches of insulation at a time and allow this amount to dry and expand before spraying again. While the insulation dries, it will likely flow over the edge of the sheet metal duct. The excess dry foam can then be cut with a small saw. All condenser air loop duct pieces, except for the rectangular-to-round transition piece, were then joined together. The duct pieces were then aligned with the plenum and taped to the inside plenum wall with duct tape to prevent leakage. Finally, the rectangular-to-round transition

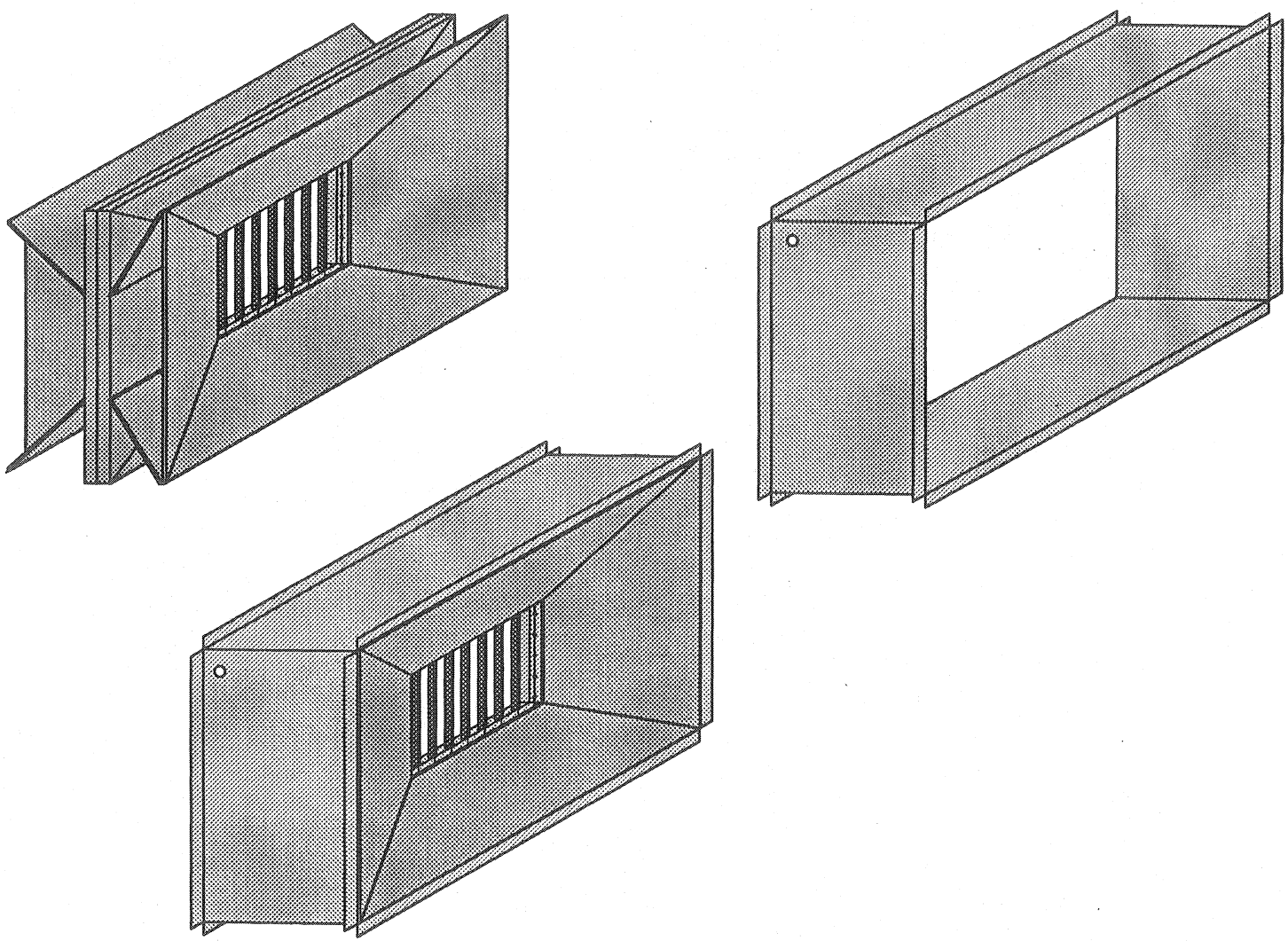

Figure 2.14: Condenser outlet measurement section (assembled).

piece was attached to the exit of the outlet measurement section and condenser fan entrance.

2.4.6 Condenser Air Loop Zone Box

To ensure accurate thermocouple measurements, the condenser air loop thermocouples are placed inside an insulated, isothermal box. We refer to this box as the condenser air loop "zone box". The condenser air loop zone box contains the electrical connections for all condenser air-side measurements. Some of these connections are output signals to the Strawberry Tree data acquisition system, while others are inputs to instrumentation (such as power). Due to the limited amount of space in the other zone boxes, not all connections on the condenser air loop zone box concern condenser air loop measurements and equipment. Table 2.2 summarizes the instrumentation connected through the condenser air loop zone box. A detailed diagram of the zone box is provided in Figure 2.15. The "name" heading in column one of Table 2.2 refers to the variable name used in Figure 2.15. As the condenser zone box diagram shows, a single thermocouple wire is used to transport the outlet air temperature signal from a separate zone box that consolidates the 40 outlet air thermocouples. A Type-T thermocouple wire must be used for connecting the signal to avoid creating "virtual" thermocouples from connections made using wires with conductive materials other than those in Type-T thermocouples. All 40 thermocouples in the separate outlet temperature grid zone box are wired in a similar manner as the inlet thermocouple grid shown in Figure 2.15.

2.5 Evaporator Air Loop Design and Construction

Like the condenser air loop, the evaporator air loop contains all equipment and components that deliver air to the evaporator. Figure 2.16 shows a diagram of the evaporator air loop. The major difference between the evaporator and condenser air loops, other than the smaller size of the ductwork, is that the air in the evaporator loop is recirculated and an electric duct heater is used to control the evaporator inlet

Table 2.2: Condenser Air Loop Zone Box Summary

Measurement (Name, Instrument)	Model No.	Serial No.	Input Signal	Output Signal
Venturi Flow Tube P In (Pcav, Pressure Trans.)	Setra 239	398563	Power Supply Rail: 24 V	Data Aq.: 0-5 V
Venturi Flow Tube ΔP (dPcav, Pressure Trans.)	Setra C239	307533	Power Supply Rail: 24 V	Data Aq.: 4-20 mA
Venturi Flow Tube T in (Tcav, Thermocouple)	Type-T	N/A	N/A	Data Aq.: Thermocouple μV
Relative Humidity (RHcao, Humidity Sensor)	Vaisala HMP35A	595725	Power Supply Rail: 24 V	Data Aq.: 0-5 V
Temp @ Humidity Probe (TRHcao, Humidity Sensor)	Vaisala HMP35A	595725	Power Supply Rail: 24 V	Data Aq.: RTD
Condenser T In (Tcai, Thermocouple Grid)	Type-T	N/A	N/A	Data Aq.: Thermocouple μV
Condenser T Out (Tcao, Thermocouple Grid)	Type-T	N/A	N/A	Data Aq.: Thermocouple μV
Refrigerant Flow Rate (mdot_micro, Micro Motion)	DS025S119SV	56767	A/C Power	Data Aq.: 4-20 mA
Refrigerant Oil % (Sonic Device)	N/A	N/A	External 12V Power	Flight Time: 0-5 V Temp: 0-5 V
Condenser Blower Set Pt. (Strawberry Tree Data Aq.)	Toshiba VF-SX 2037P	92854690	Data Aq: Square Wave	N/A
Condenser Heater Set Pt. (Strawberry Tree Data Aq.)	CAPP/USA 535-44120B0S01	964200201	Data Aq: Not Used	N/A

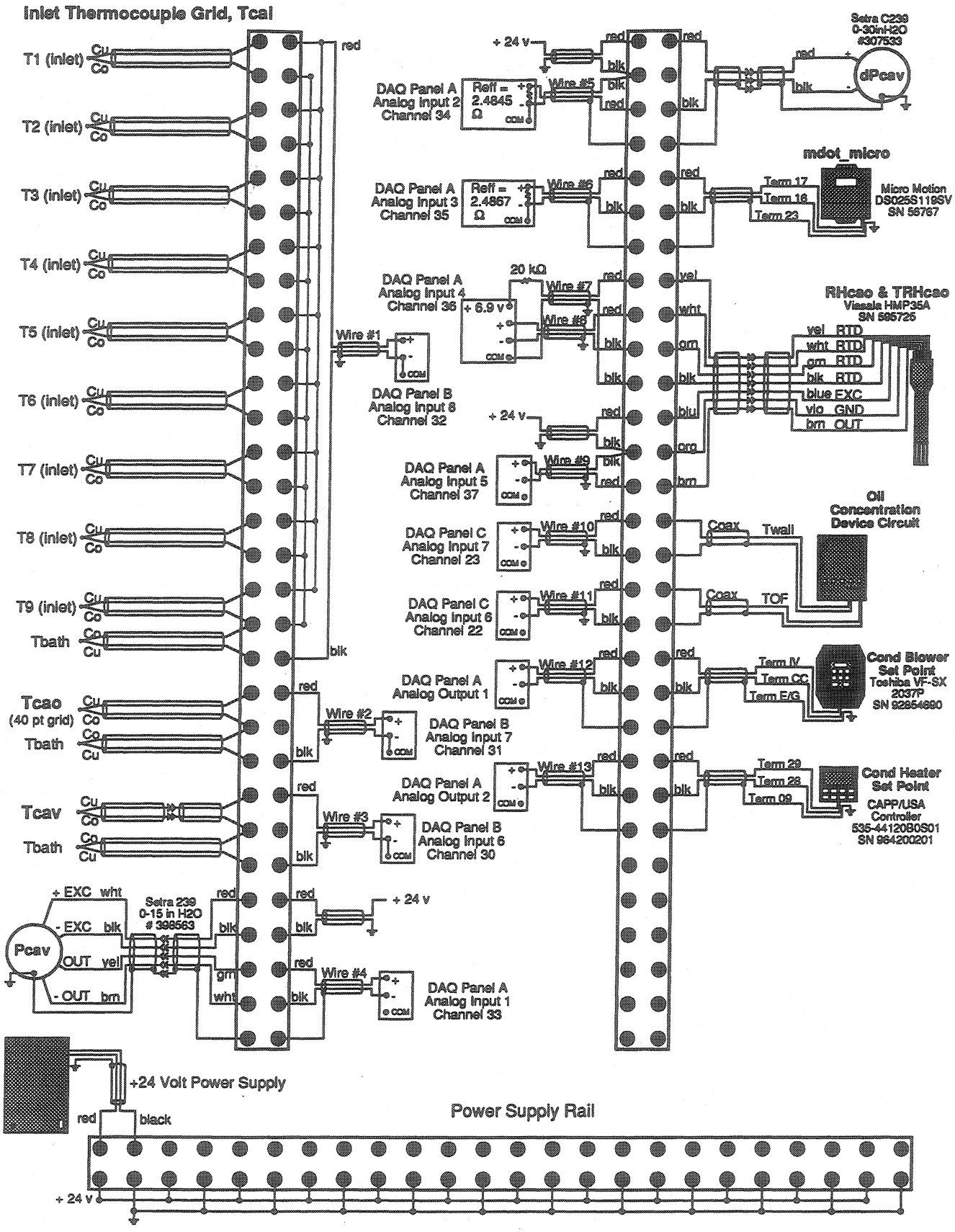

Figure 2.15: Condenser loop zone box diagram.

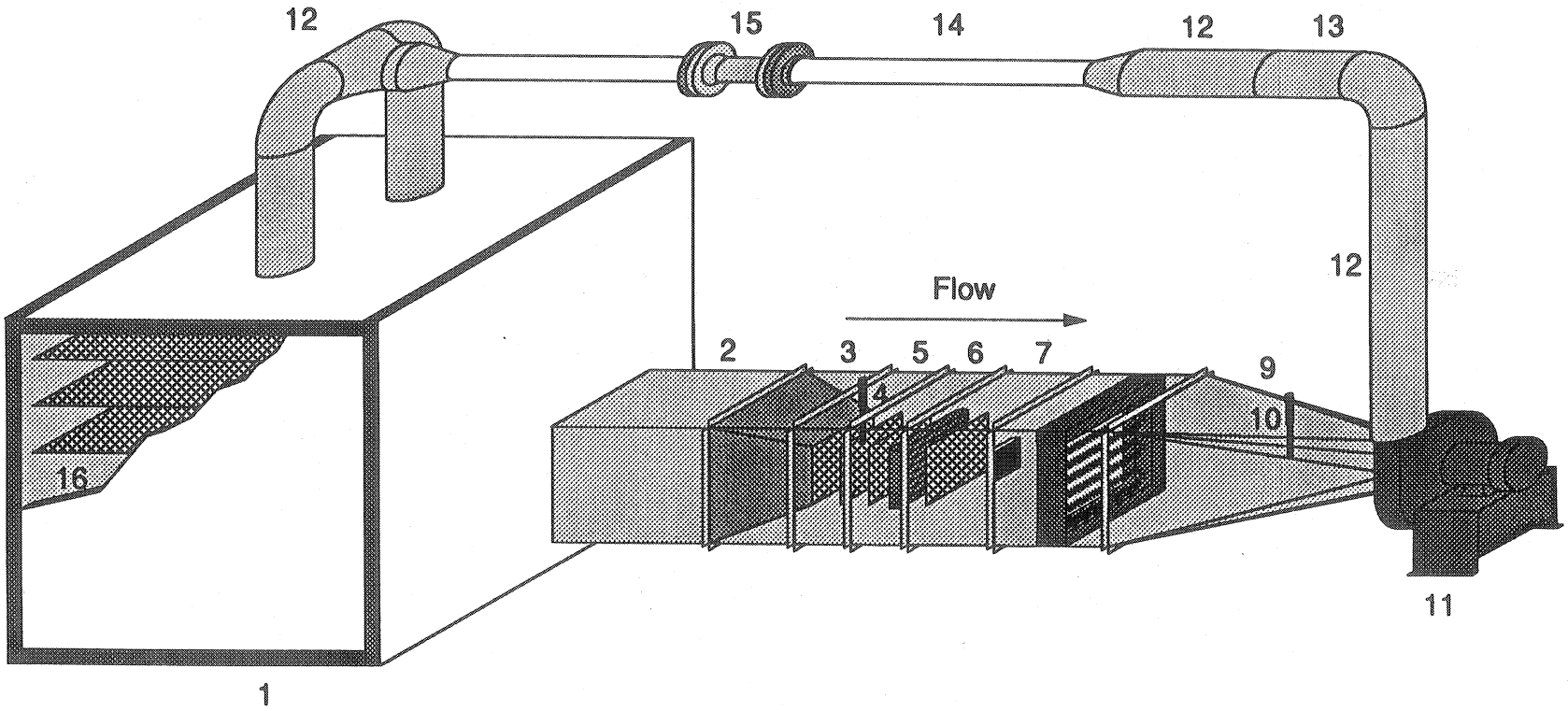

1. Plenum
2. Entrance Section
3. Reducer Section
4. Inlet Humidity Sensor
5. Inlet Measurement Section
6. Evaporator Section
7. Outlet Measurement Section
8. Duct Heater Section
9. Rectangular-to-Round Transition
10. Outlet Humidity Sensor
11. Blower
12. 6" Sheet Metal Pipe
13. Flow Straightener
14. 3" PVC Pipe
15. Venturi Flow Tube
16. Plenum Screens

Figure 2.16: Evaporator air loop. (modified from Weston, 1995)

air temperature. The heater is located before the blower so the blower can mix the air and prevent temperature stratification at the evaporator inlet. This section describes the work required to install the Ford 1994 Crown Victoria air conditioning system evaporator. For discussion relating to other aspects of the evaporator air loop, including a detailed description of the condenser air loop instrumentation, the reader should refer to the report by Weston (1995).

To install the Ford 1994 Crown Victoria evaporator, only the following test sections needed to be constructed: (a) reducer section, (b) measurement section, and (c) evaporator section. Additionally, a new test section was designed for accurately measuring the evaporator air outlet temperature. The galvanized sheet metal duct pieces used in the evaporator air loop are shown in Figure 2.17. The reader may wish to refer to Figures 2.16 and 2.17 in the following discussion.

2.5.1 Converging Section

Located after the plenum, the converging section reduces the air flow area from the sheet metal duct standard of 16 by 16 in. to the evaporator face area of 8-3/8 in. wide by 9 in. tall. The converging section is constructed of 1/4-in. plywood and covered with aluminum foil tape. The four plywood pieces that constitute the converging section are joined together with small right angle metal brackets. A drawing of the evaporator converging section is shown in Figure 2.18.

2.5.2 Inlet Measurement Section

The evaporator inlet measurement section is housed inside a 16 in. by 16 in. by 8 in. (L × H × W) galvanized sheet metal duct and contains instrumentation for measuring the evaporator air-side inlet humidity and temperature. As shown in Figure 2.19, the evaporator inlet measurement section is divided into two subsections. The first subsection contains a Vaisala Model HMP35A humidity sensor located between two flow conditioning fine-mesh screens. The second subsection contains a nine-point inlet thermocouple grid used to measure the evaporator air inlet temperature. Both subsections are constructed of 1/2-in.

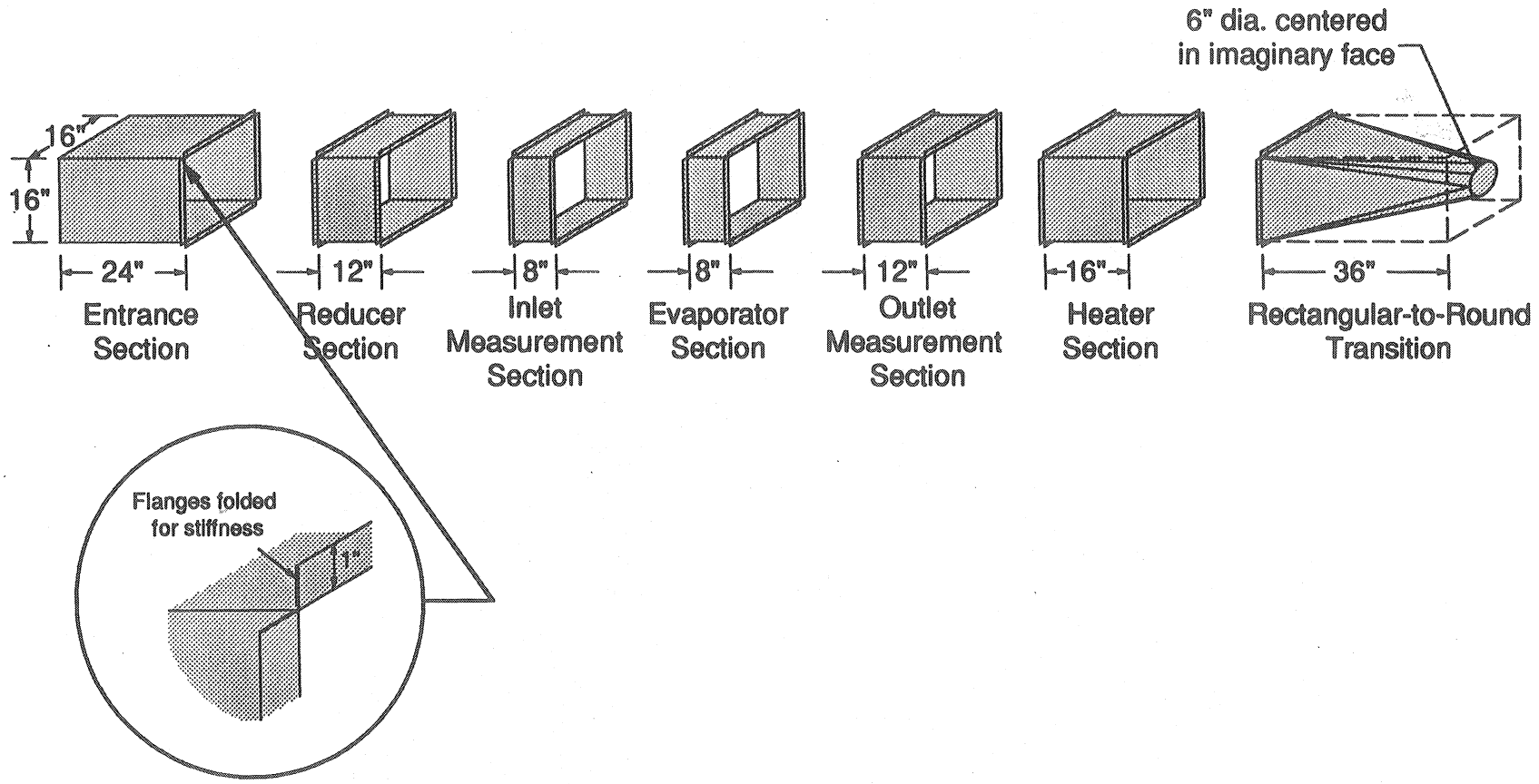

Figure 2.17: Evaporator air loop duct pieces. (modified from Weston, 1995)

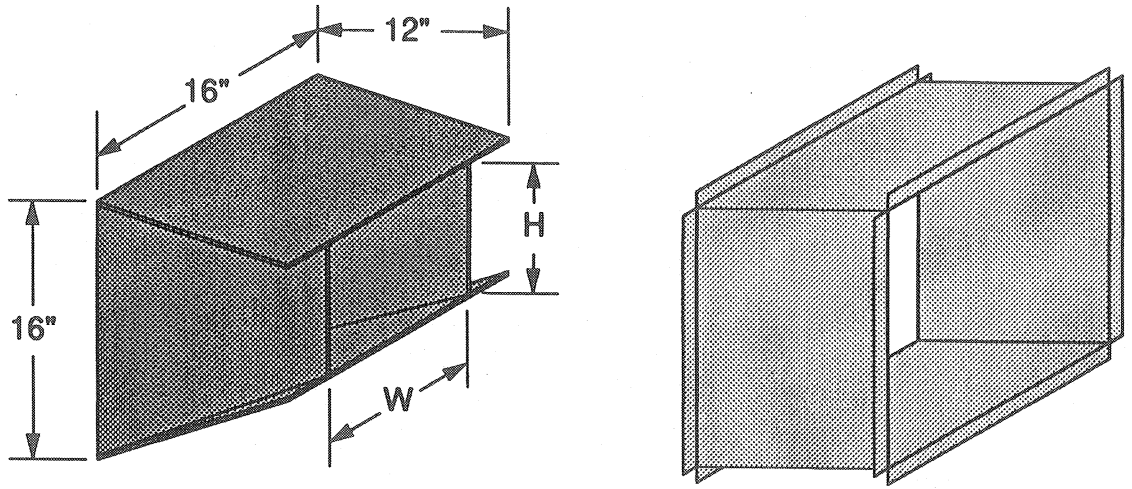

Figure 2.18: Evaporator converging section. (Weston, 1995)

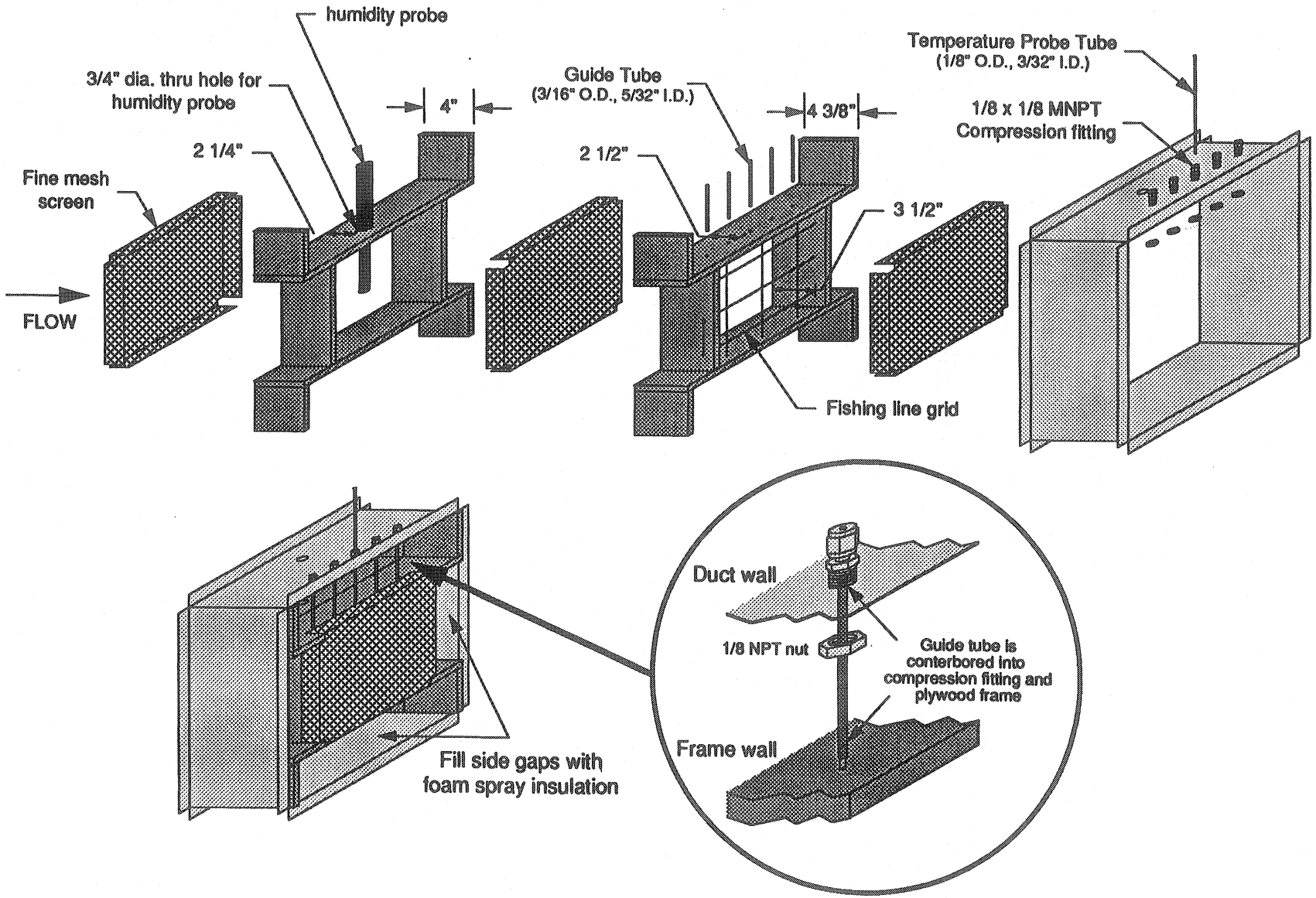

Figure 2.19: Evaporator inlet measurement section. (modified from Weston, 1995)

35plywood and covered with aluminum foil tape. The plywood frames are 9 in. tall by 8-3/8 in. wide—the exact outside dimensions of the evaporator.

The humidity probe is located 2-1/4 in. from the entrance of the humidity and flow conditioning subsection. Residing near the middle of the duct, the probe measures the relative humidity of the inlet evaporator air. To ensure a uniform velocity profile entering the thermocouple grid and the evaporator, two fine-mesh screens are attached to the inlet and outlet of the subsection plywood frame.

As shown in Figure 2.19, the inlet temperature measurement subsection is located directly downstream of the humidity and flow conditioning subsection. This subsection contains the nine-point evaporator inlet thermocouple grid and seven access ports that can be used for measuring the inlet temperature independently of the grid. The air can be assumed to be uniform at this point because it has passed through two fine-mesh screens. All nine thermocouples are equally spaced and numbered as shown in Figure 2.20. The inlet thermocouples are attached to fishing wire that is looped through small holes drilled in the plywood frame. Another fine-mesh screen is located downstream of the thermocouple grid.

2.5.3 Evaporator Section

The evaporator section houses the Ford 1994 Crown Victoria evaporator. A 1/2-in. plywood frame, covered with aluminum foil tape, is used to secure the evaporator inside the galvanized sheet metal duct. The evaporator section is shown in Figure 2.21. Two holes, cut out of the sheet metal duct, allow the evaporator refrigerant tubing to be connected to the rest of the refrigerant loop. Unlike the condenser section, the evaporator section contains a heavy-gauge sheet plastic drain pan that allows the condensate collected on the evaporator to drain into a graduated cylinder. The plastic drain pan funnels condensate into a drain hole that is secured to the galvanized sheet metal duct. During transient operation, the graduated cylinder that collects the condensate can be weighed to determine the latent load on the evaporator. The evaporator section, as with the inlet measurement section, has six access ports spaced 1.39 in. apart that allow direct

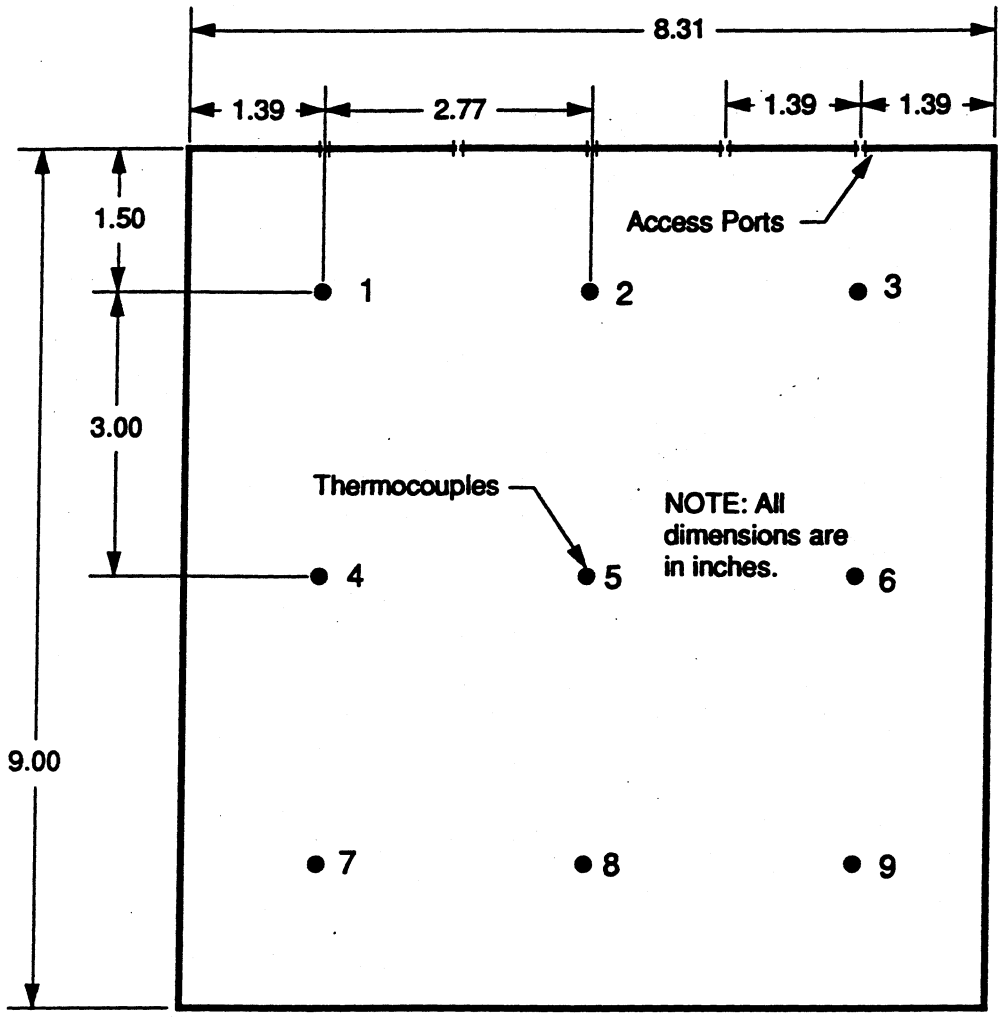

Figure 2.20: Evaporator inlet temperature grid and access port numbering and spacing (looking upstream).

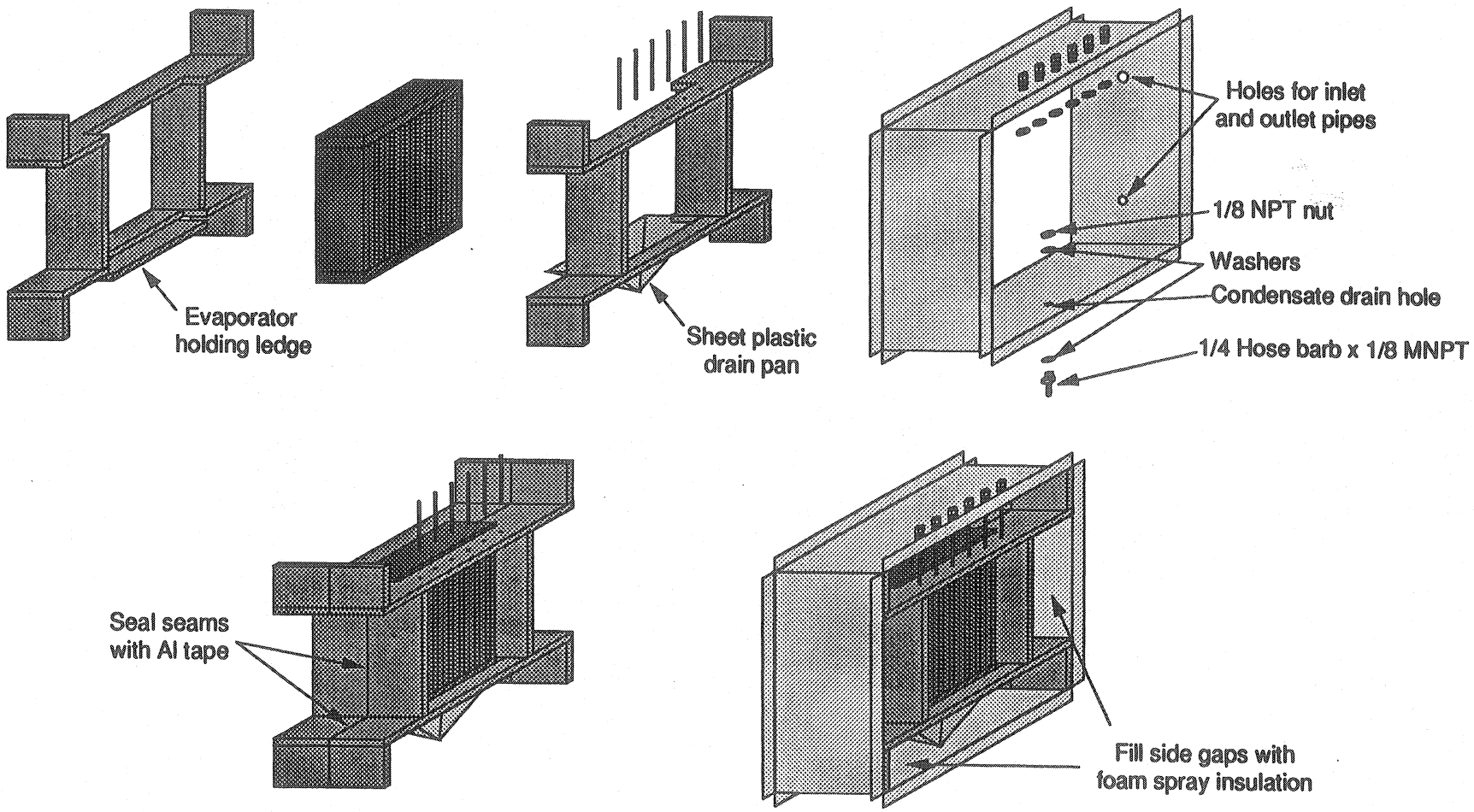

Figure 2.21: Evaporator section.

measurement of the evaporator outlet temperature independently of the outlet thermocouple grid. The outlet thermocouple grid is discussed in Section 2.5.4.

Assembling the evaporator section is somewhat more complex than the condenser section. The initial step is to put the first wood frame inside the sheet metal duct. The evaporator is then placed against the first wood frame, paying careful attention to where the evaporator refrigerant tubing fits through the duct. The second wood frame is then seated against the evaporator and all seams, except for the plastic drain pan area, are sealed with aluminum foil tape. The final step is to secure the plastic drain pan to the plywood frame with aluminum foil tape and thumbtacks and to the galvanized sheet metal duct using the fittings shown in Figure 2.21.

2.5.4 Outlet Temperature Measurement Section

The outlet temperature measurement section contains the outlet air thermocouple grid. As stated earlier, the outlet temperature profile is nonuniform, requiring a finer thermocouple grid than the nine-point grid used at the inlet of the evaporator. In a similar fashion as the condenser outlet measurement section, the flow is contracted and the thermocouple grid is located behind a row of small wood cylinders. The eight 1/4-in. diameter cylinders are spaced 1/2 in. apart and generate eddies to provide additional temperature averaging. To generate the required Reynolds number of at least 500 at the cylinder array, and to remove flow inhomogeneities (required for accurate temperature average), the flow area is contracted to approximately 25% of the evaporator face area. The converging section consists of three 1-in. thick pieces of foam insulation that incrementally decrease the flow area, as shown in Figure 2.22.

Using the method stated above, 46 thermocouples are attached to a rigid wire mesh with small wire ties and placed two cylinder diameters (1/2 in.) behind the eight rods. A schematic showing the evaporator outlet thermocouple numbering and spacing is provided in Figure 2.23.

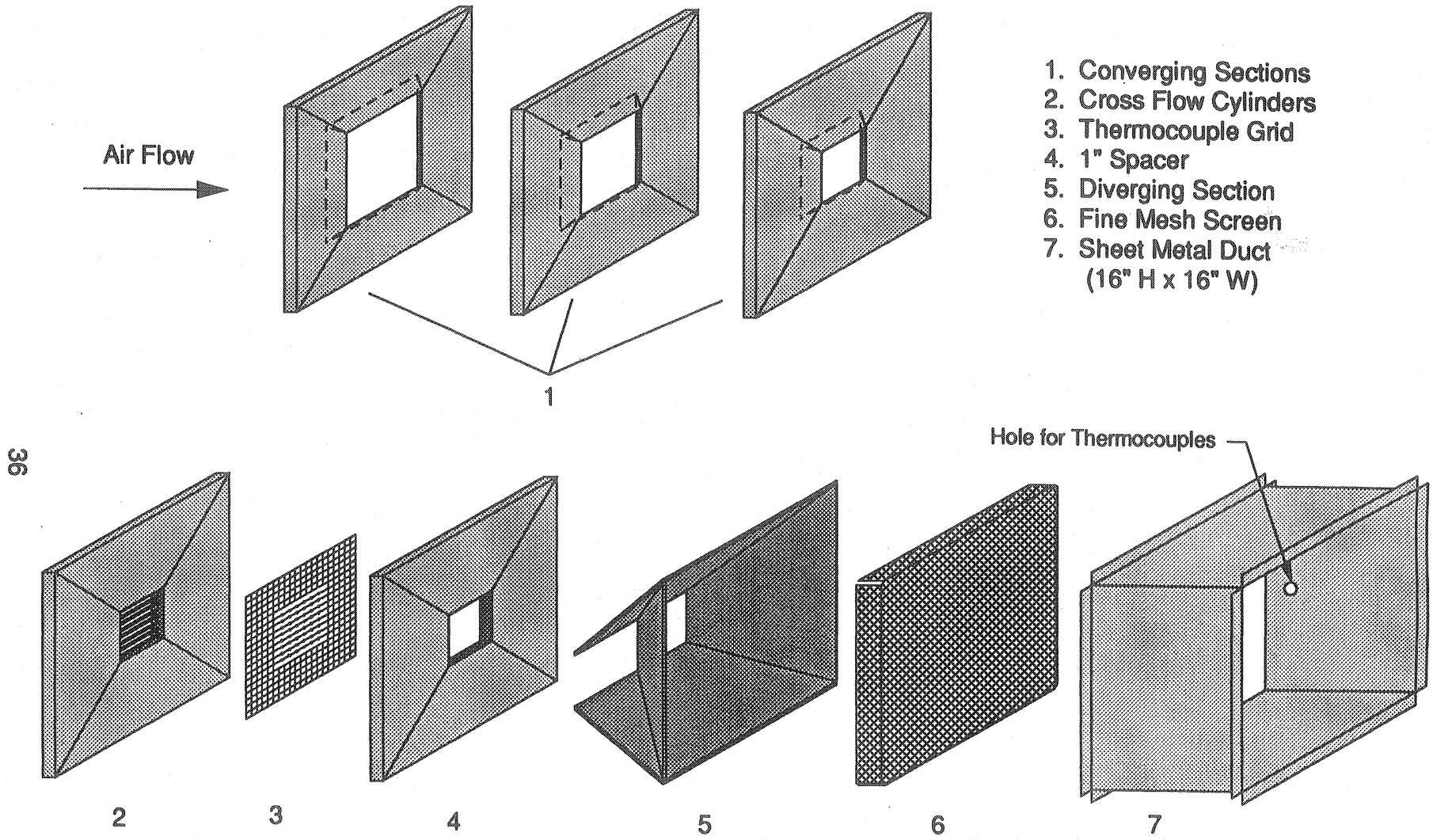

Figure 2.22: Evaporator outlet measurement section (disassembled).

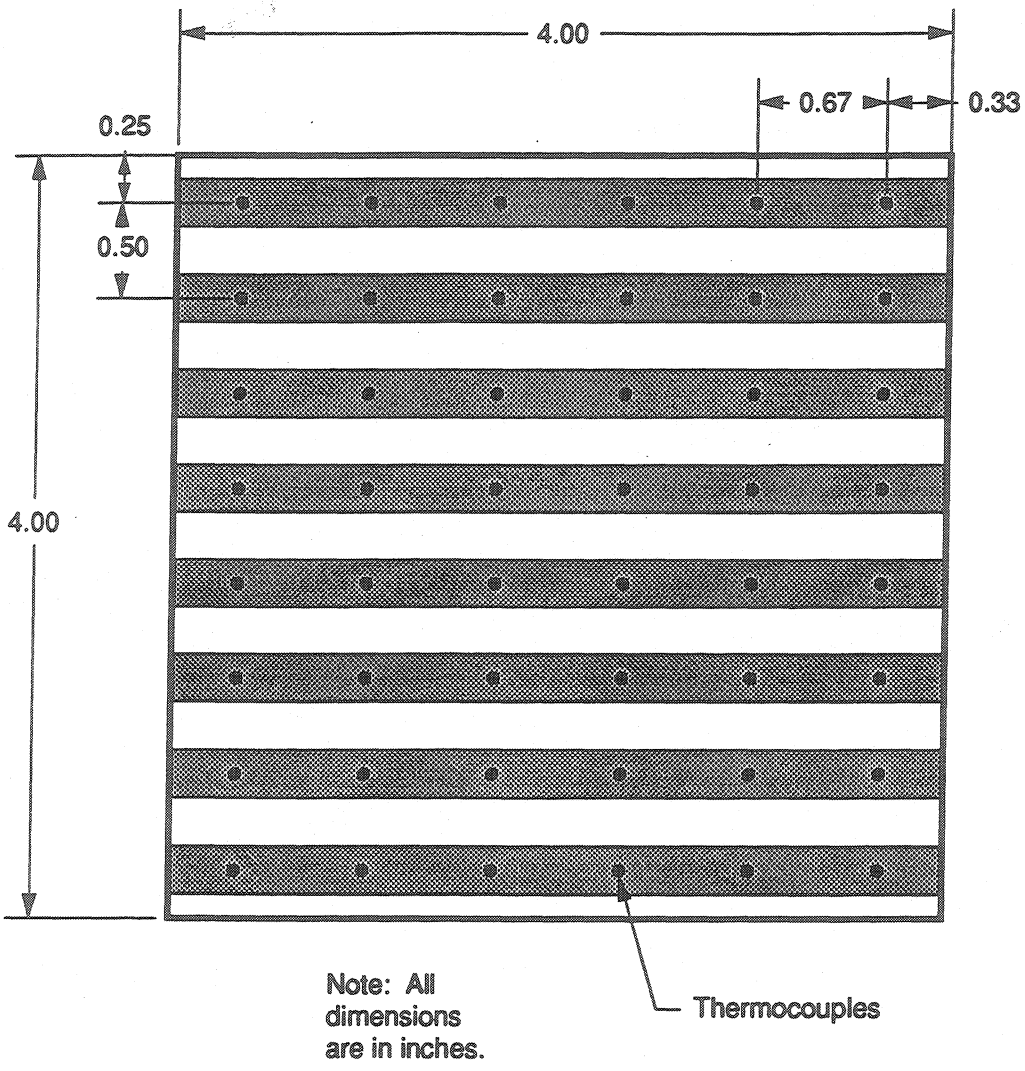

Figure 2.23: Evaporator outlet temperature grid numbering and spacing (looking upstream).

As with the condenser outlet temperature measurement section, 1-in. thick foam insulation is used to secure the eight cylinders. Holes approximately 1 in. deep, drilled into the side of the foam insulation, hold the wood cylinders in place. Because the cylinders used in the evaporator outlet measurement section are smaller than those used in the condenser outlet section, no spacer piece is needed. For this reason, the thermocouple wire mesh is attached to the cylinder foam piece —maintaining the required two diameter spacing between the cylinders and thermocouples. All 46 thermocouples are connected in parallel at an external junction box. A single thermocouple lead is used to measure the thermocouple voltage of the entire parallel grid. The resulting measured voltage is the arithmetic mean of the 46 independent thermocouples.

Downstream of the thermocouple grid is a 1/4-in. plywood diverging section. This section allows the flow to be expanded back to the original size of the galvanized sheet metal duct. A fine-mesh screen is used at the exit of the diverging section to provide nearly uniform flow to the evaporator loop duct heater. Uniform flow is required at the duct heater to prevent the heater coils from overheating. All the pieces that constitute the evaporator outlet measurement section are sealed and secured to each other with aluminum foil and putty, as shown in Figure 2.24.

As shown in Figure 2.16, the evaporator air-side outlet humidity is measured using a Vaisala Model HMP35A humidity sensor located on the rectangular-to-round transition piece downstream of the duct heater. In the evaporator air loop, inlet and outlet humidity sensors are necessary to account for the condensation of water that occurs on the evaporator surface. It was determined during data analysis that the evaporator air-side outlet humidity sensor was generating faulty readings when high evaporator inlet air temperatures were required. Faulty readings were obtained because (a) the air was not properly mixed before it was read by the sensor and, therefore, (b) the temperature at the sensor was above the maximum recommended operating limit of 140 °F.

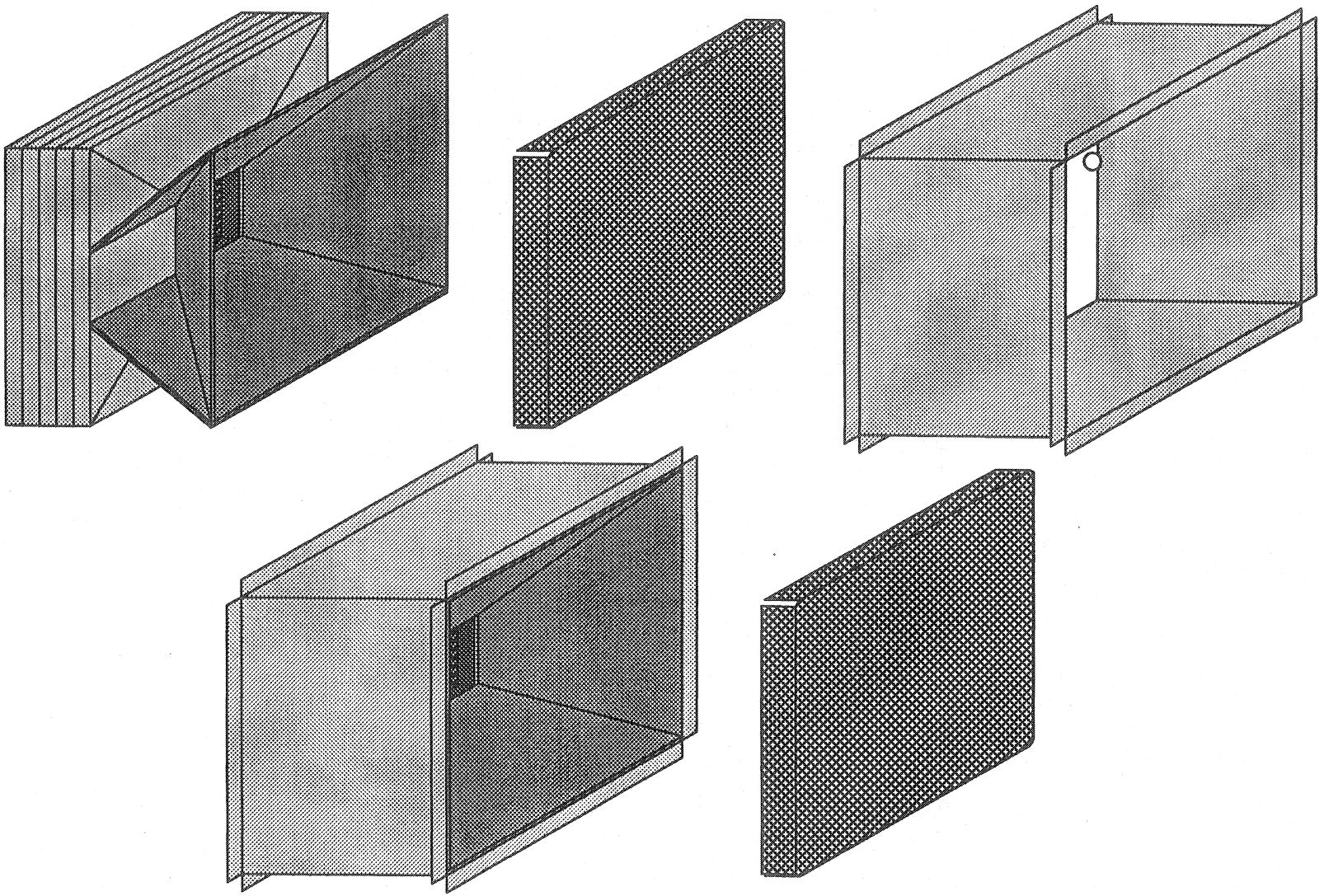

Figure 2.24: Evaporator outlet measurement section (assembled).

2.5.5 Evaporator Ductwork Assembly

The evaporator ductwork is assembled in a fashion similar as the condenser ductwork. The first step is to join and seal the inside plywood-framed ductwork with aluminum foil tape and putty while making sure no small holes exist. Small holes can cause leaks and destroy the system calorimetry. The second step is to connect the flanges on the inlet measurement and evaporator sections together using small nuts and bolts. Foam insulation is then sprayed to fill the empty space between the galvanized sheet metal duct and the wooden frame. All evaporator air loop pieces, except for the duct heater and the rectangular-to-round transition piece, are then joined together. The duct pieces are then aligned with the plenum and taped to the inside plenum wall with duct tape to prevent leakage. Finally, the duct heater and rectangular-to-round pieces are attached to the exit of the outlet measurement section and evaporator fan entrance.

2.5.6 Evaporator Air Loop Zone Box

To ensure accurate thermocouple measurements, the evaporator air loop thermocouples are located inside an insulated, isothermal box. The evaporator air loop zone box contains the electrical connections for all evaporator air-side measurements. As with the condenser air loop zone box, some of the connections are output signals to the data acquisition system, whereas others are inputs to instrumentation. In addition to housing all the evaporator air loop measurements, the zone box contains all the connections necessary to provide power to the compressor and measure the rotational speed and torque of the compressor drive motor. Table 2.3 summarizes the connections inside the evaporator zone box. A detailed diagram of the zone box is shown in Figure 2.25.

A single Type-T thermocouple wire is again used to transport the air-side outlet temperature grid signal from an external junction box to the evaporator loop zone box. A Type-T wire must be used to prevent "virtual" thermocouples from being created at all connections made with wire containing dissimilar metals. The 46

Table 2.3: Evaporator Air Loop Zone Box Summary

Measurement (Name, Instrument)	Model No.	Serial No.	Input Signal	Output Signal
Venturi Flow Tube P In (Peav, Pressure Trans.)	Setra 239	409977	Power Supply Rail: 24 V	Data Aq.: 0-5 V
Venturi Flow Tube ΔP (dPeav, Pressure Trans.)	Setra C228-1	355739	Power Supply Rail: 24 V	Data Aq.: 4-20 mA
Venturi Flow Tube T In (Teav, Thermocouple)	Type-T	N/A	N/A	Data Aq.: Thermocouple μV
Inlet Relative Humidity (RHeai, Humidity Sensor)	Vaisala HMP 35A	618479	Power Supply Rail: 24 V	Data Aq.: 0-5 V
Temp @ In Humidity Probe (TRHeai, Humidity Sensor)	Vaisala HMP 35A	618479	Power Supply Rail: 24 V	Data Aq.: RTD
Outlet Relative Humidity (RHeao, Humidity Sensor)	Vaisala HMP 35A	595698	Power Supply Rail: 24 V	Data Aq.: 0-5 V
Temp @ Out Humidity Probe (TRHeao, Humidity Sensor)	Vaisala HMP 35A	595698	Power Supply Rail: 24 V	Data Aq.: RTD
Evaporator T In (Teai, Thermocouple Grid)	Type-T	N/A	N/A	Data Aq.: Thermocouple μV
Evaporator T Out (Teao, Thermocouple Grid)	Type-T	N/A	N/A	Data Aq.: Thermocouple μV
Compressor Drive Speed (krpm, Speed Sensor)	Daytronic 3240A	2072 (8621)	External Power	Data Aq.: 0-5 V
Compressor Drive Torque (ktorque, Torque Sensor)	Daytronic 3278	2103 (31030)	External Power	Data Aq.: 0-5 V
Compressor Clutch On/Off (Strawberry Tree Output)	N/A	N/A	Data Aq: Square Wave	N/A
Evaporator Blower Set Pt. (Strawberry Tree Data Aq.)	Toshiba VF-SX 2007P	92854452	Data Aq: Square Wave	N/A
Evaporator Heater Set Pt. (Strawberry Tree Data Aq.)	CAPP/USA 535-44120B0S01	964200202	Data Aq: Not Used	N/A

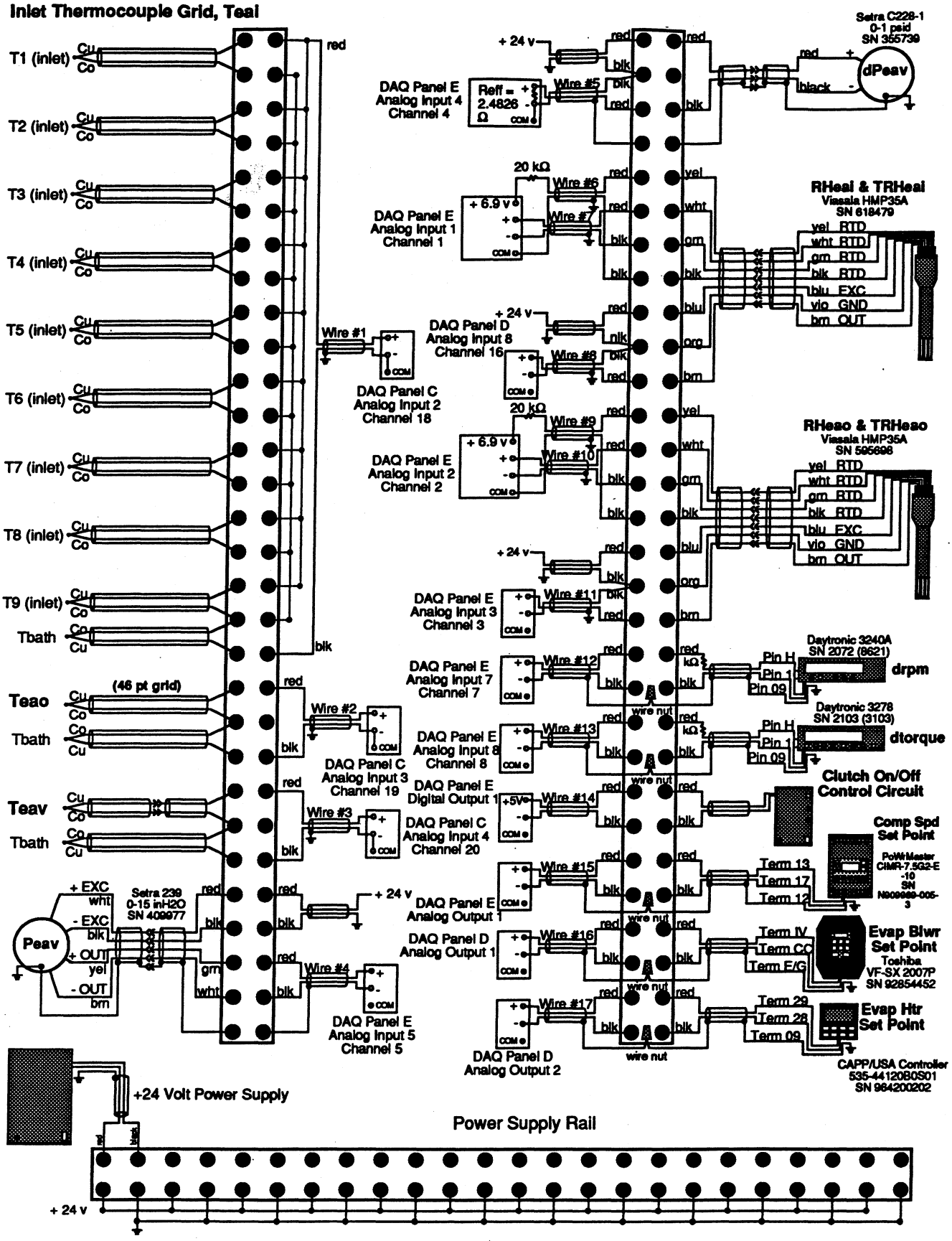

Figure 2.25: Evaporator loop zone box diagram.

thermocouples in the outlet temperature grid are wired in a similar manner as the inlet thermocouple grid shown in Figure 2.25.

2.6 Refrigerant Loop Design and Construction

The refrigerant loop contains all the refrigerant tubing that delivers R-134a refrigerant to the Ford 1994 Crown Victoria air conditioning components. This section discusses issues related to the design and construction of the 1994 Crown Victoria refrigerant loop. For other details regarding the refrigerant loop, the reader should refer to the report by Weston (1995).

2.6.1 General Description

In the refrigerant loop, circular tubing is used to connect the refrigerant sections of the Crown Victoria air conditioning components. The majority of these connections consist of copper tubing and fittings joined with silver brazing compound. Silver brazing is used because of its strength at high temperatures. In addition to the brazed connections, refrigerant hoses and Gyrolok compression fittings are used where necessary.

Because the refrigerant loop was designed (Weston, 1995) to allow for easy modifications, the general procedure for installing a new air conditioning system is to install the air-side ductwork, attach the compressor to the drive motor, and use new or cleaned refrigerant tubing to connect the components together. The refrigerant-side connections made to the Ford 1994 Crown Victoria air conditioning components are discussed in the next section.

2.6.2 Refrigerant Loop Connections

2.6.2.1 Compressor

A manifold, provided to us by Ford Motor Co., is used to attach the inlet and outlet refrigerant tubing to the Ford FS-10 compressor. The manifold provides female spring lock connections that, when mated with their male spring lock

counterparts, can be easily removed and re-attached without damaging the fittings. For this reason, male spring lock mating pieces were purchased from the 1994 Murray Temperature Control catalog. The pieces used are: (a) one 90° male 5/8-in. spring lock to #10 hose coupling (Murray No. 405973) at the inlet, and (b) one 90° male 1/2-in. spring lock to #8 hose coupling (Murray No. 405972) at the outlet. The #8 and #10 hoses were attached to the couplings with a bubble-style crimping tool specifically designed for refrigerant hoses (Murray No. 400300). Figure 2.26 shows the compressor with the fittings described above.

A 21-mm thick by 1235-mm long six groove belt (Gates Micro-V K060480), is used to connect the compressor drive pulley to the compressor. Specially designed brackets are used to attach the compressor to the test stand mounting plate. These brackets, in conjunction with the movable pulley on the compressor drive shaft, allow the compressor to be perfectly aligned to minimize vibration. Although the process of aligning the pulley can be quite tedious, it is necessary because excessive test stand vibration can cause the refrigerant-side compression fittings to loosen and leak.

2.6.2.2 Condenser

The condenser inlet and outlet tubes are attached to the refrigerant loop with Gyrolok 1/2-in. and 3/8-in., 90°-elbow compression unions, respectively. The original connections on the Crown Victoria condenser contained spring lock couplings. These couplings were removed, however, because their orientation did not allow the condenser tubing to be easily attached to the refrigerant loop. The condenser connections are shown in Figure 2.27.

2.6.2.3 Throttling Device

The orifice tube throttling device is contained inside a 1/2-in. nominal diameter aluminum tube. Using a flathead screwdriver, small indentations were made on the outside of the aluminum tube to prevent the orifice tube from sliding inside the

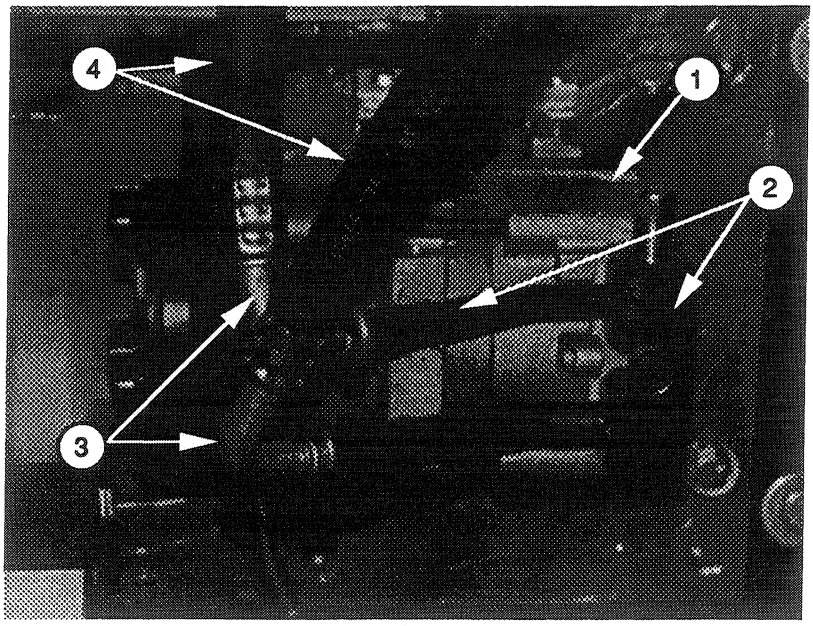

1. Compressor
2. Manifold
3. Spring-Lock Couplings
4. Refrigerant Hoses

Figure 2.26: Compressor refrigerant loop connections.

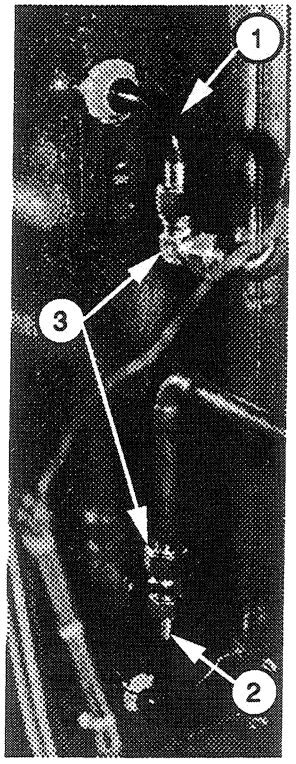

1. Inlet Tube
2. Outlet Tube
3. Compression Fittings

Figure 2.27: Condenser refrigerant loop connections.

refrigerant tubing. Gyrolok 1/2-in. compression fittings are again used to connect the orifice tube to the rest of the refrigerant loop, as shown in Figure 2.28.

2.6.2.4 Evaporator

Though somewhat more complicated to connect than the other components, the evaporator is attached to the refrigerant loop with both compression fittings and hose couplings. At the inlet, a Gyrolok 90°-elbow compression union is used to mate the 1/2-in. copper refrigerant tube to the 1/2-in. circular aluminum tube already attached to the evaporator. Figure 2.29 shows the evaporator inlet refrigerant connection.

In the standard 1994 Crown Victoria system, the accumulator is threaded to a fitting connected to the evaporator outlet tube. This configuration, however, is not possible in our system because the evaporator outlet pressure and temperature need to be measured. To allow space for the pressure and temperature measurement, and to be able to use the threaded connection on the evaporator, a straight male 5/8-in. insert "o" ring to #10 hose fitting (Murray No. 405010) is used at the evaporator outlet. The #10 hose is connected to the copper refrigerant tube with a hose to metal compression splicer (Murray No. 401052), as shown in Figure 2.30.

2.6.2.5 Accumulator

As stated above, the accumulator inlet contains a 5/8-in. male threaded connection. For this reason, a 90° 5/8-in. female O-ring to #10 hose fitting (Murray No. 406903) is used to connect the refrigerant loop to the accumulator inlet. The accumulator outlet is connected to the refrigerant loop with a straight male 3/4-in. spring lock to #12 hose coupling (Murray No. 405074). Figure 2.31 shows the accumulator refrigerant loop connections.

A summary of all the fittings used to connect the refrigerant loop to the Ford 1994 Crown Victoria components is provided in Table 2.4.

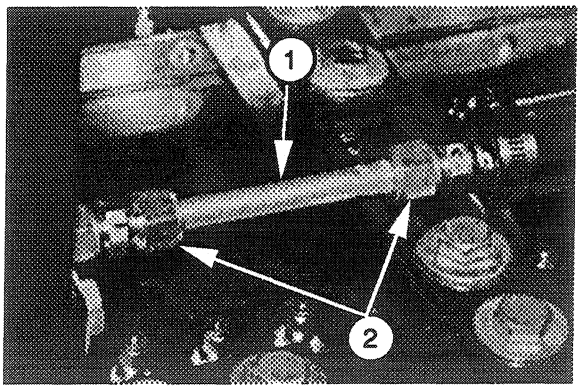

1. Aluminum Tube (orifice tube inside)
2. Compression Fittings

Figure 2.28: Orifice tube refrigerant loop connections.

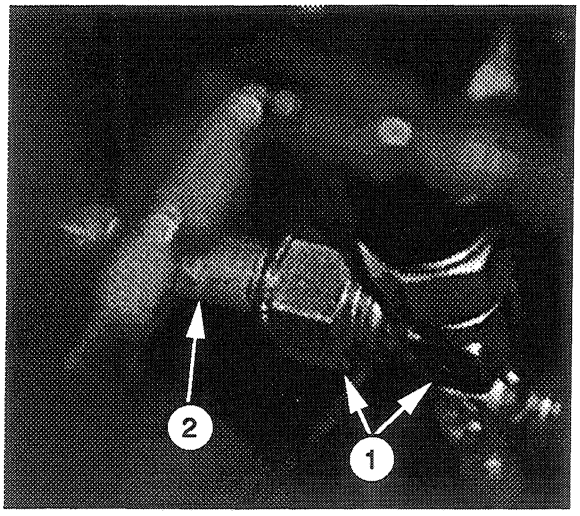

1. 90° Elbow Compression Fitting
2. Aluminum Tube

Figure 2.29: Evaporator inlet refrigerant loop connection.

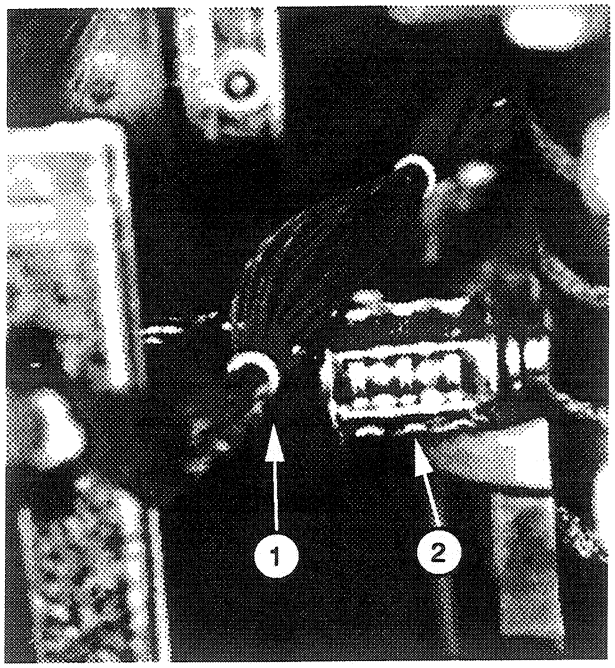

1. #10 Refrigerant Hose
2. Hose to Metal Compression Splicer

Figure 2.30: Evaporator outlet refrigerant loop connection.

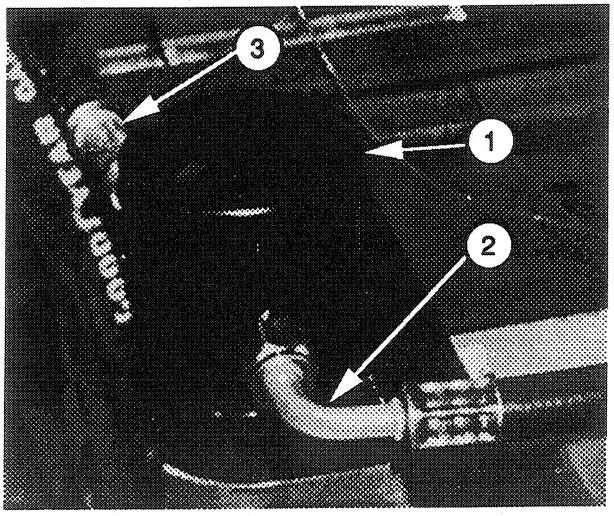

1. Accumulator
2. Inlet Fitting
3. Outlet Fitting

Figure 2.31: Accumulator refrigerant loop connections.

Table 2.4: Fittings Used for Connecting Crown Victoria Components to Refrigerant Loop

Component	Fitting Description	Part No.
Compressor Manifold Inlet	90° male 5/8-in. spring lock to #10 hose	Murray 405973
Compressor Manifold Outlet	90° male 1/2-in. spring lock to #8 hose	Murray 405972
Condenser Inlet	1/2-in. 90° elbow compression union	Hoke Gyrolok 8LU
Condenser Outlet	3/8-in. 90° elbow compression union	Hoke Gyrolok 6LU
Throttling Device (Orifice Tube) Inlet	1/2-in. 90° elbow compression union	Hoke Gyrolok 8LU
Throttling Device (Orifice Tube) Outlet	1/2-in. 90° elbow compression union	Hoke Gyrolok 8LU
Evaporator Inlet	1/2-in. 90° elbow compression union	Hoke Gyrolok 8LU
Evaporator Outlet	straight male 5/8-in. insert O-ring to #10 hose	Murray 405010
Accumulator Inlet	90° 5/8-in. female O-ring to #10 hose	Murray 406903
Accumulator Outlet	straight male 3/4-in. spring lock to #12 hose	Murray 405074

2.6.3 Sight Glasses

To provide further insight into the refrigerant flow characteristics, five 8-in. long circular glass tubes, surrounded by a polycarbonate plastic shield, are placed at critical locations throughout the refrigerant loop. As shown in the system schematic, Figure 2.32, these five "sight glasses" are at the following locations: (a) condenser inlet, (b) between condenser outlet and liquid-line venturi inlet, (c) evaporator inlet, (d) evaporator outlet, and (e) compressor inlet. A typical sight glass is shown in Figure 2.33. The sight glasses are extremely valuable for quickly diagnosing problems such as the following:

- low charge level, characterized by two-phase refrigerant (bubbly flow) at the condenser outlet sight glass,
- inadequate oil circulation, characterized by little or no oil being visible on the inside walls of the vapor line sight glasses,
- lack of subcool exiting the condenser, again characterized by bubbly flow at the condenser outlet sight glass, and
- lack of superheat exiting the evaporator, characterized by misted flow at the evaporator outlet sight glass.

In addition to diagnosing problems, the sight glasses are used during normal test stand operation to determine refrigerant flow regimes. The reader should refer to the report by Weston (1995) for additional details on sight glass design and construction.

2.6.4 Pressure and Temperature Measurements

Since the long-term goal of our project is to develop and test a transient computer model for mobile air conditioning systems, an abundance of instrumentation is located throughout the refrigerant loop. Perhaps the most critical measurements, in conjunction with mass flow rate, are pressure and temperature. These measurements are important because pressure and temperature measurements are used to calculate single phase refrigerant enthalpies. Inaccurate readings can lead to incorrect system calorimetry. Another important issue is that

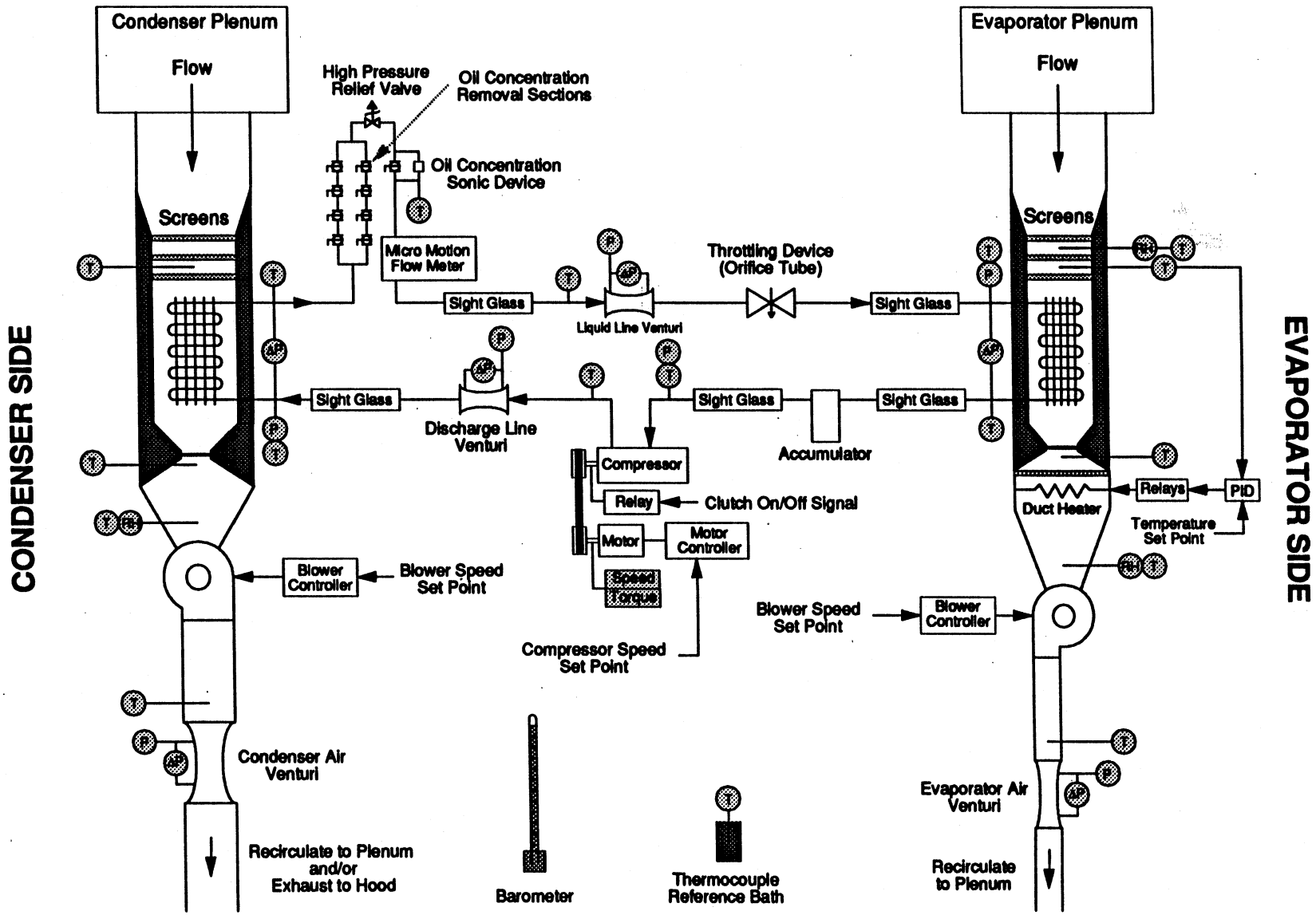

Figure 2.32: Test facility instrumentation schematic. (modified from Weston, 1995)

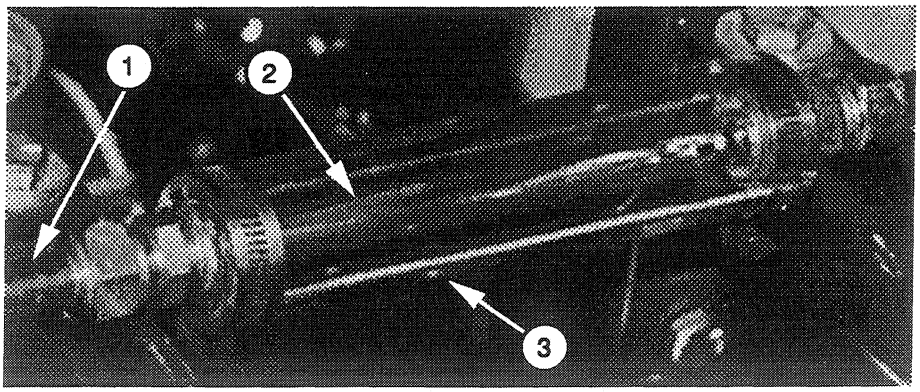

1. Refrigerant Tube
2. Sight Glass
3. Polycarbonate Sight Glass Shield

Figure 2.33: Typical refrigerant loop sight glass.

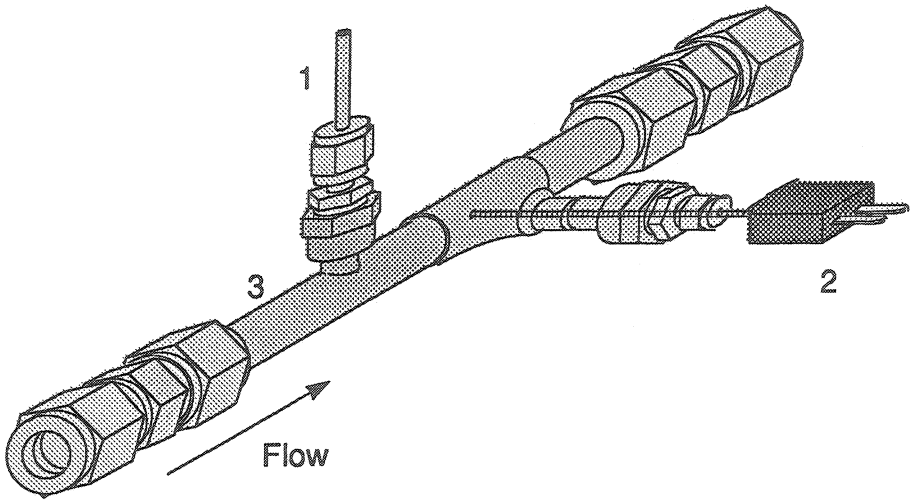

1. Pressure Transducer Connection
2. 3" Type-T Thermocouple Probe
3. Main Refrigerant Channel

Figure 2.34: Typical refrigerant loop pressure and temperature tap.

refrigerant pressures and temperatures must be measured as close to each other as possible. To facilitate this, pressure and temperature taps, similar to the one shown in Figure 2.34, are widely used.

As shown in the system schematic (Figure 2.32), refrigerant pressure and temperature are measured at the entrance and exit of the compressor, the condenser, and the evaporator—the components that account for and create energy transfer in the system. Pressure and temperature are also measured at the entrance of the refrigerant-side venturis. The reader may wish to refer to the system schematic frequently throughout the remainder of this chapter.

All pressure transducers were calibrated using a very accurate dead weight tester. A valve has been placed across the low and high pressure ports of the differential pressure transducers, as shown in Figure 2.35, so that zero offset readings can be obtained when the system is charged with refrigerant. Table 2.5 contains descriptions of the pressure transducers and their calibration results. All pressure transducers, except for the Sensotec transducers discussed earlier, require a 24-VDC power input.

As shown in Figure 2.34, Type-T immersion thermocouple probes are used to measure refrigerant-side temperatures. The 3-in. length probes were purchased from Omega Engineering (Part No. TMQSS-062U-3). For other information concerning thermocouple selection and installation the reader should refer to the report by Weston (1995).

2.6.5 Flow Rate Measurements

Because it is a fundamental parameter required to calculate heat transfer, refrigerant-side mass flow rate measurements must be reliable and accurate. Two methods are used to measure the refrigerant-side mass flow rate. The first method involves using two refrigerant-line venturi flow tubes in conjunction with differential pressure transducers. As shown in Figure 2.32, one venturi is located on the vapor line (after compressor and before condenser) and the other on the liquid line (after condenser and before throttling device). Figure 2.36 shows the vapor-line venturi

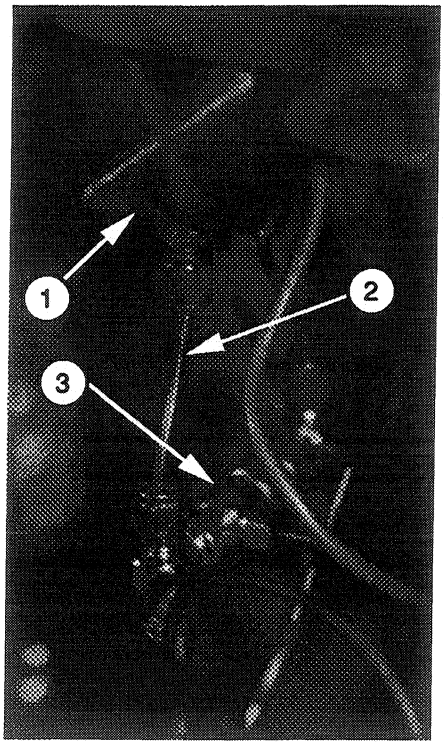

1. Pressure Transducer
2. Copper Tube
3. Cross Valve

Figure 2.35: Differential pressure transducer cross valve assembly.

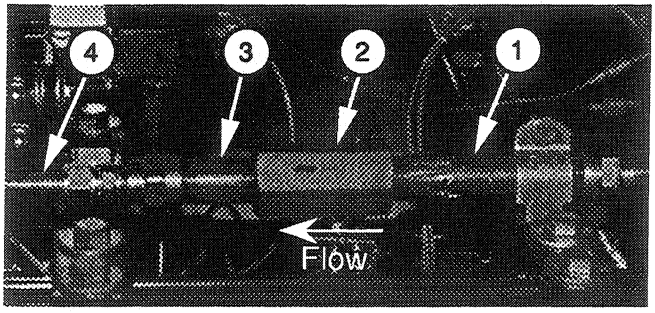

1. Entrance Section
2. Venturi Flow Tube
3. Exit Section
4. Refrigerant Tube

Figure 2.36: Vapor-line venturi flow tube.

Table 2.5: Pressure Tranducer Description and Calibration Results

Description (Variable Name)	Pressure Range	Model	Serial No.	Output Range	Calibration Curve Fit
Evaporator Inlet Refrigerant Rressure (Peri)	0-100 psig	Setra 207	247866	0-5 V	P(psig)=20.038(V)-2.6437
Evaporator Refrigerant Pressure Drop (dPer)	0-25 psid	Setra 228-I	258209	0-5 V	P(psid)=5.1463(V)-0.25249
Compressor Inlet Refrigerant Pressure (Pkri)	0-100 psig	Setra 207	270489	0-5V	P(psig)=20.38(V)-2.0578
Comp Outlet Refrigerant Press (Pkro), Discharge Venturi Inlet Ref Press (Pdv)	0-500 psig	Setra 207	202281	0-5V	P(psig)=121.07(V)-13.389
Discharge Venturi Refrigerant Pressure Differential (dPdv)	0-1 psid	Sensotec Z	411077	Input Dependent	$P(psid)=1.0144(mV_{out}/V_{in})-0.0022797$
Condenser Inlet Refrigerant Pressure (Pcri)	0-500 psig	Setra 207	253458	0-5V	P(psig)=100.63(V)-9.2972
Condenser Refrigerant Pressure Drop (dPcr)	0-25 psid	Setra 228-I	258208	0-5 V	P(psid)=4.9448(V)-2.55
Liquid Venturi Inlet Refrigerant Pressure (Plv)	0-500 psig	Setra 207	253459	0-5V	P(psig)=100.86(V)-7.0731
Liquid Venturi Refrigerant Pressure Differential (dPlv)	0-0.5 psid	Sensotec Z	437090	Input Dependent	$P(psid)=0.50393(mV_{out}/V_{in})-0.001313$
Evaporator Air Flow Venturi Inlet Pressure (Peav)	0-15 inH2O	Setra 239	40997	0-5 V	P(inH2O)=3.0014(V)-0.061338 P(psig)=0.10833(V)-0.0021936
Evaporator Air Flow Venturi Pressure Differential (dPeav)	0-1 psid	Setra C228-I	355739	4-20 mA	P(psid)=0.065652(mA)-0.26203
Condenser Air Flow Venturi Inlet Pressure (Pcav)	0-15 inH2O	Setra 239	398563	0-5 V	P(inH2O)=2.9698(V)-0.95581 P(psig)=0.10719(V)-0.034478
Condenser Air Flow Venturi Pressure Differential (dPcav)	0-30 inH2O	Setra C239	307533	4-20 mA	P(in H2O)=1.8956(mA)-7.6934 P(psid)=0.06841(mA)-0.27766

flow tube installed in the system. A drawing showing the typical venturi pressure transducer connections is provided in Figure 2.37. The second method for measuring refrigerant mass flow rate involves using a Micro Motion coriolis-effect flow meter (Model D25).

To obtain reliable mass flow rate readings from the venturi flow tubes, the refrigerant-side venturis must first be calibrated. Calibration was achieved by comparing the flow rates obtained by the very accurate (approximately ± 0.2%) Micro Motion meter and the two venturi flow tubes. Through a series of tests covering a wide range of mass flow rates, the correct venturi discharge coefficient was determined and henceforth applied to the venturi equation. The results of the refrigerant-side venturi calibrations are presented in Chapter 3.

When measuring the refrigerant mass flow rate with the vapor-line venturi, it is important to observe the flow rate being displayed by the data acquisition system. This is important because the oil flowing with the refrigerant can sometimes cause an incorrect venturi mass flow rate to be reported. What creates this error is the surface tension of the oil causing oil to be pulled into the small 1/8 in. pressure transducer lines. Because the vapor-line venturi pressure transducer has a range of only 0-1 psid, the effect of the oil surface tension is significant and therefore does not allow the correct pressure to be transmitted to the differential pressure transducer. A quick solution to this problem is to periodically open the cross valve attached to the differential pressure transducer for a few minutes. To permanently solve the problem, larger diameter pressure transducer tubing should be installed on the vapor-line venturi.

2.6.6 Oil Concentration Optimization

According to our contacts at Ford Motor Co., the typical amount of oil circulating in the refrigerant loop for the 1994 Crown Victoria system operating under normal conditions is 3% by mass. Because of this recommendation, the 3% oil condition was our target before extensive data would be collected. On our test stand, as shown in Figure 2.32, there are two methods for measuring oil concentration. The

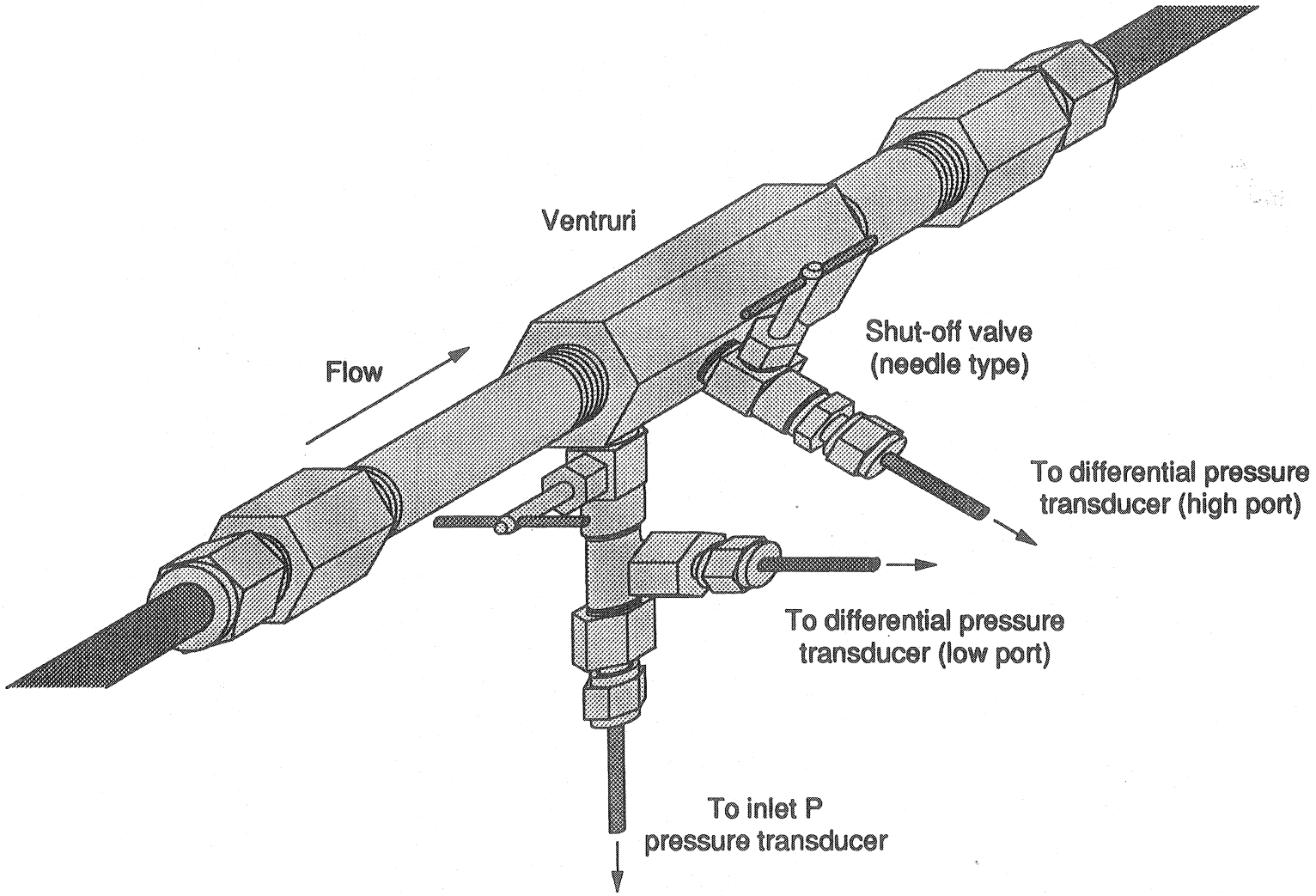

Figure 2.37: Refrigerant-side venturi pressure transducer connections. (Weston, 1995)

first method uses a sonic device, developed by another investigator in our project, to measure real-time oil concentration. Although this method shows great promise, it is still under development and no quantitative data from this device is used in our study.

The second method requires that a small section of refrigerant tubing, containing approximately 3 gm. of refrigerant-oil mixture, be removed. The section is then weighed and allowed to expand through a cascade impactor. A cascade impactor is a device that incrementally separates particles (such as oil droplets) of varying diameters. The separation is achieved as large particles, with relatively higher momentum than the mainstream particles, "impact out" on surfaces inside the cascade impactor. As the refrigerant escapes through the impactor, the oil is deposited on the inside surfaces of the impactor and on small pieces of circular filter paper. The small pieces of paper are then be used to collect the excess oil on the impactor surfaces and weighed. The mass of the oil collected on the tissue paper, divided by the total mass removed from the small refrigerant tube, is the fraction of oil in the circulating refrigerant-oil mixture. Even though this method is highly accurate and repeatable, a small amount of refrigerant is lost each time a sample is removed from the system. After repeated tests, the amount of refrigerant removed can become significant enough to affect the heat transfer characteristics of the air conditioning system.

Due to the abundance of pressure transducer tubing in our test stand, the initial amount of oil circulating was considerably lower (< 1%) than the 3% recommended by Ford. Using the method for determining oil concentration described in the previous paragraph, FS-10 compressor oil was added in 30 ml increments until the amount of oil circulating was approximately 3%. To add the oil, 30 ml was poured into a 8 in. long by 1 in. diameter cylinder that was then charged with refrigerant vapor from the high pressure side of the refrigerant loop (compressor outlet). The pressurized cylinder and oil mixture was then turned upside down and discharged into the low pressure vapor section of the test loop (compressor inlet). As oil was being added to the refrigerant loop, increasingly higher amounts of oil were visible on the inside walls of the sight glasses.

2.6.7 Refrigerant Loop Zone Box

The refrigerant loop zone box is an insulated and isothermal chamber that contains the electrical connections for all refrigerant-side pressure and temperature measurements. As with the two other zone boxes, some of the connections are outputs to the data acquisition system, whereas others are inputs to instrumentation. Table 2.6 summarizes the refrigerant loop zone box connections. Due to the abundance of refrigerant-side instrumentation, the refrigerant loop zone box contains only refrigerant-side connections. Five gage pressure and four differential pressure transducers, as well as eight thermocouples and a thermistor, are connected through this zone box, as shown in Figure 2.38. The thermistor shown in Figure 2.38 is located inside a constant temperature bath that is used as a reference for all the thermocouples in the test stand. Unlike the other zone boxes, the refrigerant loop zone box has access to both 5- and 24-VDC power supplies.

Table 2.6: Refrigerant Loop Zone Box Summary

Measurement (Name, Instrument)	Model No.	Serial No.	Input Signal	Output Signal
Evaporator Ref. T In (Teri, Thermocouple Probe)	Type-T	N/A	N/A	Data Aq.: Thermocouple μV
Evaporator Ref. T Out (Tero, Thermocouple Probe)	Type-T	N/A	N/A	Data Aq.: Thermocouple μV
Condenser Ref. T In (Tcri, Thermocouple Probe)	Type-T	N/A	N/A	Data Aq.: Thermocouple μV
Condenser Ref. T Out (Tcro, Thermocouple Probe)	Type-T	N/A	N/A	Data Aq.: Thermocouple μV
Compressor T In (Tkri, Thermocouple Probe)	Type-T	N/A	N/A	Data Aq.: Thermocouple μV
Compressor T Out (Tkro, Thermocouple Probe)	Type-T	N/A	N/A	Data Aq.: Thermocouple μV
Liquid Venturi T In (Tlv, Thermocouple Probe)	Type-T	N/A	N/A	Data Aq.: Thermocouple μV
Oil Section T (Toil, Thermocouple Probe)	Type-T	N/A	N/A	Data Aq.: Thermocouple μV
Evaporator Ref. P In (Peri, Pressure Trans.)	Setra 207	247866	Power Supply Rail: 24 V	Data Aq: 0-5 V
Condenser Ref. P In (Pcri, Pressure Trans.)	Setra 207	253458	Power Supply Rail: 24 V	Data Aq: 0-5 V
Compressor Ref. P In (Pkri, Pressure Trans.)	Setra 207	270489	Power Supply Rail: 24 V	Data Aq: 0-5 V
Compressor Ref. P Out (Pkro, Pressure Trans.)	Setra 207	202281	Power Supply Rail: 24 V	Data Aq: 0-5 V
Liquid Venturi P (Plv, Pressure Trans.)	Setra 207	253459	Power Supply Rail: 24 V	Data Aq: 0-5 V
Evaporator Ref. ΔP (dPer, Pressure Trans.)	Setra 228-1	258209	Power Supply Rail: 24 V	Data Aq: 0-5 V
Condenser Ref. ΔP (dPcr, Pressure Trans.)	Setra 228-1	258208	Power Supply Rail: 24 V	Data Aq: 0-5 V
Discharge Venturi ΔP (dPdv, Pressure Trans.)	Sensotec Z	411077	Power Supply Rail: 5 V	Data Aq: Input Dependent
Liquid Venturi ΔP (dPlv, Pressure Trans.)	Sensotec Z	437090	Power Supply Rail: 5 V	Data Aq: Input Dependent
Reference Bath T (Tbath, Thermistor)	Omega ON-970	44032	Power Supply Rail: 5 V	Data Aq: Input Dependent

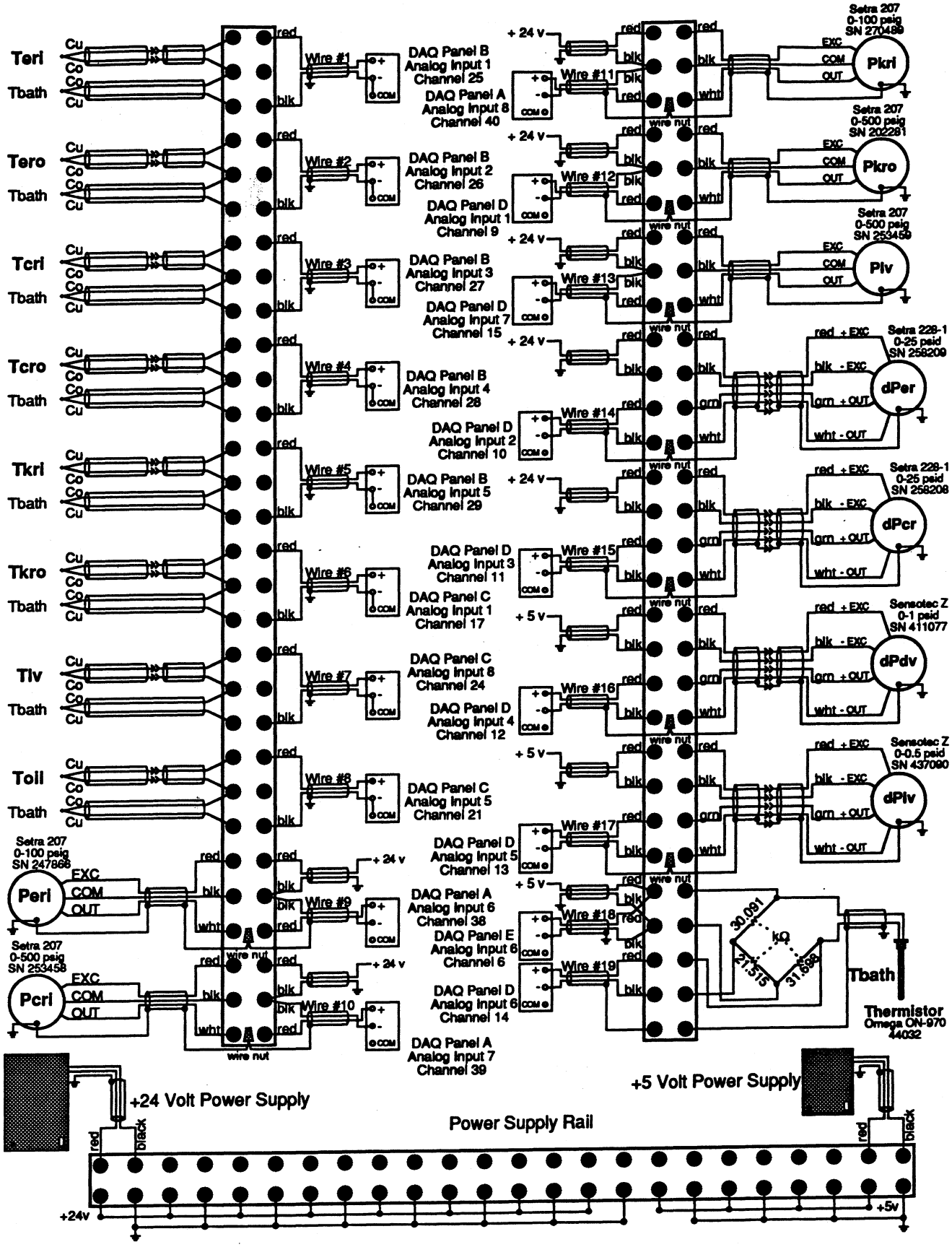

Figure 2.38: Refrigerant loop zone box diagram.

3. EXPERIMENTAL RESULTS AND ANALYSIS

3.1 Introduction

Two major efforts are discussed in this chapter. The first effort, presented in Section 3.2, involves the calibration and validation of the test stand. Test stand validation is critical to ensure the data collected during transient testing is correct. The second effort is presented in Section 3.3 and contains preliminary transient results intended to show the capabilities of the current control system used in the test stand. These results are "preliminary" because the current control system is not intended for complicated transient control. At the time of writing, a more advanced transient control system is being installed in the test stand. Forthcoming reports will contain more complicated transient patterns and, consequently, more detailed analyses.

3.2 Steady-state Results and Analysis

Although the overall goal of our project is to develop and validate a transient computer model for mobile air conditioners, the test facility must first be validated to ensure the accuracy of the data collected. To this end, a goal of achieving the best possible system calorimetry was set and a series of steady-state tests were conducted to analyze the system calorimetry. The steady-state tests were also used to calibrate the two refrigerant-side venturi flow tubes which measure refrigerant mass flow rate. Accurate results are critical because during transient operation the refrigerant charge migrates between the evaporator and the condenser, therefore creating different mass flow rates in the refrigerant-side venturis. This section discusses the results of the steady-state tests.

3.2.1 Energy Balance Program Description and Calculations

The energy balance program, again used to analyze the steady-state system calorimetry, serves one major purpose: to calculate and compare the evaporator and condenser air-side and refrigerant-side heat transfer rates. In the process of determining the heat transfer rates, the program calculates other valuable variables

such as air-side and refrigerant-side mass flow rate. The energy balance equations were solved using the Engineering Equation Solver (EES) because it contains built-in property routines for refrigerants (R-134a in this case) and most common substances.

All instrumentation variables are recorded with the Strawberry Tree data acquisition system in their raw form (volts, milli-amps, μ-volts, etc.). Their values are then imported into the EES energy balance program, which after a series of calculations using instrumentation calibration curves and equations, determines their physical values (temperature, pressure, enthalpy, heat transfer rate). The remainder of this section is devoted to discussing the energy balance program calculations. For completeness, the entire energy balance program is provided in Appendix A.

3.2.1.1 Temperature

The energy balance program requires two steps to calculate a thermocouple temperature. The first step determines the equivalent Type-T thermocouple voltage of the thermistor located inside the water-filled constant temperature bath using the following equations:

$$T_{bath(°F)} = 164.96\left(\frac{V_{tmstr}}{V_{5V}}\right) + 60.96, \tag{3.1}$$

$$T_{bath(°C)} = \frac{5}{9}\left(T_{bath(°F)} - 32\right), \tag{3.2}$$

$$\begin{aligned} V_{Tbath} = {} & C_0 + C_1 T_{bath(°C)} + C_2 T_{bath(°C)}^{2} + C_3 T_{bath(°C)}^{3} \\ & + C_4 T_{bath(°C)}^{4} + C_5 T_{bath(°C)}^{5} + C_6 T_{bath(°C)}^{6} \\ & + C_7 T_{bath(°C)}^{7} + C_8 T_{bath(°C)}^{8} + C_9 T_{bath(°C)}^{9} \\ & + C_{10} T_{bath(°C)}^{10} + C_{11} T_{bath(°C)}^{11} + C_{12} T_{bath(°C)}^{12} \\ & + C_{13} T_{bath(°C)}^{13} + C_{14} T_{bath(°C)}^{14} \end{aligned}, \tag{3.3}$$

where T_{bath} is the bath temperature, V_{tmstr} is the recorded thermistor voltage in VDC, V_{5V} is the voltage applied to the thermistor using the 5 VDC power supply in VDC, and V_{Tbath} is the equivalent thermocouple voltage in mVDC determined from the IPS-

90 Tables in the CRC Handbook of Chemistry and Physics (Lide & Frederikse, 1994). The coefficients for Equation 3.3 are provided in Appendix A. This previous step is required because all single thermocouples and thermocouple grids are referenced to the constant temperature bath. The second step is to add the equivalent thermocouple voltage determined above to the relative Type-T thermocouple voltage recorded by the data acquisition system and calculate the temperature using the following equation:

$$T_{(°C)} = c_0 + c_1 V + c_2 V^2 + c_3 V^3 + c_4 V^4 + c_5 V^5 + c_6 V^6 + c_7 V^7, \tag{3.4}$$

where T is the temperature at the particular thermocouple probe and V is the thermocouple voltage in mVDC. The coefficients for Equation 3.4 are again provided in Appendix A. All thermocouple voltages in the test stand are calculated using the method described above.

3.2.1.2 Pressure

To calculate pressure, the energy balance program transforms the gage pressure and differential pressure transducer outputs, either in VDC or mA, to pressure using the calibration equations discussed in Chapter 2. All of the transducers, except for the Sensotec Model Z differential pressure transducers, have an offset output. The offset output is the transducer output generated when no pressure is applied to the transducer. A typical equation used to calculate pressure is:

$$P = m(V_{out} - V_{offset}) + P_{atm}, \tag{3.5}$$

where P is the absolute or differential pressure in psi, m is the calibration equation slope in psi/VDC, V_{out} is the output voltage recorded by the data acquisition system in VDC, V_{offset} is the offset voltage in VDC, and P_{atm} is the pressure in the laboratory room.

3.2.1.3 Enthalpy

Because it defines the amount of energy in a specific substance, the enthalpy is a very important calculation in the energy balance program. Enthalpy, as with other properties, is calculated automatically in EES. For the refrigerant-side enthalpy function in EES, only the pressure and temperature of the substance (R-134a) are needed, as shown below.

$$h_{R134a} = \text{Enthalpy}(\text{R134a},\ T = T_1,\ P = P_1), \tag{3.6}$$

where T is the temperature in °F and P is the pressure in psia. To account for moisture in the air, the air-side enthalpy is calculated by adding the air enthalpy and the steam enthalpy. EES contains property routines for automatically calculating the enthalpy of air and water mixtures, but these routines are not as accurate as the method described above. For this reason, the air-side enthalpy is determined using the following set of equations:

$$\omega = \text{HumRat}(\text{Air}H_2O,\ T = TRH,\ P = P,\ R = RH/100), \tag{3.7}$$

$$\begin{aligned} h = {} & \text{Enthalpy}(\text{Air},\ T = T) \\ & + \omega[\text{Enthalpy}(\text{Steam},\ T = T,\ x = 1)] \end{aligned} \tag{3.8}$$

HumRat and Enthalpy are both internal EES functions. The arguments to the humidity ratio function (Equation 3.7) are temperature at the relative humidity sensor TRH in °F, pressure P in psia, and relative humidity R. The humidity ratio ω is used to calculate the enthalpy of the air-water mixture using Equation 3.8., where h is the total enthalpy and x is the steam quality.

3.2.1.4 Mass Flow Rate

There are five different mass flow rates calculated in the energy balance program. Three of these are in the refrigerant loop: discharge-line venturi, liquid-

line venturi, and Micro Motion coriolis-effect meter; whereas the other two are in the air loops: condenser venturi and evaporator venturi. The Micro Motion refrigerant-side mass flow rate is determined using the following calibration equation supplied by the manufacturer:

$$\dot{m}_{micro} = 25.0(A_{micro} - 4.00), \tag{3.9}$$

where $\dot{m}_{micro}$ is the refrigerant mass flow rate in lb_m/hr and A_{micro} is the signal recorded by the data acquisition system in mA.

As one might assume, the process for determining the mass flow rate for the four venturis is quite different than that for the Micro Motion. However, because all venturi mass flow rates are calculated in a similar fashion, the following discussion is general in nature and applies to all four venturis.

The theoretical equation for calculating venturi mass flow rate is derived by combining the conservation of mass and conservation of momentum equations. The equation used to calculate the actual mass flow rate is shown below as Equation 3.10. Except for the two factors C and F_a, the actual mass flow rate equation is identical to the theoretical mass flow rate equation.

$$\dot{m} = (CA_2F_a)\sqrt{\frac{2\rho_1(P_1 - P_2)}{\frac{\rho_1}{\rho_2} - \beta^4}} \tag{3.10}$$

The variable C in Equation 3.10 is the venturi discharge coefficient—a unitless coefficient that represents the ratio of actual to theoretical rate of flow. For classical venturis, the discharge coefficient is usually about 0.98-0.99. However, since our venturis are not classical venturis, the discharge coefficient must be determined by calibration. The calibration results will be discussed later in this chapter. For completeness, the size of the four venturis and the calibrated discharge coefficients, are shown in Table 3.1.

The variable F_a in the mass flow rate equation is a unitless factor that accounts for the thermal expansion of the venturi material. It is defined as:

$$F_a = \left[1+\alpha(T-68)^2\right], \tag{3.11}$$

where α is the thermal expansion factor of the venturi material (1.0×10^{-5} 1/°F for the brass refrigerant-side venturis and 6.7×10^{-6} 1/°F for the steel air-side venturis) and T is the venturi temperature in °F.

In Equation 3.10, ρ_1 and P_1 are the flowing substance density and pressure at the venturi entrance, ρ_2 and P_2 are the density and pressure at the throat, β is the throat to entrance inside diameter ratio, and A_2 is the throat area.

Table 3.1: Venturi Size and Discharge Coefficient

Venturi	Throat Diameter, d (in.)	Diameter Ratio (Throat/Entrance), β	Discharge Coefficient, C
Refrigerant-side Discharge Line	0.3750	0.4091	0.910
Refrigerant-side Liquid Line	0.1890	0.2625	0.954
Air-side Condenser	4.4913	0.7336	0.825
Air-side Evaporator	1.8767	0.6084	0.940

3.2.1.5 Energy Balance

To calculate energy balances, the EES program first determines the heat transfer rates for the condenser and evaporator air-side and refrigerant-side loops. These are calculated using the following equations:

$$\dot{q}_{ref} = \dot{m}_{ref}\left(h_{ref,out} - h_{ref,in}\right) \tag{3.12}$$

$$\dot{q}_{air} = \dot{m}_{air}\left(h_{air,out} - h_{air,in}\right) \tag{3.13}$$

Two energy balances, evaporator and condenser, are calculated in the EES energy balance program. Both calculations use the following equation:

$$E_{bal} = \left(\frac{\dot{q}_{ref} - \dot{q}_{air}}{\dot{q}_{ref}} \right) \times 100\% \qquad (3.14)$$

As can be seen by examining Equation 3.14, a positive energy balance indicates a higher refrigerant-side than air-side heat transfer rate and a negative energy balance indicates the opposite.

Several variables are more critical than others when calculating the final energy balance. Because several of these variables can have a greater effect on the energy balance calculation, the test stand operator must ensure that the instrumentation that generates these variables is working properly. The three most critical variables used in the energy balance calculations are: humidity, temperature, and flow rate.

3.2.2 Steady-state Test Plan

To ensure that correct data could be obtained from the test stand, a test plan encompassing a wide range of operating conditions was developed. The test plan contains a list of tests that covers the entire operating range of each controllable steady-state parameter on the test stand. The steady-state test plan is shown in Table 3.2. The actual tests were conducted in a random order, not in the order shown in Table 3.2.

The compressor motor drive speed, condenser blower drive speed, and evaporator blower drive speed are designated in Table 3.2 in terms of the variable-frequency drive Hz, with the approximate compressor speed in revolutions per minute (RPM) and blower flow rate in cubic feet per minute (CFM) shown in parentheses. A setting of 20 Hz corresponds to 1/3 (20Hz/60Hz) of the maximum operating range of the drive. Because of the relatively small amount of air flow rate required in the evaporator air loop, the evaporator variable-frequency drive can be run at speeds higher than 60 Hz. For the opposite reason, the maximum setting for the compressor variable-frequency drive is 56.5 Hz.

The settings in Table 3.2 were selected from initial tests that determined the maximum and minimum compressor RPM and blower flow rates. Several of the

Table 3.2: Steady State Test Plan

Test No.	Compressor Speed Hz (RPM)	Cond Air Blower Spd Hz (CFM)	Cond Air In Temp °F	Evap Air Blower Spd Hz (CFM)	Evap Air In Temp °F
1	20 (1100)	25 (750)	Ambient	30 (130)	90
2	20 (1100)	25 (750)	Ambient	42.5 (200)	75
3	20 (1100)	25 (750)	Ambient	42.5 (200)	90
4	20 (1100)	25 (750)	Ambient	42.5 (200)	110
5	20 (1100)	25 (750)	Ambient	42.5 (200)	125
6	20 (1100)	25 (750)	Ambient	60 (280)	110
7	20 (1100)	25 (750)	Ambient	77.5 (360)	75
8	20 (1100)	25 (750)	Ambient	77.5 (360)	110
9	20 (1100)	40.8 (1200)	Ambient	30 (130)	90
10	20 (1100)	40.8 (1200)	Ambient	42.5 (200)	90
11	20 (1100)	40.8 (1200)	Ambient	60 (280)	110
12	20 (1100)	40.8 (1200)	Ambient	77.5 (360)	75
13	20 (1100)	40.8 (1200)	Ambient	77.5 (360)	110
14	20 (1100)	56.6 (1650)	Ambient	30 (130)	90
15	20 (1100)	56.6 (1650)	Ambient	42.5 (200)	90
16	20 (1100)	56.6 (1650)	Ambient	60 (280)	110
17	20 (1100)	56.6 (1650)	Ambient	77.5 (360)	75
18	20 (1100)	56.6 (1650)	Ambient	77.5 (360)	110
19	40 (2300)	25 (750)	Ambient	30 (130)	90
20	40 (2300)	25 (750)	Ambient	42.5 (200)	90
21	40 (2300)	25 (750)	Ambient	60 (280)	110
22	40 (2300)	25 (750)	Ambient	77.5 (360)	75
23	40 (2300)	25 (750)	Ambient	77.5 (360)	110
24	40 (2300)	40.8 (1200)	Ambient	30 (130)	90
25	40 (2300)	40.8 (1200)	Ambient	42.5 (200)	90
26	40 (2300)	40.8 (1200)	Ambient	60 (280)	75
27	40 (2300)	40.8 (1200)	Ambient	60 (280)	90
28	40 (2300)	40.8 (1200)	Ambient	60 (280)	110
29	40 (2300)	40.8 (1200)	Ambient	60 (280)	125
30	40 (2300)	40.8 (1200)	Ambient	77.5 (360)	75
31	40 (2300)	40.8 (1200)	Ambient	77.5 (360)	110
32	40 (2300)	56.6 (1650)	Ambient	30 (130)	90

Table 3.2 cont.: Steady State Test Plan

Test No.	Compressor Speed Hz (RPM)	Cond Air Blower Spd Hz (CFM)	Cond Air In Temp °F	Evap Air Blower Spd Hz (CFM)	Evap Air In Temp °F
33	40 (2300)	56.6 (1650)	Ambient	42.5 (200)	90
34	40 (2300)	56.6 (1650)	Ambient	60 (280)	110
35	40 (2300)	56.6 (1650)	Ambient	77.5 (360)	75
36	40 (2300)	56.6 (1650)	Ambient	77.5 (360)	110
37	60 (3500)	25 (750)	Ambient	30 (130)	90
38	60 (3500)	25 (750)	Ambient	42.5 (200)	90
39	60 (3500)	25 (750)	Ambient	60 (280)	110
40	60 (3500)	25 (750)	Ambient	77.5 (360)	75
41	60 (3500)	25 (750)	Ambient	77.5 (360)	110
42	60 (3500)	40.8 (1200)	Ambient	30 (130)	90
43	60 (3500)	40.8 (1200)	Ambient	42.5 (200)	90
44	60 (3500)	40.8 (1200)	Ambient	60 (280)	110
45	60 (3500)	40.8 (1200)	Ambient	77.5 (360)	75
46	60 (3500)	40.8 (1200)	Ambient	77.5 (360)	110
47	60 (3500)	56.6 (1650)	Ambient	30 (130)	90
48	60 (3500)	56.6 (1650)	Ambient	30 (130)	110
49	60 (3500)	56.6 (1650)	Ambient	30 (130)	125
50	60 (3500)	56.6 (1650)	Ambient	42.5 (200)	90
51	60 (3500)	56.6 (1650)	Ambient	60 (280)	110
52	60 (3500)	56.6 (1650)	Ambient	77.5 (360)	75
53	60 (3500)	56.6 (1650)	Ambient	77.5 (360)	110

tests in the steady-state test plan could either not be conducted or had to be altered because of the following reasons: (a) insufficient air flow to the evaporator air loop duct heater, resulting in overheating and consequent tripping of the heater circuit, and (b) lack of superheated refrigerant at the evaporator outlet, a requirement for calculating the evaporator refrigerant-side heat transfer. For verification purposes, a number of tests were repeated. The results discussed in the following section contain data from 68 steady-state tests—50 from the original test plan and 18 repeated.

3.2.3 Calorimetry Results

Using the data from the test plan described in the previous section, condenser and evaporator energy balances were calculated using the energy balance equations and EES. These results are presented in the two following sections.

3.2.3.1 Condenser

The condenser calorimetry results are shown in Figure 3.1. This figure contains a plot of the air-side versus refrigerant-side heat transfer for the condenser. The majority of the points are contained within lines that represent a ± 5% calorimetry. It should be noted that ± 5% is considered quite good because of the wide range of operating conditions tested. All of the test points lie within ± 10%. The average error for the condenser heat transfer is -0.2%—meaning that, for the tests conducted, the air-side shows slightly more heat transfer than the refrigerant-side. The standard deviation of the error (σ) in the energy balance is 4.9% and the average absolute error is 4.0%. These last two values can be interpreted as meaning that approximately 68% of the test points lie within ± 4.9% of the theoretical heat transfer line and that the average test point is 4.0% from the theoretical line. Because of the large number of tests conducted, the root-mean-square (RMS) error is identical to the standard deviation.

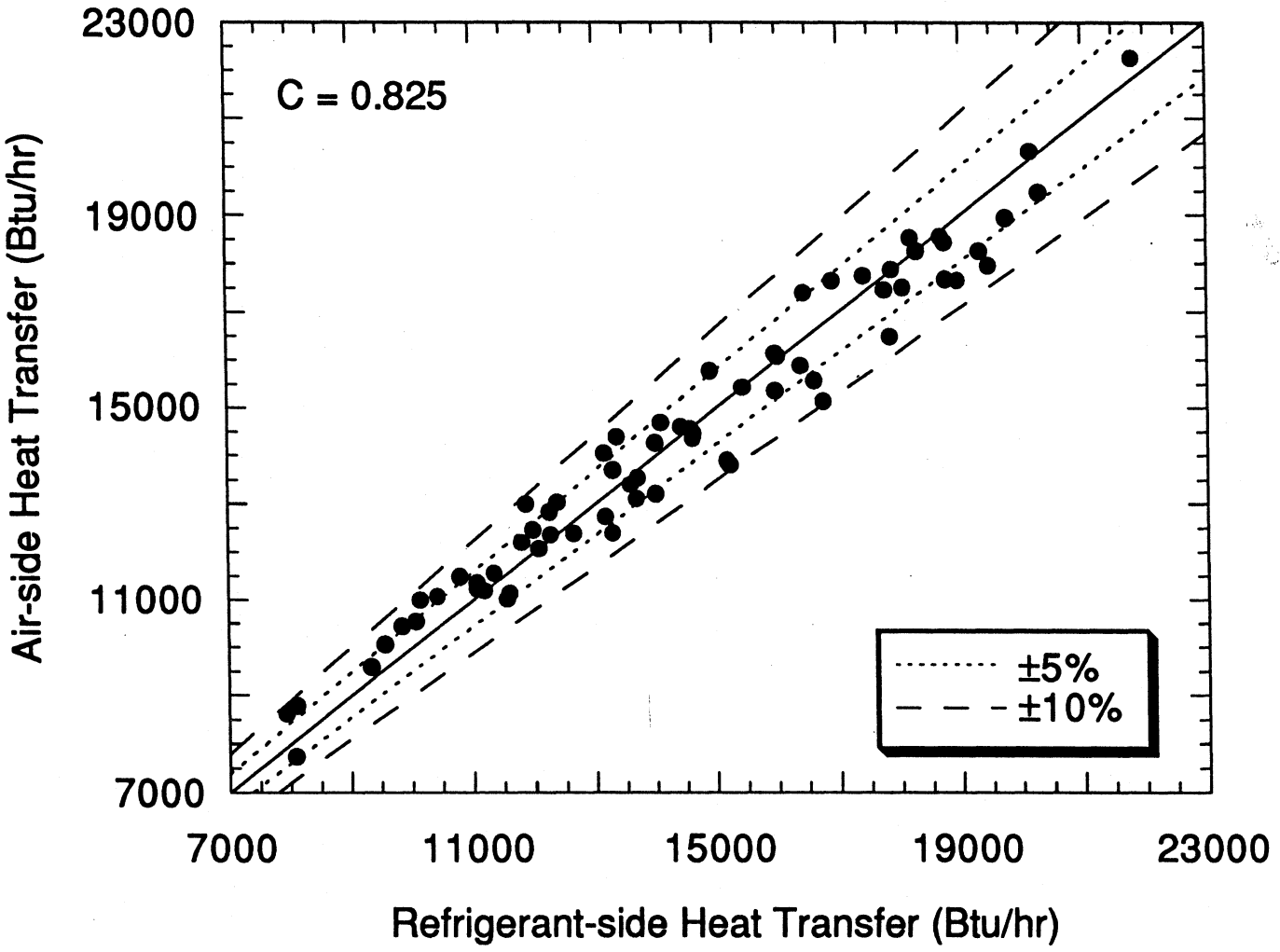

Figure 3.1: Condenser air-side versus refrigerant-side calorimetry.

3.2.3.2 Evaporator

The evaporator calorimetry results are slightly better than the condenser, as shown in Figure 3.2. Again, considering the wide range of operating conditions tested, the results are quite good, as the majority of the test points lie within ± 5% of the theoretical straight line and all of them lie within ± 10%. The average evaporator heat transfer error is -0.2%, once again showing a slightly higher air-side than refrigerant-side heat transfer. Approximately 68% of the test points lie within the standard deviation (σ) of ± 4.0% of the theoretical heat transfer line. The average absolute error of the evaporator heat transfer is 3.2%. Because of the large number of test conducted, the root-mean-square (RMS) error is again identical to the standard deviation.

The slightly better evaporator than condenser heat transfer results are likely due to several reasons. The first reason is that the condenser air-side flow rate has a range of approximately 900 CFM, while the evaporator air-side flow rate has a range of only 230 CFM. The condenser air-side venturi therefore measures flow rates over a larger range than the more limited and therefore better "matched" evaporator air-side venturi. For this reason, the standard deviation of the error is higher in the condenser calorimetry than in the evaporator calorimetry. The second reason for the evaporator calorimetry results being slightly better than the condenser is that the evaporator air-loop is a closed system. Because it is a closed system, the evaporator blower does not have to work against the sometimes fluctuating pressures being transmitted to the condenser blower through the exhaust hood.

3.2.4 Venturi Calibration Results

As stated above, the four venturis in the test stand were calibrated using the data collected from the steady-state test plan. The venturi calibration results are discussed in the following sections.

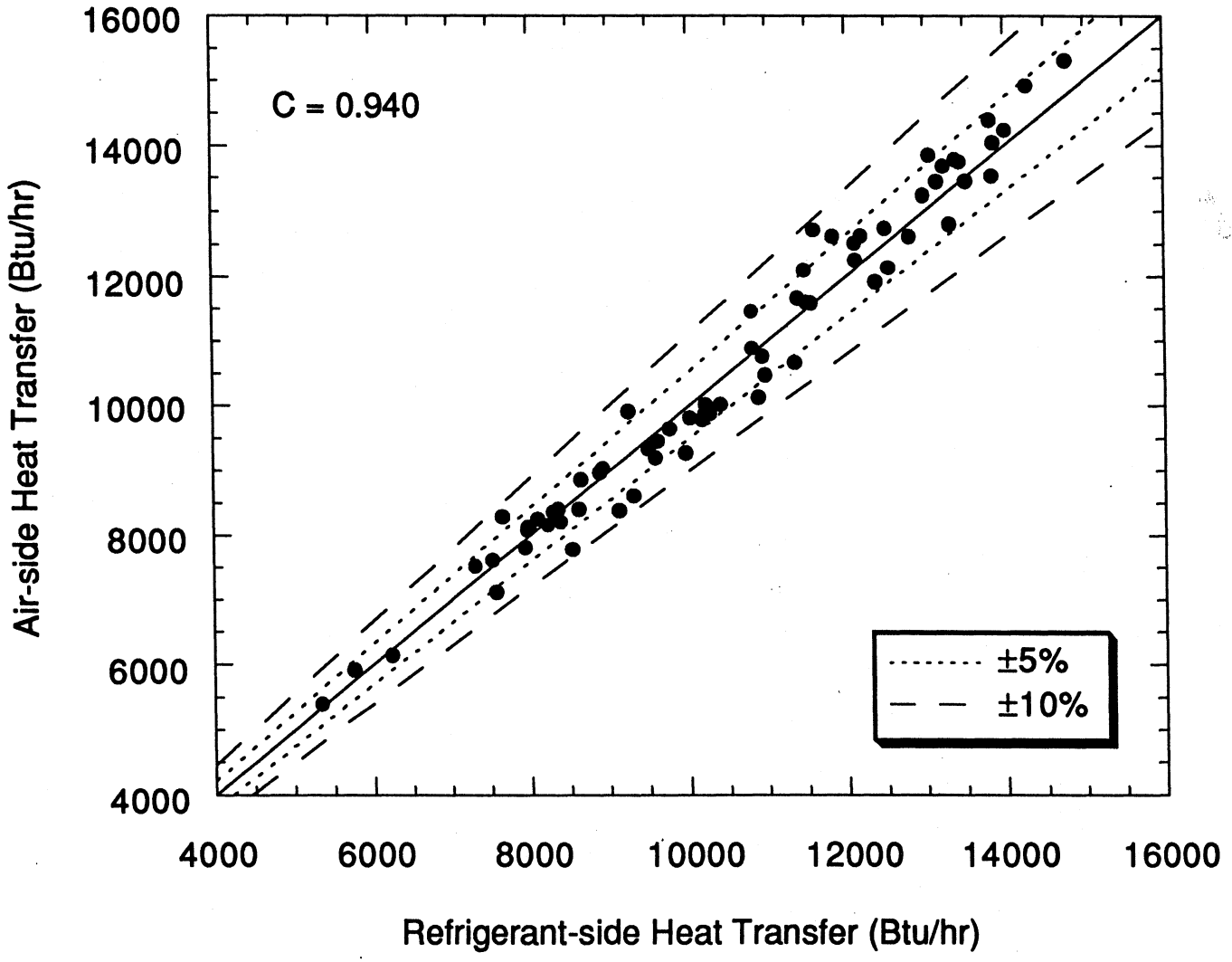

Figure 3.2: Evaporator air-side versus refrigerant-side calorimetry.

3.2.4.1 Air-side

The air-side venturi calibration results were used to generate the energy balance plots shown in Figures 3.1 and 3.2. The condenser and evaporator air-side venturi discharge coefficients were found to be 0.825 and 0.940, respectively. These values are quite different than those shown in the report by Weston (1995) because the they were obtained from an in-situ calibration using air as the substance flowing through the venturis. The results reported by Weston were obtained from calibrations using water as the substance flowing through the air-side venturis. Since water is essentially incompressible, it cannot be used to simulate the actual phenomenon taking place in the test stand air loops. For this reason, the discharge coefficient values stated in this report should be used in place of those reported by Weston.

3.2.4.2 Refrigerant-side Discharge Line

As stated in Chapter 2, the refrigerant-side discharge-line venturi is located on the high pressure/high temperature refrigerant line between the compressor and the condenser. This venturi was calibrated by comparing the mass flow rate results with the very accurate Micro Motion coriolis-effect meter using the data collected from the test plan. The calibration results are shown in Figure 3.3. The discharge coefficient C for the refrigerant-side discharge-line venturi was found to be 0.910. Even though a wide range of operating conditions were tested, a large majority of the test points line within ± 5% of the theoretical line. The average discharge-line venturi error is -0.1%—meaning that, for the data points collected, the discharge-line venturi shows slightly more mass flow rate than the Micro Motion. The standard deviation of the error (σ) for the venturi versus Micro Motion mass flow rate is 3.7% and the average absolute error is 2.9%. These results are considered quite good, as approximately 68% of the test plan points lie within ± 3.7% of the theoretical mass flow rate line and the average test point is only 2.9% from the theoretical line. As with the energy balance results, the large number of tests conducted makes the RMS error identical to the standard deviation.

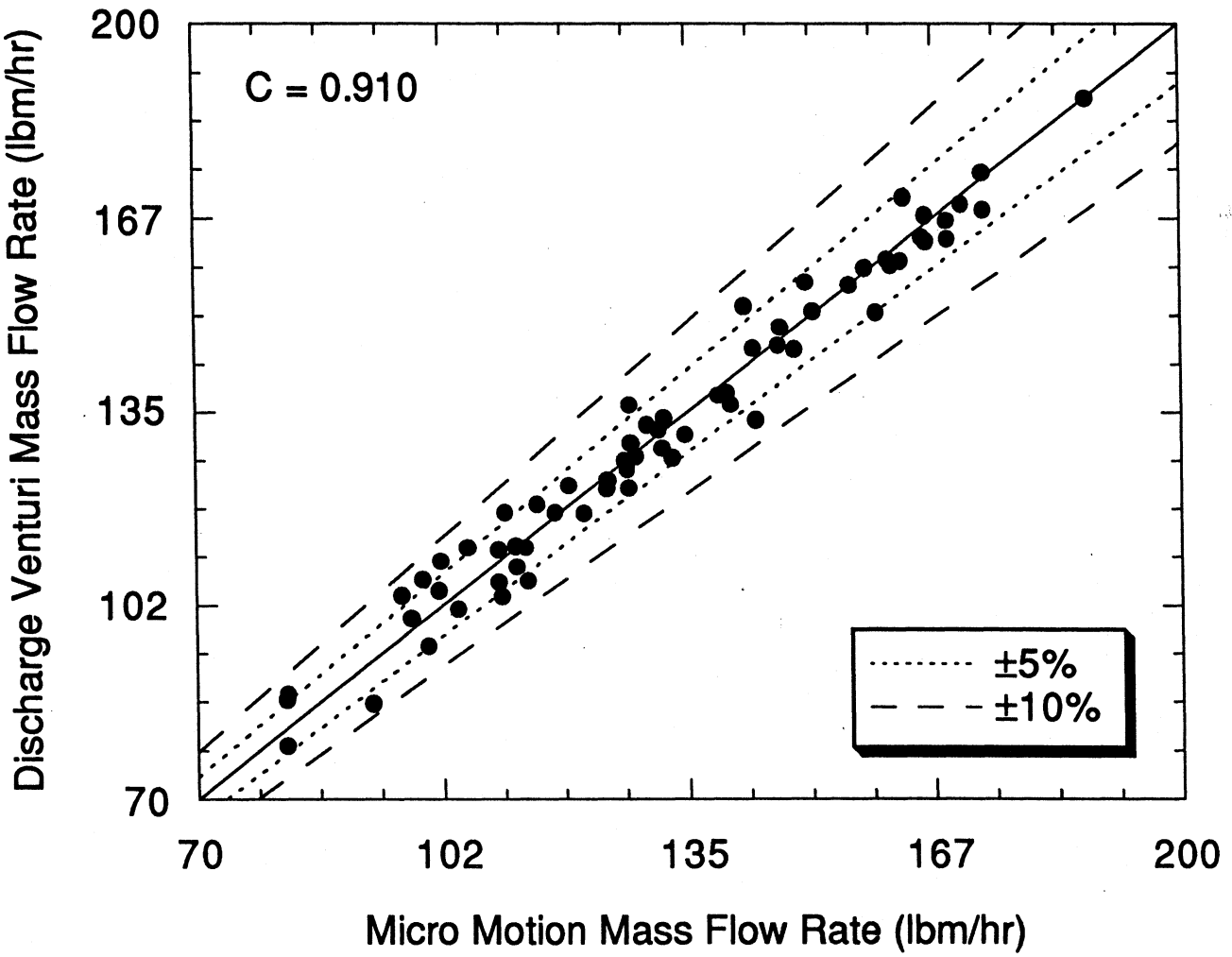

Figure 3.3: Discharge-line venturi versus Micro Motion mass flow rate.

3.2.4.3 Refrigerant-side Liquid Line

The refrigerant-side liquid-line venturi, located between the condenser and the orifice tube throttling device, was calibrated by comparing the mass flow rates of the venturi with the mass flow rates of the Micro Motion coriolis-effect meter. As shown in Figure 3.4, the calibration results yielded a venturi discharge coefficient of 0.954. All but one of the test points lie within ± 5% of the theoretical mass flow rate line. The average error for the liquid venturi mass flow rate is -0.1%. Because of the large number of data points collected, one can say that approximately 68% of the test points line within one standard deviation, or 1.9%, of the theoretical line. The average absolute error of the venturi mass flow rate is 1.4%. Again, the RMS is error is identical to the standard deviation.

The reader should not be surprised by the fact that the best results were obtained from the liquid-line venturi. A couple of phenomenon may contribute to this result. The first phenomenon, though probably the least important, is that the liquid-line venturi and the Micro Motion are both located between the condenser and throttling device and both mass flow rate devices have liquid refrigerant running through them. The likely reason for the liquid-line venturi results being better than the discharge-line venturi results is that the refrigerant-oil mixture flowing around the loop is in a single phase at the liquid-line venturi, whereas it is a liquid-vapor mixture of refrigerant and oil at the discharge-line venturi.

Because good results were obtained from the calibration of the venturis, they can comfortably be used to collect transient data. By having two calibrated refrigerant-line venturis, the refrigerant charge migration that occurs during transient operation can be studied and documented. The results of the four calibrated venturis in the test stand are summarized in Table 3.3.

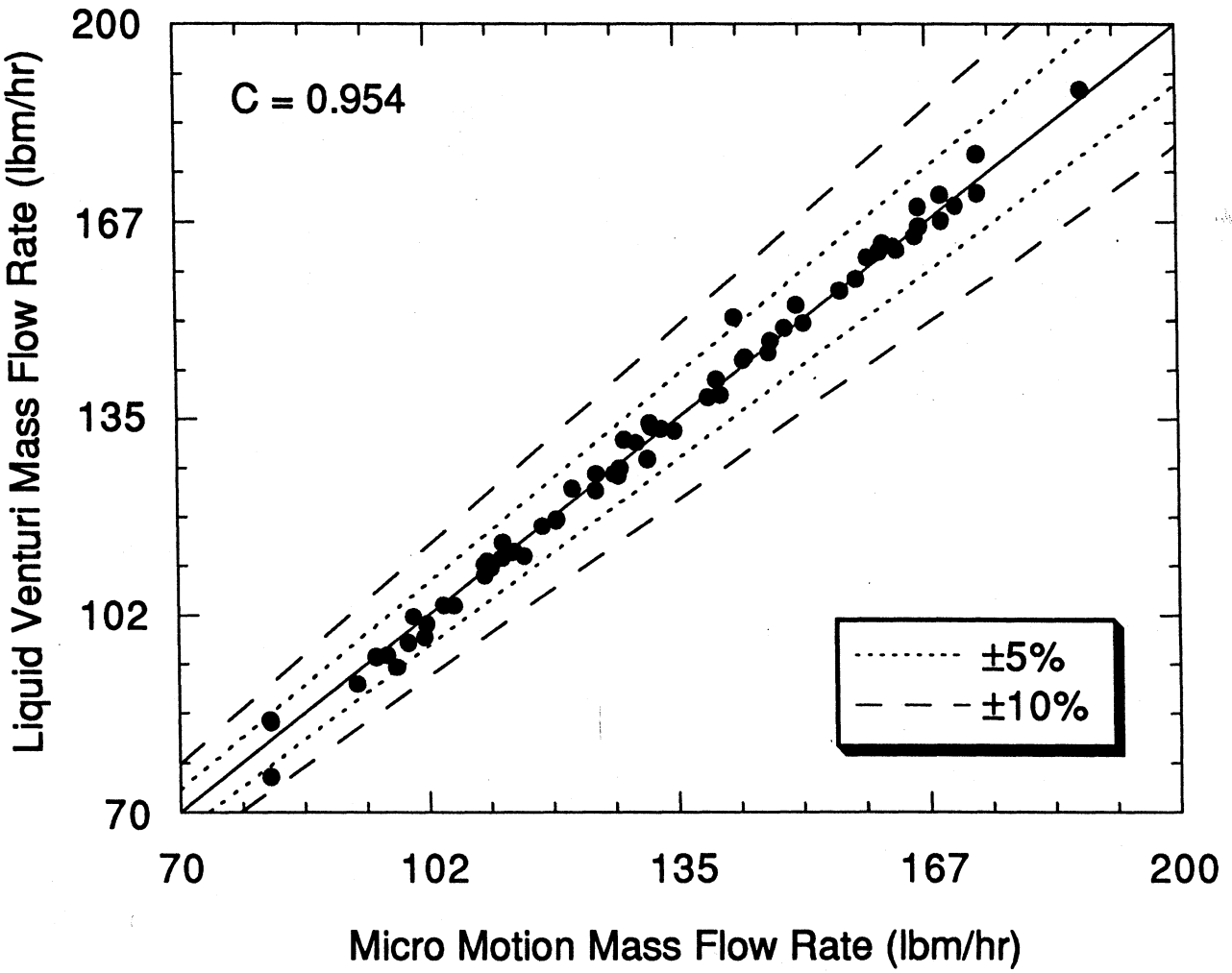

Figure 3.4: Liquid-line venturi versus Micro Motion mass flow rate.

Table 3.3: Venturi Calibration Results Summary

Venturi	Avg. Error, %	Std. Dev. of Error, σ, %	Avg. Absolute Error, %	Discharge Coefficient, C
Air-side Condenser	-0.2	4.9	4.0	0.825
Air-side Evaporator	-0.2	4.0	3.2	0.940
Refrigerant-side Discharge Line	-0.1	3.7	2.9	0.910
Refrigerant-side Liquid Line	-0.1	1.9	1.4	0.954

3.3 Transient Results and Analysis

The transient results presented in this section are intended to show the flexibility of the mobile air conditioning test stand. Transient data was collected as the Ford 1994 Crown Victoria air conditioning system responded to naturally-induced transients such as cabin pulldown and pressure-cycled compressor clutch, and pre-programmed transients such as time-cycled compressor clutch and simulated driving conditions. This section discusses the results of these transient tests. Because evaporator analysis can be considerably more meaningful than condenser analysis, the majority of the results presented in this section are concerned with evaporator refrigerant-side and air-side temperatures. Future reports from this project will contain additional results.

3.3.1 Cabin Pulldown

"Cabin pulldown" refers to the lowering of the temperature (and consequently humidity) inside a vehicle by an air conditioning system from a high, uncomfortable temperature to a low, more comfortable temperature. In our test stand, the cabin temperature is simulated by recording the air-side temperature entering the evaporator. After the air exits the evaporator, as shown in Figure 2.32, it passes through a duct heater, a blower, and the evaporator plenum before entering the

evaporator again. The duct heater is used to simulate the thermal load on a vehicle and the plenum is used to simulate the vehicle cabin. Three types of pulldown tests were conducted to reduce the evaporator air-side inlet temperature (vehicle cabin temperature) from 110 °F to 60 °F. The pulldown types tested were: (1) a free response test where the duct heater is turned off, (2) a linear pulldown test where the heater controller is programmed to reduce the cabin temperature linearly over several time periods, and (3) an exponential pulldown test where the heater controller is programmed to reduce the cabin temperature exponentially in 14 min.. Figure 3.5 shows the evaporator air-side inlet temperature for the three types of pulldown tests.

As stated in the previous paragraph, the evaporator air-side inlet temperature is set to 110 °F before the compressor clutch is engaged. The conditions for the test stand components, shown in Table 3.4, were constant for the three types of pulldown tests. These conditions were selected because they are representative of the conditions a mobile air conditioning system may encounter during pulldown.

Table 3.4: Pulldown Test Conditions

Compressor Speed (RPM)	Cond. Air Flow (CFM)	Cond. Air In Temp (°F)	Evap. Air Flow (CFM)	Evap. Air In Temp (°F)
1150	800	Ambient	280	110 initial

To conduct the linear pulldown tests, the evaporator duct heater was programmed to reduce the evaporator air-side inlet temperature linearly from 110 to 60 °F at several different rates. Figure 3.6 shows the actual and theoretical evaporator air-side inlet temperature for linear rates of 6, 14, and 22 min.. Due to the large time constant associated with the duct heater being far upstream of the evaporator air-side inlet, the temperature followed the unheated temperature profile for the first minute of the tests before the heater "recovered" and was able to control the temperature linearly. The effects of the large time constant, however, lasted through as many as 6 min. for the 22 min. pulldown case. The large time constant of the heater control circuit is also responsible for the slight one to two minute offset in

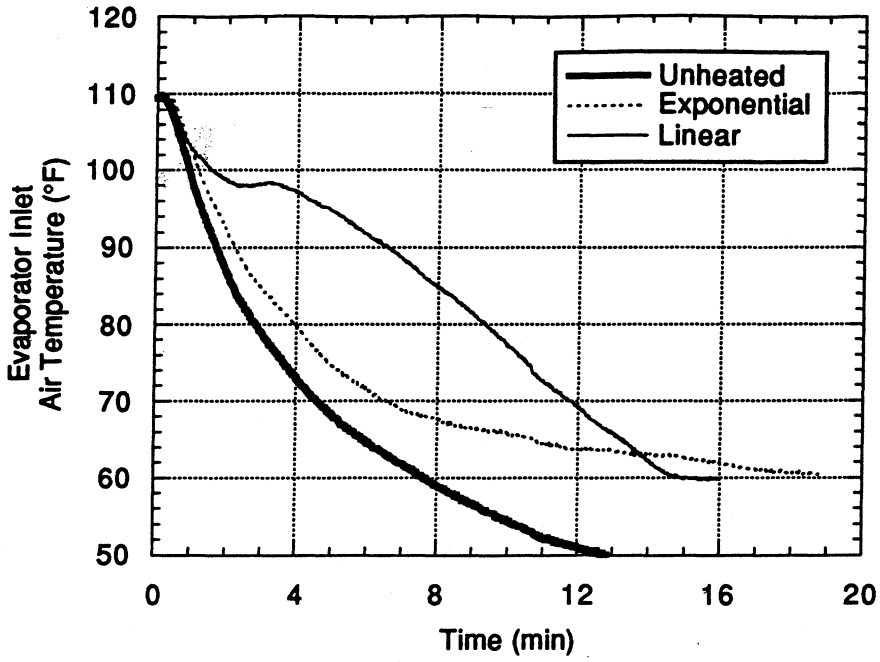

Figure 3.5: Pulldown transients tested.

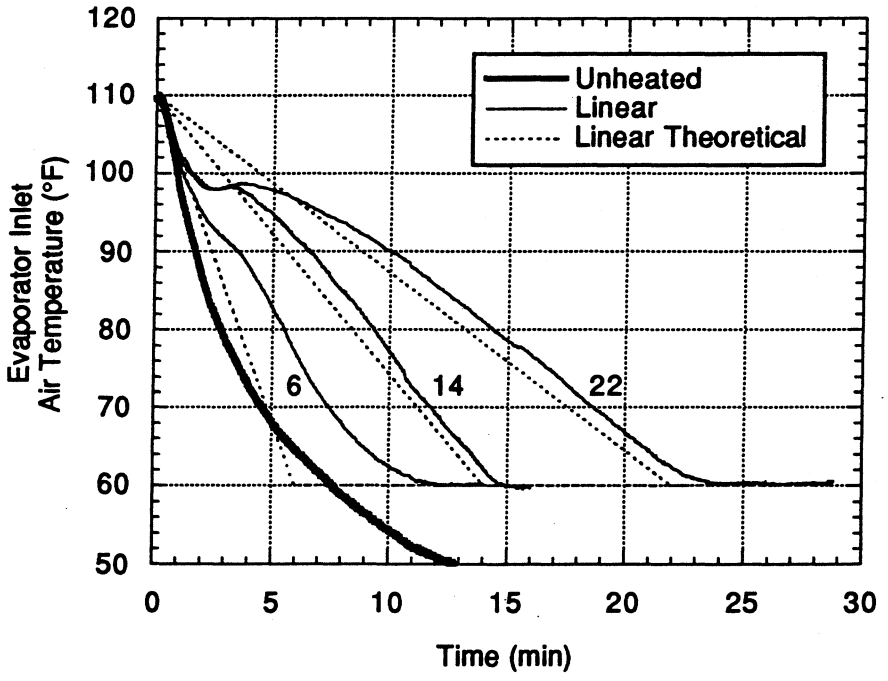

Figure 3.6: Linear 6, 14, and 22 min. pulldown transients.

the time required to reach 60 °F for the 14 and 22 min. cases. The large discrepancy between the actual and theoretical inlet temperatures for the 6 min. linear pulldown can be attributed to the fact that the air conditioning system cannot reduce the evaporator inlet temperature any faster than it can when the duct heater is turned off. The inlet temperature for the unheated pulldown can be interpreted as being the fastest possible pulldown for the Ford 1994 Crown Victoria air conditioning system under the conditions in Table 3.4. Additionally, the unheated case can be used to determine the maximum slope of the pulldown line at any given evaporator air-side inlet temperature.

The evaporator air-side inlet and outlet temperatures for the 14 min. linear pulldown case are shown in Figure 3.7. Because the evaporator air-side outlet temperature depends on the inlet temperature, it is not surprising the outlet temperature follows a similar profile as the inlet. The effects of the large time constant associated with the heater are especially noticeable in this figure since the inlet temperature does not begin to drop until approximately one minute after the compressor clutch is engaged. This result can be interpreted as meaning that one minute elapses before the effects generated by the system being turned on reach the evaporator air-side inlet.

As shown in Figure 3.8, the evaporator air-side outlet temperature for the exponential pulldown case again follows a similar pattern as the inlet temperature. A delay of approximately one minute in the evaporator air-side inlet temperature was also experienced due to the large time constant of the duct heater. However, because this pulldown is exponential, the inlet temperature follows a similar pattern as the theoretical inlet temperature.

3.3.2 Pressure-cycled Compressor Clutch

A common method used to control air conditioning systems, especially when a system uses an orifice tube as a throttling device, involves engaging and disengaging the compressor clutch. This method is used to prevent the condensate on the evaporator surface from freezing. For this reason, several tests were

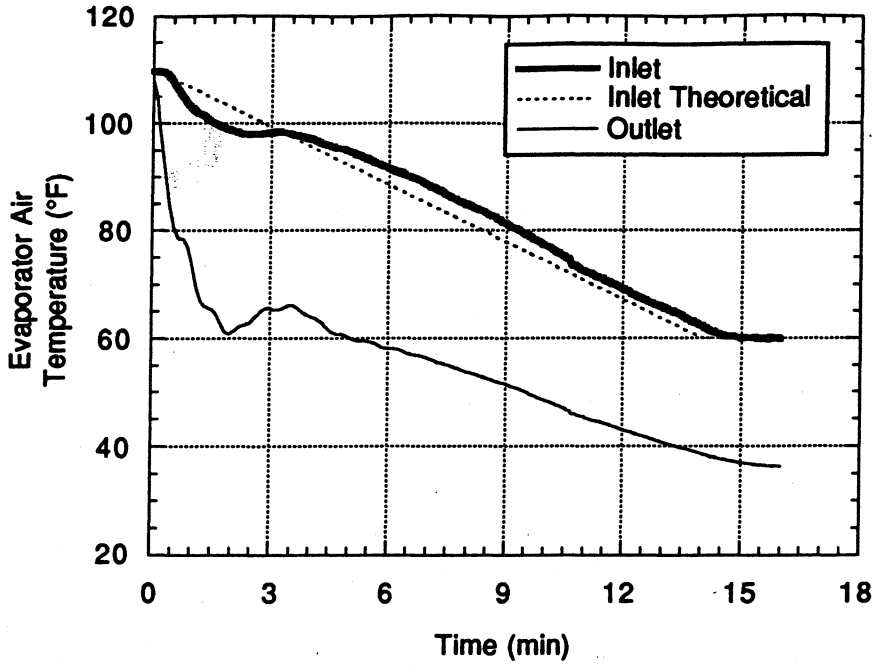

Figure 3.7: Evaporator air-side temperatures for 14 min. linear pulldown.

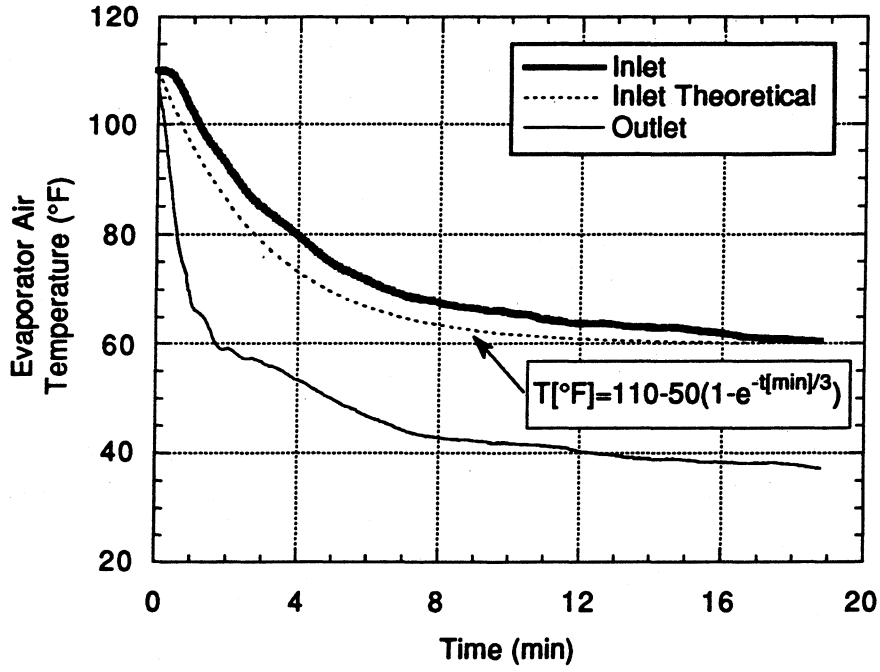

Figure 3.8: Evaporator air-side temperatures for 14 min. exponential pulldown.

conducted in which the compressor clutch was cycled as the evaporator refrigerant outlet pressure traveled between two sets of upper and lower limits. The first set of limits, clutch engaged at 45 psig and disengaged at 24 psig (45/24), were suggested by our sponsors at Ford Motor Company. A second set of limits, clutch engaged at 50 psig and disengaged at 20 psig (50/20), was selected to explore the effects that a wider range of operating pressures would have on the system.

For all the pressure-cycled tests, the evaporator air loop duct heater was programmed to maintain an evaporator air-side inlet temperature of 90 °F. The conditions for the test stand components, shown in Table 3.5, were constant for all the pressure-cycled clutch tests. These conditions were also used for the time-cycled clutch tests that will be discussed in Section 3.3.3.

Table 3.5: Pressure-cycled and Time-cycled Clutch Test Conditions

Compressor Speed (RPM)	Cond. Air Flow (CFM)	Cond. Air In Temp (°F)	Evap. Air Flow (CFM)	Evap. Air In Temp (°F)
1150	800	Ambient	215	90

For all the pressure-cycled tests, data were collected from the time the system was turned on until the system reached a steady-state. To demonstrate the pulldown that occurs after the system is started, the evaporator air-side outlet temperature is shown in Figure 3.9 for the test with a 45/24 pressure-cycled clutch. The spikes in Figure 3.9 represent the times when the clutch was engaged and disengaged. As can be seen in this figure, the evaporator outlet temperature reaches a quasi steady-state value. For the remainder of the figures, the data plotted are for shorter periods of time while the system was operating under quasi steady-state conditions. Three engaged compressor clutch cycles are shown in all the figures. The reader should keep in mind that the time span shown in the upcoming figures is 70 s for the 45/24 pressure-cycled clutch case and 150 s for the 50/20 pressure-cycled clutch case so that three complete on cycles could be shown on each graph. The time span for the 50/20 pressure cycled clutch case is larger

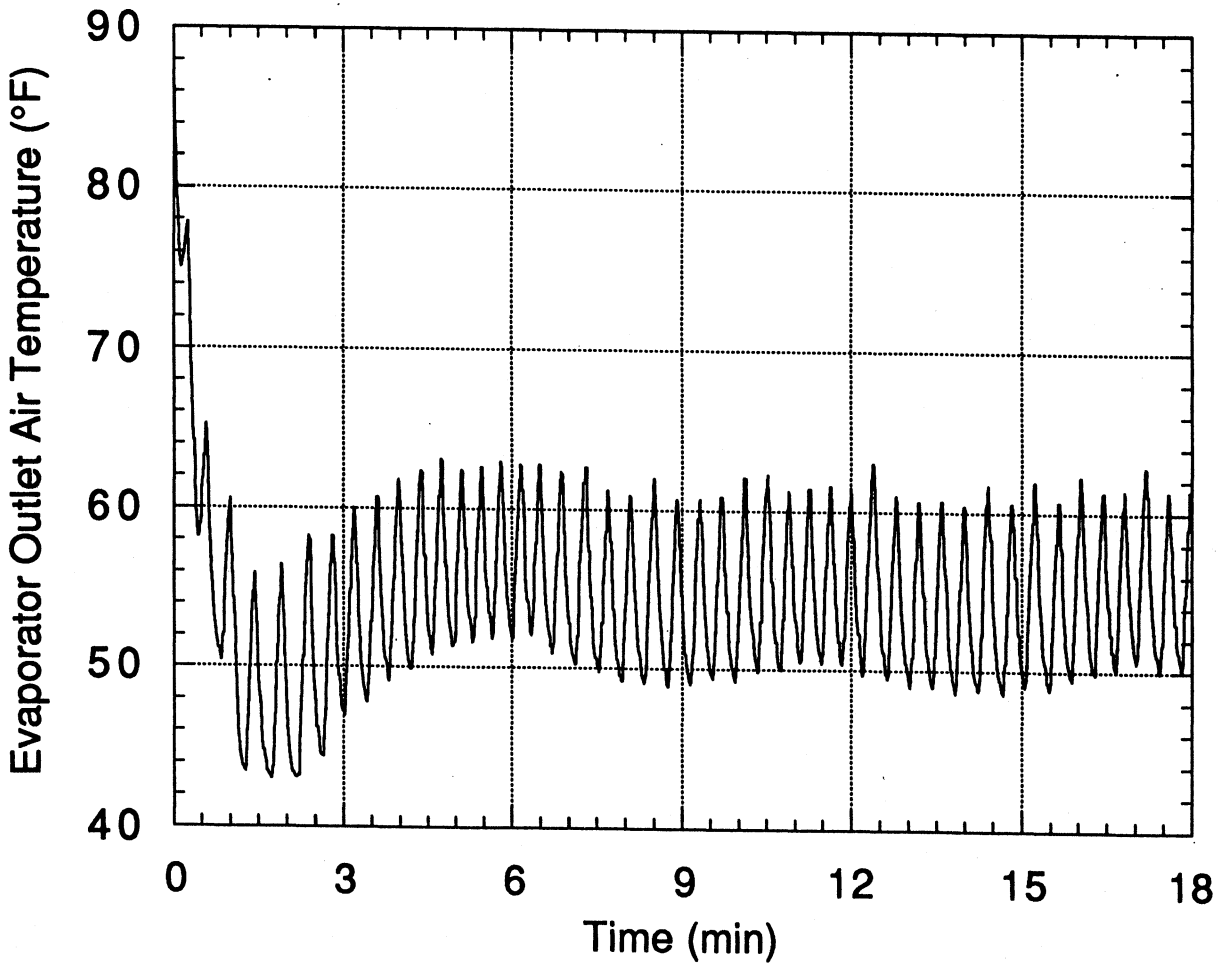

Figure 3.9: Evaporator air-side outlet temperature pulldown for 45/24 pressure-cycled clutch.

because of the greater difference in refrigerant outlet pressure that the system must go through before the clutch can be engaged and disengaged.

Figures 3.10 and 3.11 show the evaporator refrigerant inlet temperature and outlet pressure along with the compressor torque. Obviously, the compressor torque and outlet pressure were chosen to show when the clutch is engaged and disengaged. The slight deviations from the theoretical cycling pressures evident in Figures 3.10 and 3.11 are due to the zero offset of the pressure transducers used to measure the evaporator refrigerant-side outlet pressure. As might be expected, the temperature and pressure in the evaporator decrease when the clutch is engaged and increase when the clutch is disengaged. The maximum compressor torque occurs at the moment the clutch is engaged and is 92 in.-lb for the 45/24 case and 95 in.-lb for the 50/20 case. The torque is higher for the 50/20 case because the off cycle last longer and the compressor has to pump additional refrigerant that has been emptied into the evaporator from the high pressure side of the air conditioning system. Additionally, the high initial torque in the compressor can be caused by small amounts of liquid refrigerant passing through the compressor during start-up. As the on cycle proceeds, the compressor torque decreases because of the lower amount of refrigerant it has to pump through the refrigerant loop. As the clutch is disengaged, the compressor torque is reduced to approximately zero.

The refrigerant inlet temperature is shown in Figures 3.10 and 3.11 along with the outlet pressure because the compressor clutch is often cycled to prevent the freezing of condensate on the evaporator surface. The average refrigerant-side inlet temperature is 35 °F for both pressure-cycled cases—clearly high enough to prevent the freezing of condensate. Because the time required to complete a on/off cycle is longer for the 50/20 pressure-cycled case, the refrigerant inlet temperature (and therefore inlet/outlet pressure) has a larger temperature range (30 °F versus 20 °F) than the 45/24 pressure-cycled case.

As can be seen in Figures 3.10 and 3.11, the refrigerant inlet temperature and outlet pressure follow a similar pattern. This is not surprising because (1) the refrigerant entering the evaporator is saturated and the saturation temperature of R-134a in °F is almost the same as the saturation pressure in psig, and (2) the

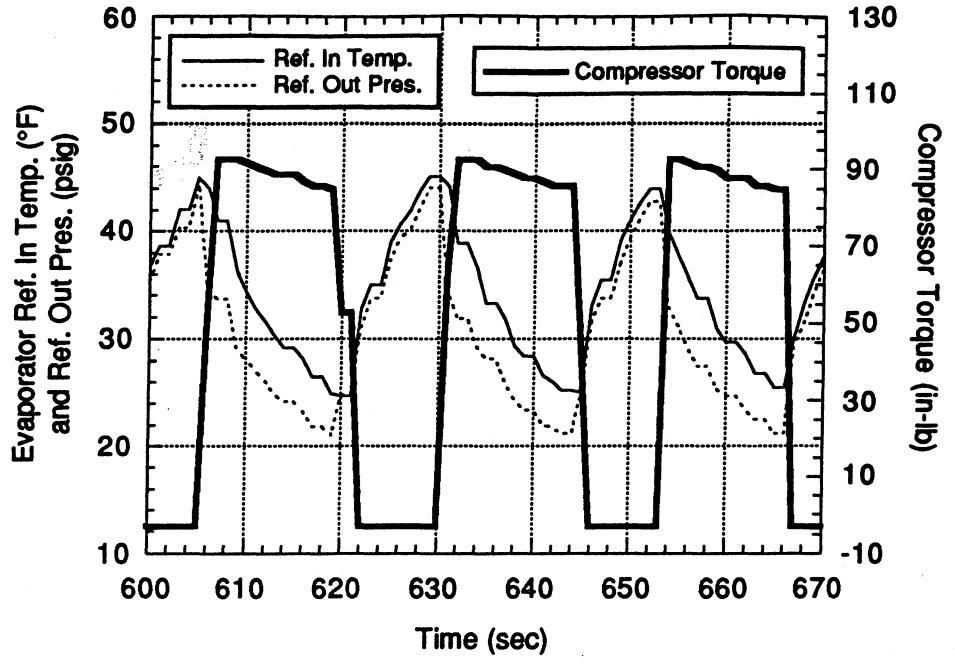

Figure 3.10: Evaporator refrigerant-side pressure and temperature for pressure-cycled clutch (on at 45 psig, off at 24 psig).

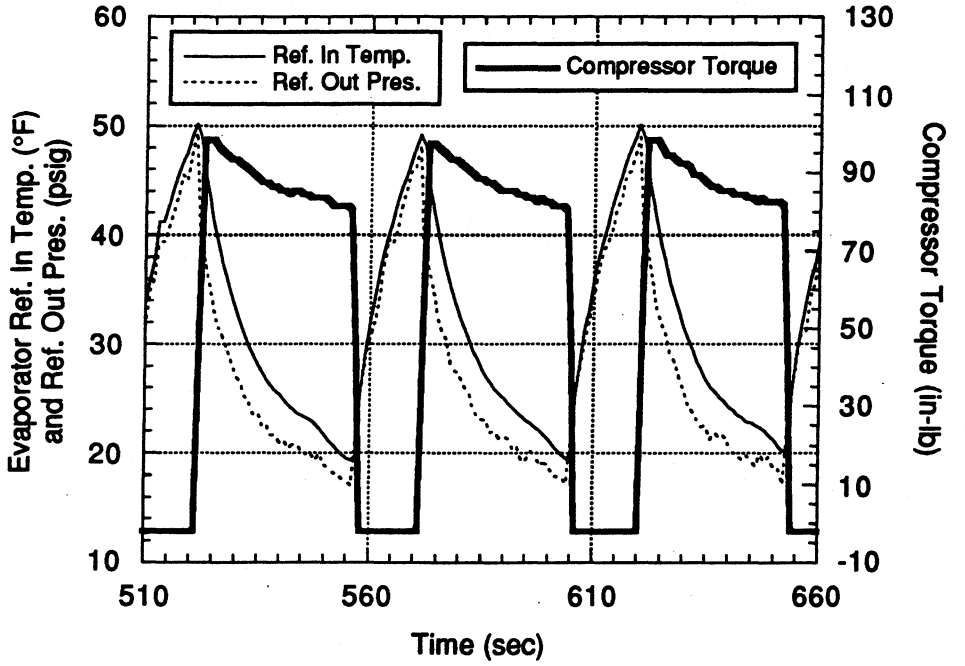

Figure 3.11: Evaporator refrigerant-side pressure and temperature for pressure-cycled clutch (on at 50 psig, off at 20 psig).

refrigerant-side differential pressure is small compared to the gage pressure, therefore making the outlet pressure essentially the same as the inlet. Because the evaporator pressures follow a similar pattern as the inlet refrigerant temperature, the remaining analysis will be limited to showing the evaporator temperatures. Analogous conclusions can be made about the evaporator refrigerant-side pressures.

Figures 3.12 and 3.13, which show the evaporator air-side temperatures for both pressure-cycled clutch cases, are used to examine the effects of clutch cycling on evaporator air-side temperatures. The inlet temperature for the 45/24 case remains essentially constant, whereas the temperature for the 50/20 case oscillates slightly. No oscillations are noticed in the 45/24 case because the clutch cycles occur too fast for the effects to propagate all the way down to the evaporator inlet temperature. Because the outlet temperature measurement is located directly downstream of the evaporator, the effects of clutch cycling on the air-side outlet temperature are quite noticeable for both clutch cycling cases. For both cases, the temperatures average approximately 55 °F with an oscillation of approximately ± 5 °F. The fact that the air-side outlet temperatures for both pressure-cycled clutch cases oscillate about the same value means that a 90 °F inlet air temperature, using the test stand conditions in Table 3.5, will generate an outlet temperature of 55 °F for cycling periods shorter than a certain limit.

The results for the evaporator refrigerant-side temperatures, shown in Figures 3.14 and 3.15, combine the effects discussed in the previous two paragraphs. The refrigerant-side inlet and outlet temperatures both oscillate as the clutch is engaged and disengaged. Also, both temperatures oscillate about the same approximate values: 35 °F for the inlet and 74 °F for the outlet. As expected, the refrigerant-side temperatures increase when the clutch is engaged and decrease when the clutch is disengaged.

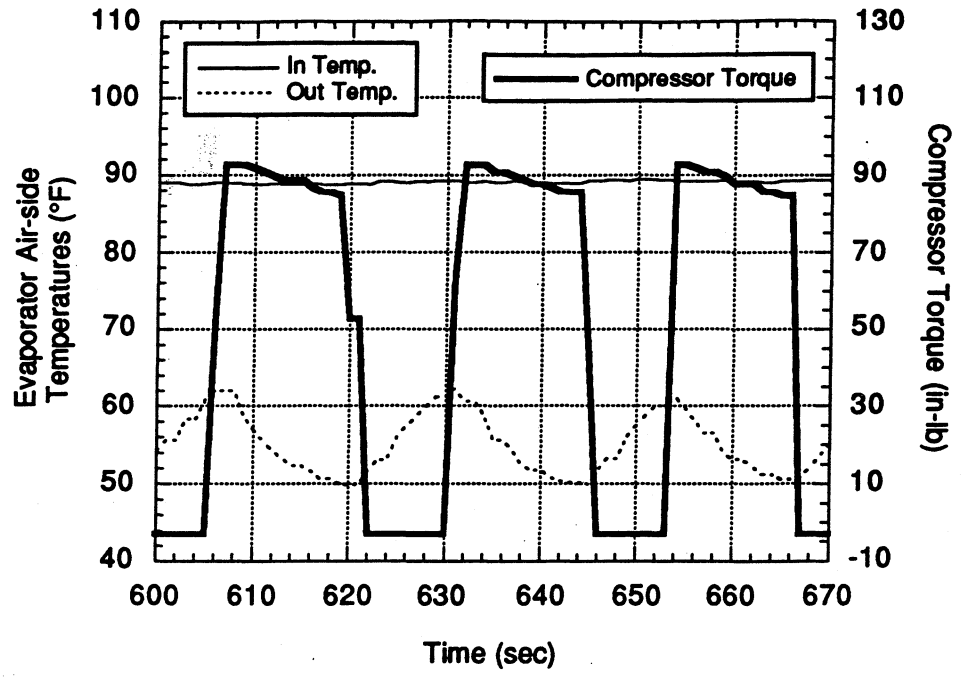

Figure 3.12: Evaporator air-side temperatures for pressure-cycled clutch (on at 45 psig, off at 24 psig).

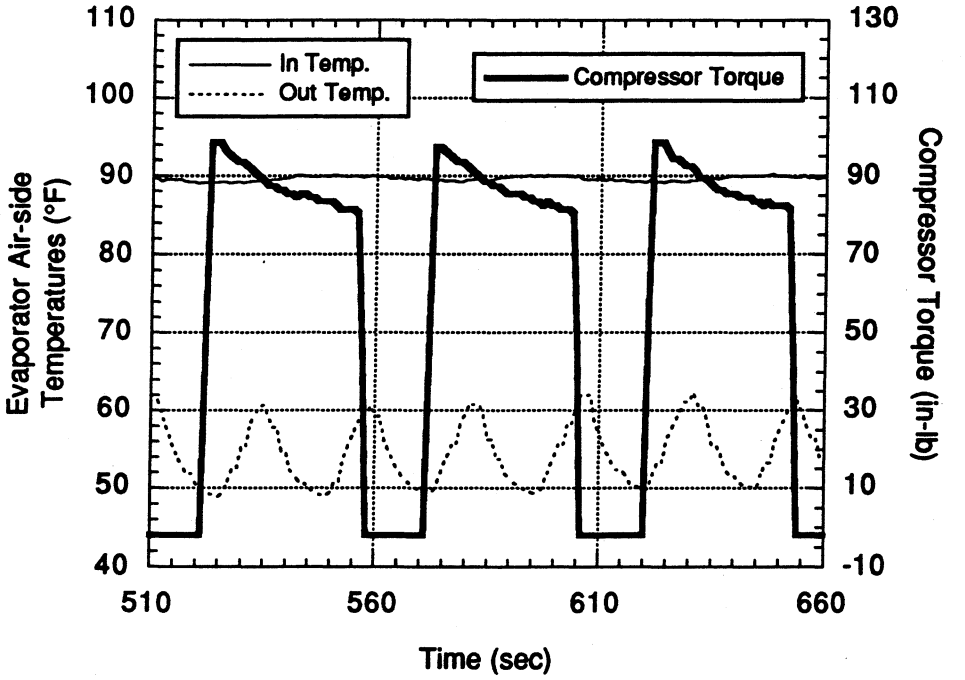

Figure 3.13: Evaporator air-side temperatures for pressure-cycled clutch (on at 50 psig, off at 20psig).

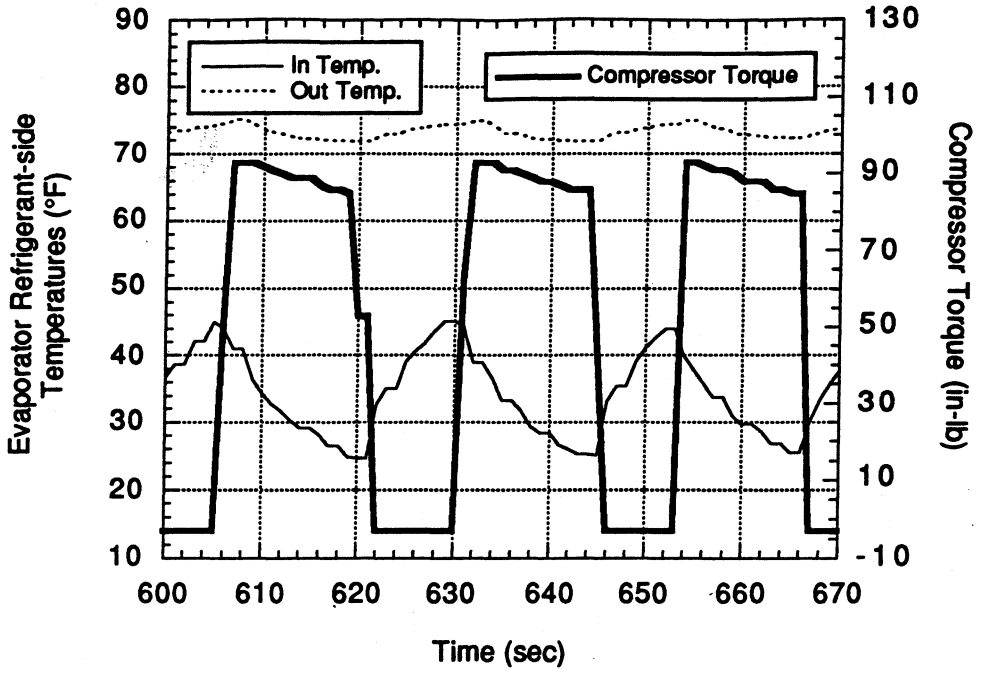

Figure 3.14: Evaporator refrigerant-side temperatures for pressure-cycled clutch (on at 45 psig, off at 24 psig).

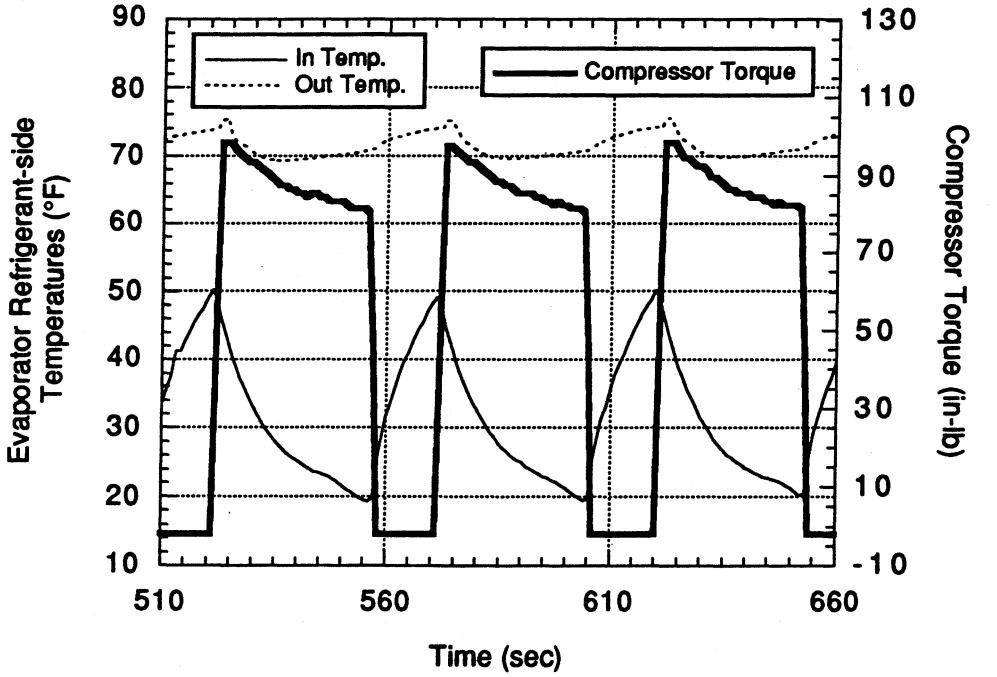

Figure 3.15: Evaporator refrigerant-side temperatures for pressure-cycled clutch (on at 50 psig, off at 20 psig).

3.3.3 Time-cycled Compressor Clutch

To examine how the Ford 1994 Crown Victoria air conditioning system responds to pre-programmed transients, several different time-determined patterns for compressor clutch cycling are tested. These patterns are: (1) clutch on for 80 s and off for 20 s (80/20), (2) clutch on for 20 s and off for 80 s (20/80), (3) clutch on for 8 s and off for 2 s (8/2), and (4) clutch on for 2 s and off for 8 s (2/8). This section is devoted to the discussion of the effects of these clutch cycling patterns on the evaporator air-side and refrigerant-side temperatures.

Figures 3.16 and 3.17 show the evaporator air-side temperatures for the 80/20 and 20/80 time-cycled clutch cases. Both figures show the inlet temperature oscillating ± 3-5 °F about an average inlet temperature of 89-90 °F. The oscillations in the air-side inlet temperature are due to the large distance, and therefore large time constant, between with the duct heater and the inlet temperature measurement. The air-side outlet temperature oscillates as the compressor clutch is cycled. When the compressor clutch is engaged, the outlet temperature decreases sharply as a greater amount of heat transfer occurs between the air-side and refrigerant-side. A greater amount of heat transfer occurs because of the large difference between the air-side inlet and refrigerant-side inlet temperatures. The outlet temperature increases sharply when the clutch is disengaged as less throttled refrigerant is provided to the condenser and therefore less heat transfer occurs. The outlet temperature oscillations are greater for the 20/80 case because the long off cycle allows the outlet temperature to approach the inlet temperature, whereas in the 80/20 case, the compressor clutch is not off long enough for the outlet temperature to approach the inlet temperature. As with the pressure-cycled clutch, the maximum compressor torque is greater for the case that has a longer off cycle (the 20/80 case) because the compressor has to initially pump a great deal of refrigerant that has been discharged into the evaporator. In terms of passenger comfort, the 80/20 case is preferable because the outlet air temperature variations are smaller and, as in the pressure-cycled cases, an average outlet temperature of 55 °F is maintained. The

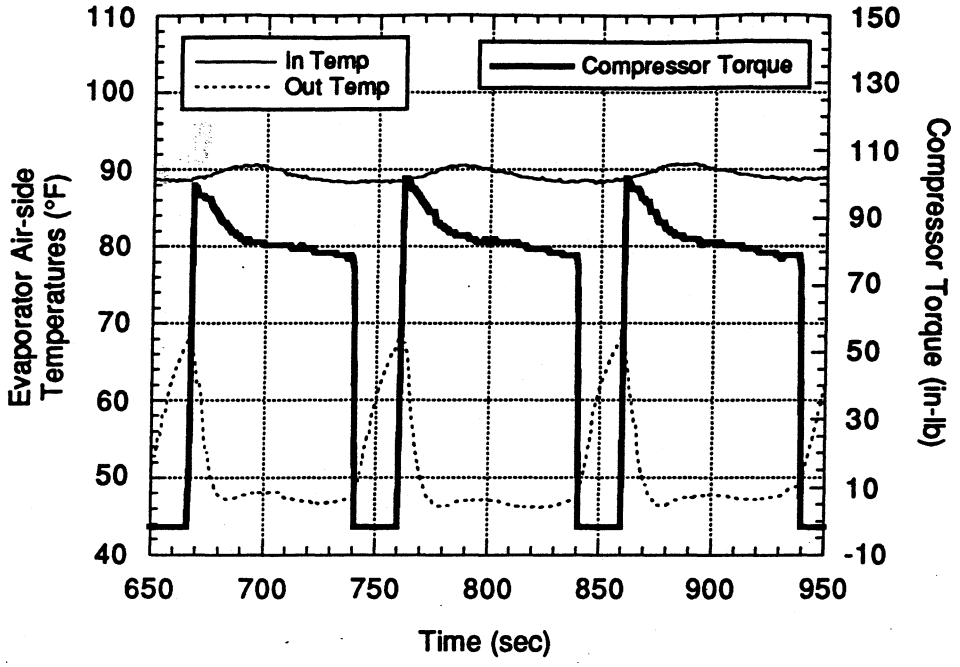

Figure 3.16: Evaporator air-side temperatures for time-cycled clutch (on for 80 s, off for 20 s).

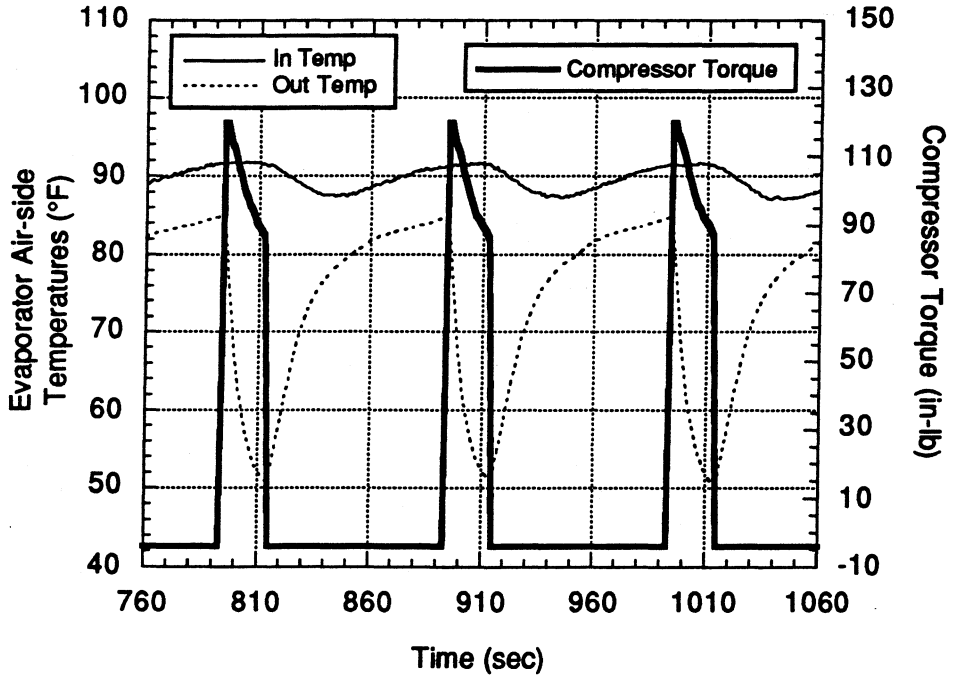

Figure 3.17: Evaporator air-side temperatures for time-cycled clutch (on for 20 s, off for 80 s).

20/80 case is impractical and inadequate because it cannot maintain a low enough average evaporator outlet temperature.

Even more so than the air-side temperatures, the evaporator refrigerant-side temperatures, shown in Figures 3.18 and 3.19, depend on the clutch cycling. Both temperatures decrease when the compressor clutch is engaged and increase when it is disengaged. As expected, the refrigerant-side temperatures are lower for the 80/20 case where the compressor clutch is engaged for a longer fraction of the cycle. For both cases, though, the average refrigerant-side inlet temperature remains near or above the 32 °F limit required to prevent the freezing of condensate on the evaporator surface.

Figures 3.20 and 3.21 show the evaporator air-side inlet and outlet temperatures for the 8/2 and 2/8 time-cycled compressor clutch cases. Because the period for an entire cycle is so short, the evaporator inlet temperature is unaffected in both cases. This is not true for the evaporator outlet temperatures. For the 8/2 case, the average outlet temperature is approximately 52 °F with small fluctuations occurring as the compressor clutch is engaged and disengaged. For the 2/8 case, the temperature fluctuations are slightly higher and have an average of approximately 67 °F. Unlike the 8/2 case, the relatively high average outlet temperature for the 2/8 case is not low enough to provide a comfortable passenger environment. As with all the other cases in which the compressor clutch is off for a longer fraction of the cycle than it is on, the 2/8 case has peak torque values higher than the 8/2 case.

The evaporator refrigerant-side temperatures for the 8/2 and 2/8 time-cycled compressor clutch cases are shown in Figures 3.22 and 3.23. As with the majority of the pressure- and time-cycled clutch cases, the inlet and outlet temperatures decrease when the compressor clutch is engaged and increase when the clutch is disengaged. The inlet temperature fluctuations, though comparable, are again greater in the 2/8 case than in the 8/2 case. The outlet temperature for the 8/2 case remains virtually constant because the cycle period is so small and the compressor is on for most of the cycle. The opposite is true for the 2/8 case, where the small on cycle causes greater fluctuations in the refrigerant-side outlet temperature.

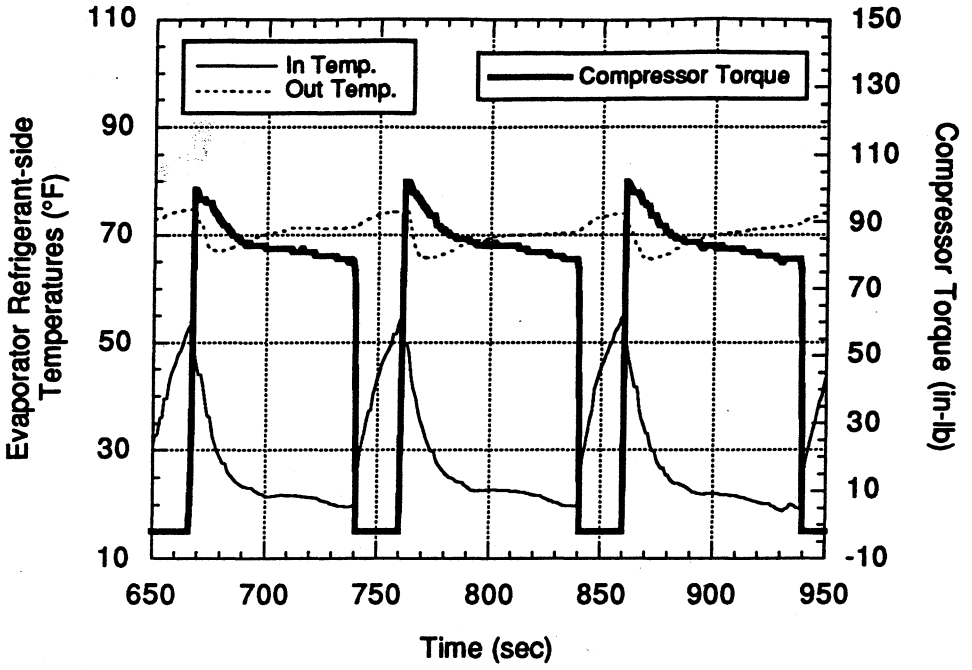

Figure 3.18: Evaporator refrigerant-side temperatures for time-cycled clutch (on for 80 s, off for 20 s).

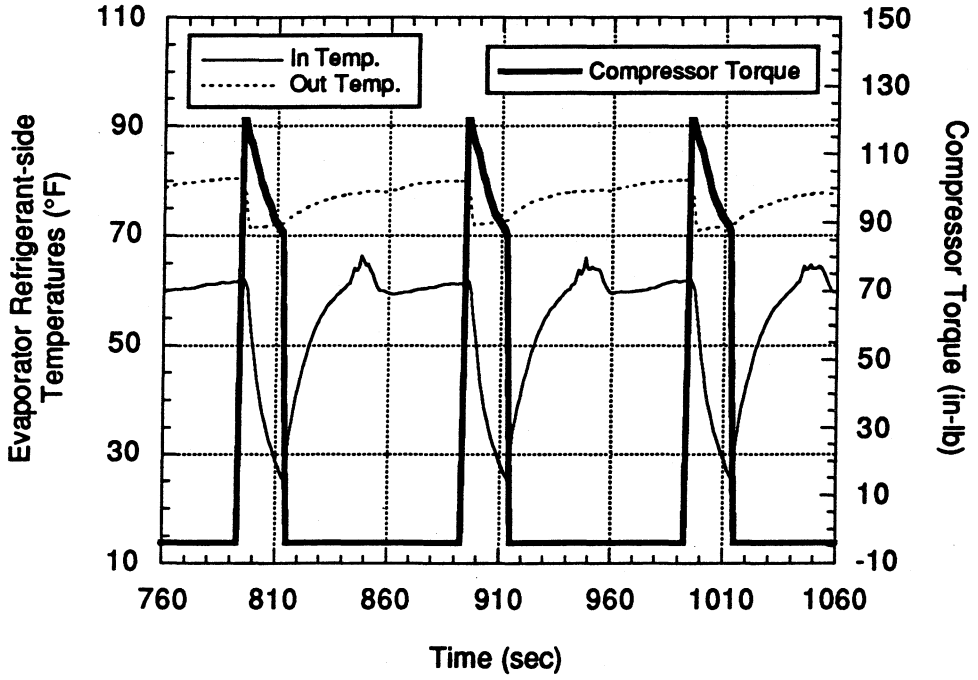

Figure 3.19: Evaporator refrigerant-side temperatures for time-cycled clutch (on for 20 s, off for 80 s).

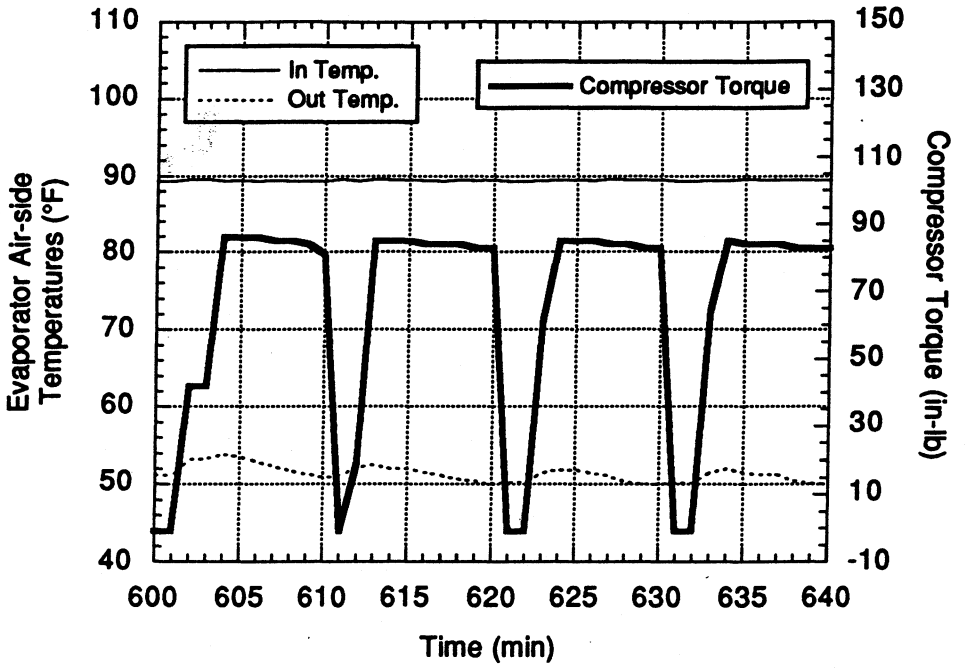

Figure 3.20: Evaporator air-side temperatures for time-cycled clutch (on for 8 s, off for 2 s).

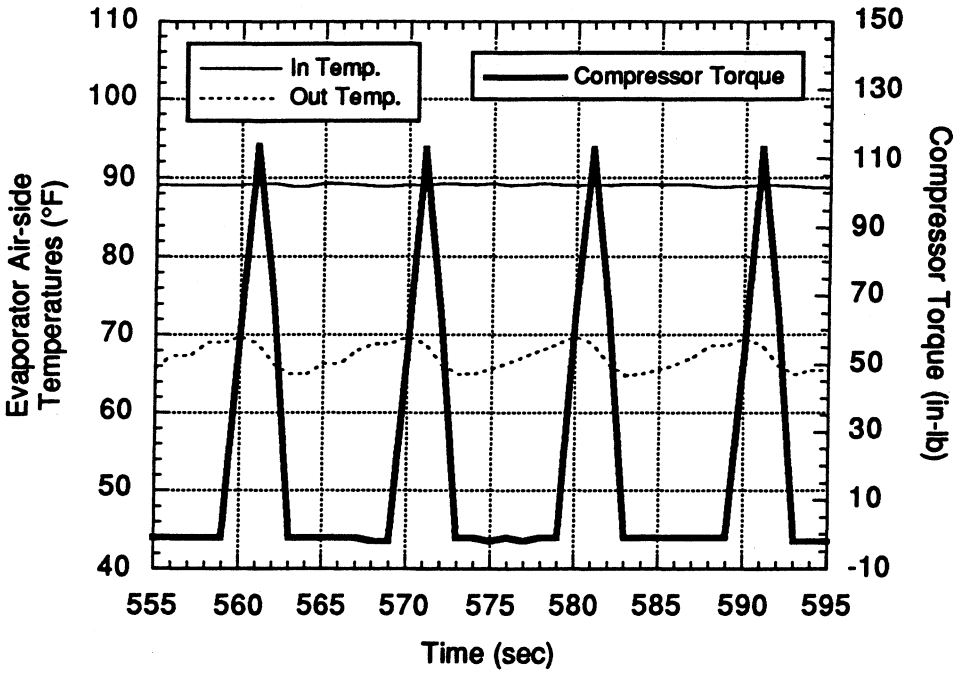

Figure 3.21: Evaporator air-side temperatures for time-cycled clutch (on for 2 s, off for 8 s).

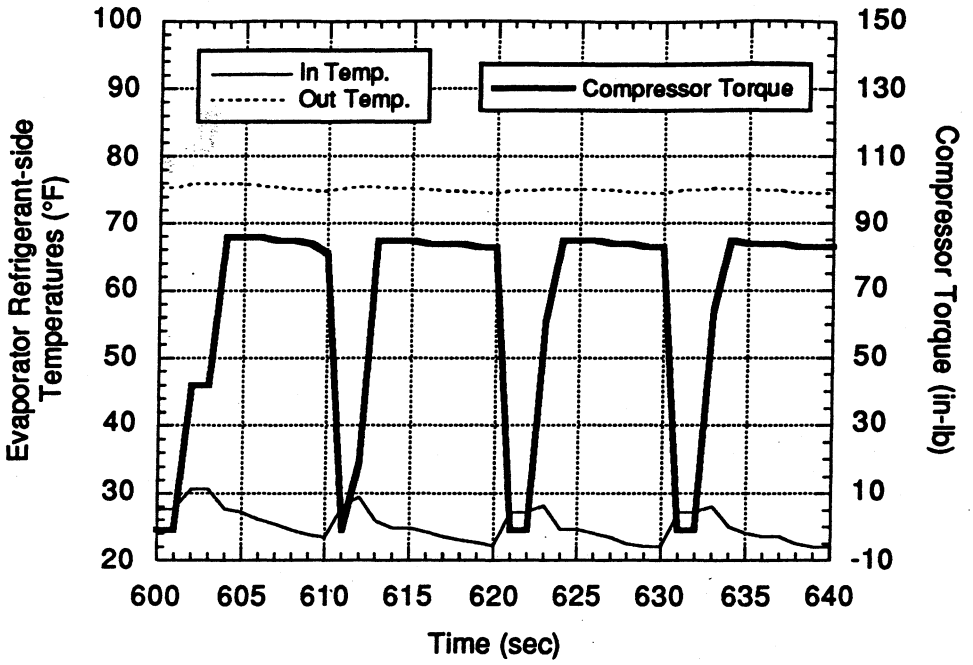

Figure 3.22: Evaporator refrigerant-side temperatures for time-cycled clutch (on for 8 s, off for 2 s).

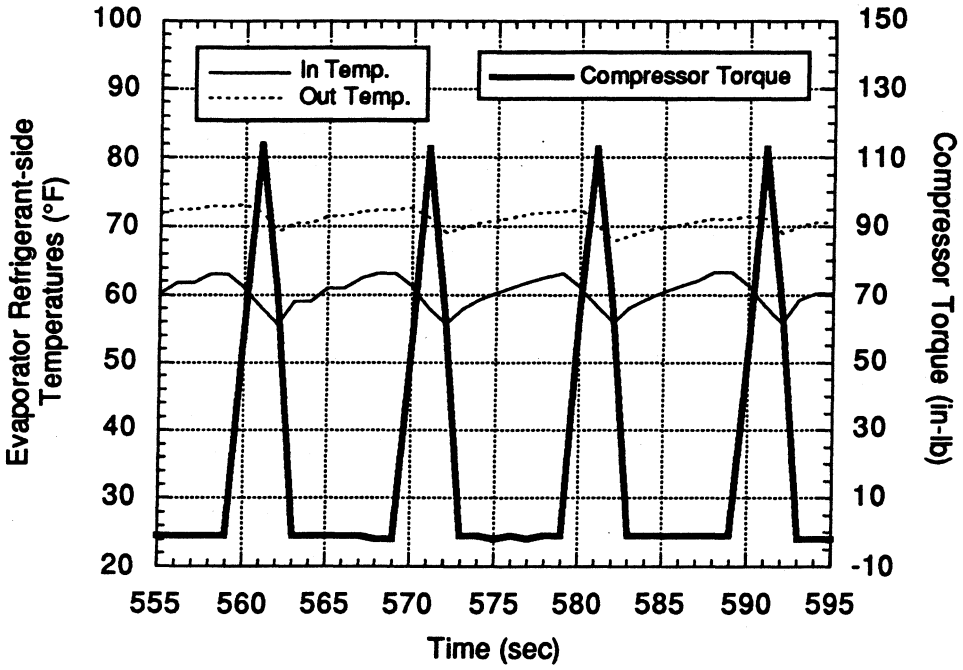

Figure 3.23: Evaporator refrigerant-side temperatures for time-cycled clutch (on for 2 s, off for 8 s).

It has been determined through the analyses in the previous paragraphs that the time cycles where the compressor is on for a greater fraction of the cycle period (the 80/20 and 8/2 cases) will generate lower evaporator air-side outlet temperature and therefore provide greater passenger comfort. Of these two cases, the 8/2 case provides lower evaporator air-side outlet temperatures. However, there is a payoff for the lower outlet temperatures because, since the clutch is cycled so frequently, there will be additional wear on the clutch and the surfaces inside the compressor. A clutch cycling pattern where the compressor clutch is cycled somewhere in between the 80/20 and 8/2 cases, such as those induced by natural phenomenon and shown in the pressure-cycled section, presents a better compromise between clutch and compressor wear and passenger comfort.

3.3.4 Simulated Driving Cycle

In the simulated driving cycle tests, the Ford 1994 Crown Victoria air conditioning components are operated at conditions that simulated their exposure to a vehicle-induced driving cycle. To simulate a driving cycle, the compressor speed and condenser blower flow rates are ramped simultaneously. Because most compressors are connected to the vehicle engine drive shaft with belts, the compressor speed change is caused by vehicle acceleration and the condenser blower change is caused by the increasing amount of air passing across the condenser as the vehicle achieves higher speeds. For the driving cycle, the compressor speed was set to 1150 RPM for 20 s to simulate the vehicle idling at a stop light. The idling was then followed by a 15 s acceleration to 3050 RPM. The 3050 RPM compressor speed was maintained for 120 s before being reduced to the original idle speed of 1150 RPM by a 10 s deceleration. While the compressor speed was being changed, the condenser speed was simultaneously ramped from 800 to 1600 CFM to simulate the additional air being provided to the condenser. Figure 3.24 shows the compressor speed and condenser air flow rate patterns for the simulated driving cycle. The settings for the test stand components are shown in Table 3.6. Other than the compressor speed and condenser air flow rate

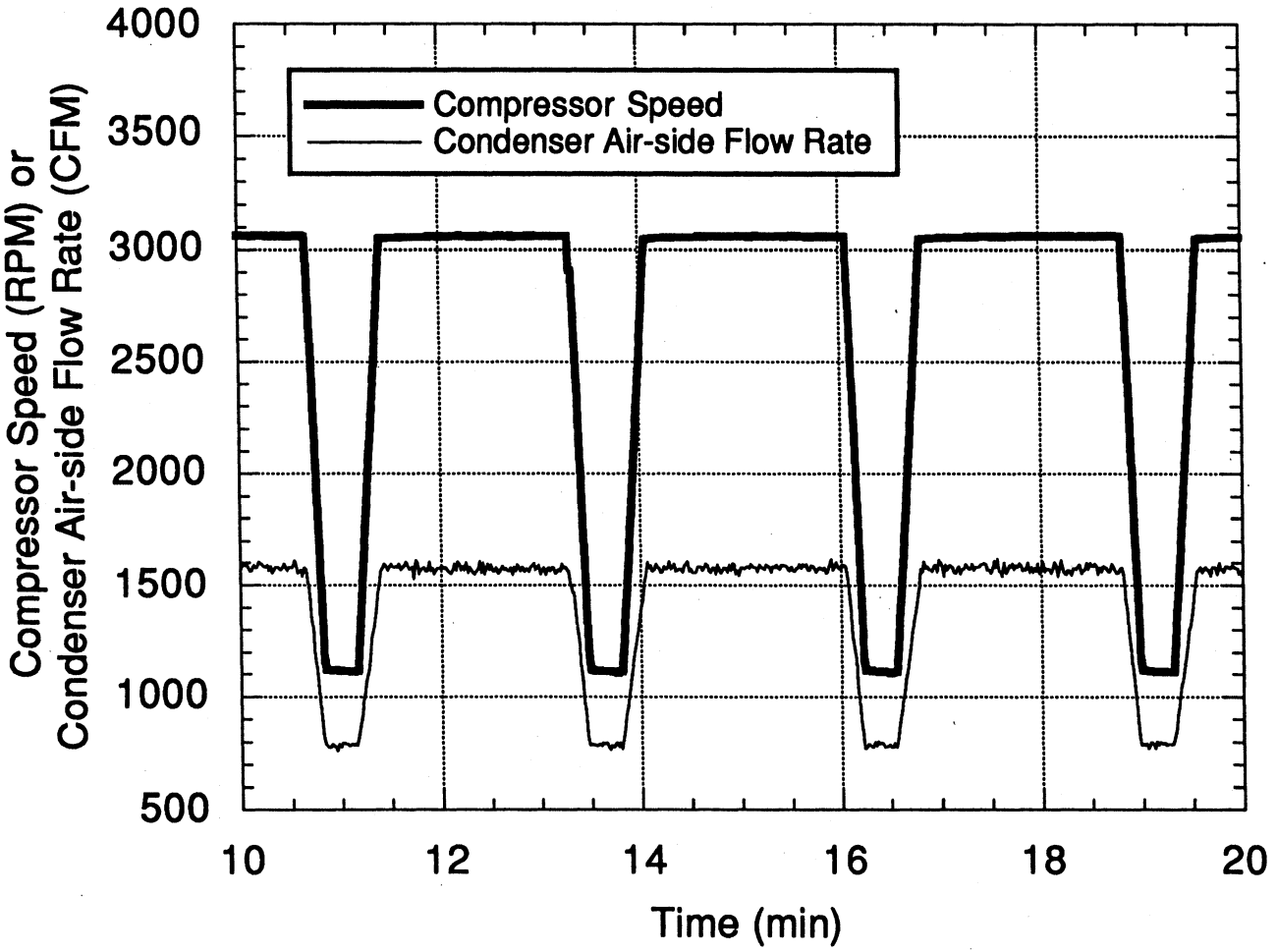

Figure 3.24: Compressor speed and condenser air-side flow rate for simulated driving cycle.

oscillations, these settings are the same as those used for the pressure-cycled and time-cycled clutch tests. Tests were done with the conditions in Table 3.6 using a continuously-engaged clutch and a 50/20 pressure-cycled clutch.

Table 3.6: Simulated Driving Cycle Test Conditions

Compressor Speed (RPM)	Cond. Air Flow (CFM)	Cond. Air In Temp (°F)	Evap. Air Flow (CFM)	Evap. Air In Temp (°F)
1150-3050	800-1600	Ambient	215	90

As with the pressure-cycled and time-cycled tests, the following discussion will be limited to the evaporator air-side and refrigerant-side temperatures. The following figures contain the compressor speed instead of the torque so that the reader can know the driving cycle stage.

Figures 3.25 and 3.26 show the evaporator air-side inlet and outlet temperatures for the driving cycles with a continuously-engaged clutch and a 50/20 pressure-cycled clutch. When comparing the compressor speed in each graph, one can clearly note the spikes in the pressure-cycled clutch case that are caused when the clutch is engaged. The clutch cycling only has a slight effect on the air-side inlet temperature, with the clutch cycling case temperature being slightly more jagged, but generally following the same pattern as the continuously-engaged clutch. Another trend in both figures, though not as noticeable in the clutch-cycled case, is that the outlet temperature increases and decreases as the compressor speed increases and decreases. This is opposite to what was experienced in the previous pressure-cycled and time-cycled tests. The reason for this opposite trend is that, in this driving simulation, the condenser air flow rate is changed simultaneously with the compressor speed. A commonly observed phenomenon is that an increase in condenser flow rate causes a decrease in refrigerant mass flow rate. Because of the decrease in refrigerant mass flow rate, there is less heat transfer, causing the air-side evaporator outlet temperature to be raised.

Some of the trends observed in the evaporator refrigerant-side temperatures, shown in Figure 3.27 and 3.28, are similar to those observed in the evaporator air-

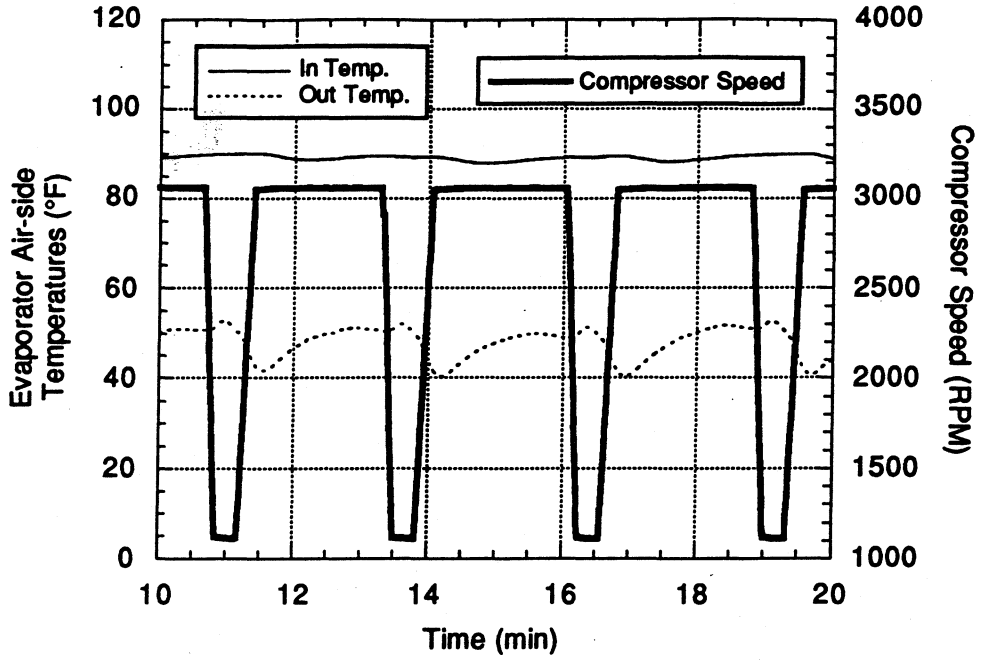

Figure 3.25: Evaporator air-side temperatures for simulated driving cycle with continuously-engaged clutch.

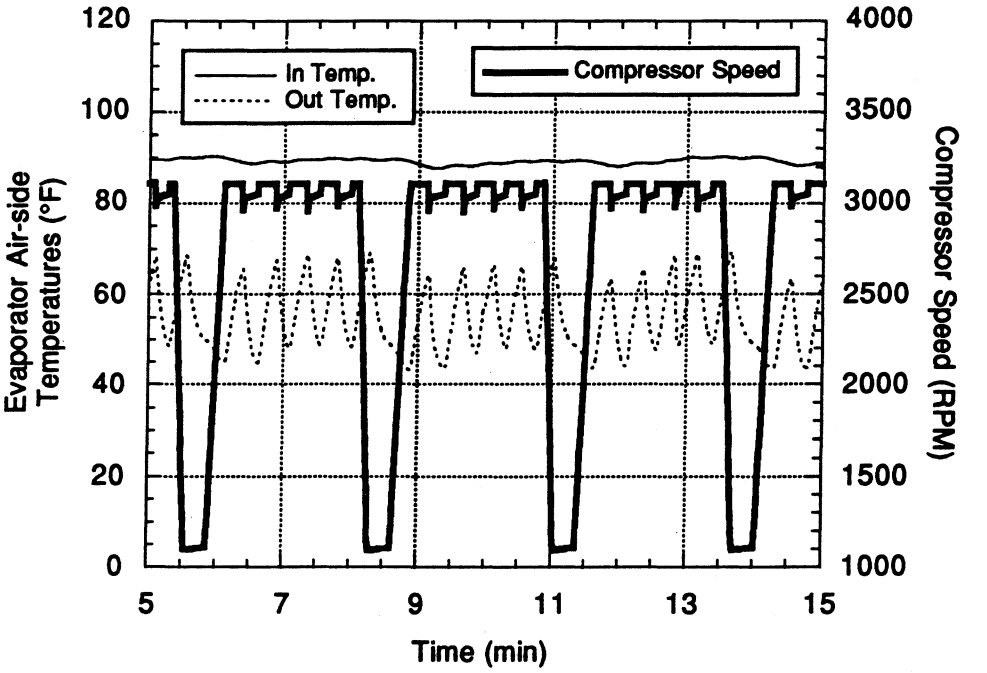

Figure 3.26: Evaporator air-side temperatures for simulated driving cycle with 50/20 pressure-cycled clutch.

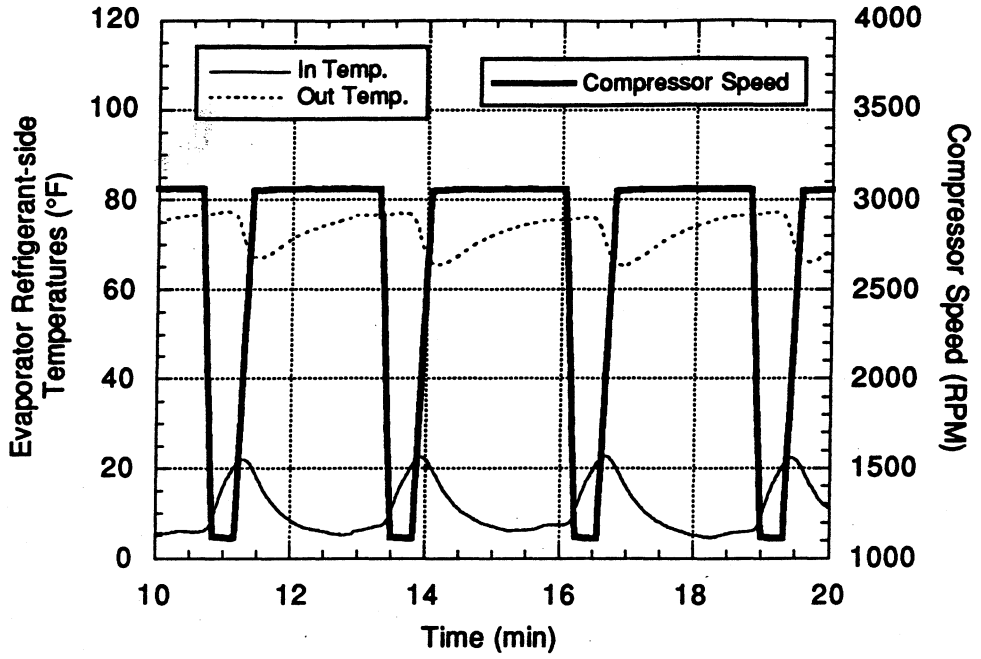

Figure 3.27: Evaporator refrigerant-side temperatures for simulated driving cycle with continuously-engaged clutch.

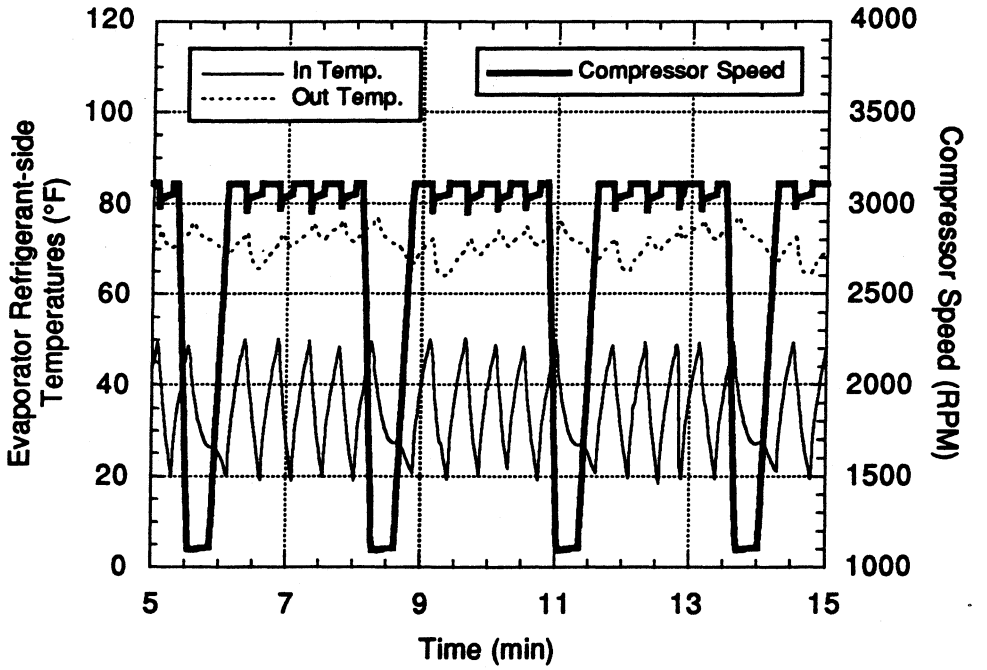

Figure 3.28: Evaporator refrigerant-side temperatures for simulated driving cycle with 50/20 pressure-cycled clutch.

side temperatures. In the case with the continuously-engaged compressor clutch, the inlet refrigerant-side temperature increases during low compressor speeds and decreases during high compressor speeds. This is not surprising because during high compressor speeds there is a greater pressure differential across the orifice tube throttling device. The greater pressure differential causes the refrigerant at the evaporator inlet to be at a lower pressure and, because it is saturated, a lower temperature. In the 50/20 pressure-cycled case, this trend cannot be observed because the effects of the cycling clutch dominate those of the throttling device. For both the continuously-engaged clutch and the 50/20 pressure-cycled clutch cases, the refrigerant-side outlet temperatures increase during high compressor speeds. The reason for this is the same as that explained in the previous paragraph—the effect of increasing the condenser air-side flow rate dominates over the increase in compressor speed, therefore resulting in higher evaporator refrigerant-side outlet temperatures during the portions of the driving cycle with high compressor speeds.

Because the average outlet air-side temperature is lower for the test with the continuously-engaged clutch than for the 50/20 pressure-cycled clutch (48 °F versus 58 °F), the temperature of the vehicle cabin will be reduced faster, providing greater passenger comfort. There is a trade-off, however, because in the continuously-engaged clutch case the average refrigerant-side inlet temperature is extremely low (10 °F) when compared to the temperature for the pressure-cycled clutch (35 °F). Clearly, the continuously-engaged clutch case is unfavorable because the refrigerant-side inlet temperature is too low and the condensate on the evaporator surface will freeze.

4. CONCLUSIONS AND RECOMMENDATIONS

4.1 Conclusions

With the work discussed in this report, the following conclusions can be drawn.

- Because most of the points lie within ± 5% of the theoretical heat transfer line, the goal of achieving good calorimetry was reached; therefore allowing for further testing of the air conditioning system operating under transient conditions.
- The instrumentation in the test stand generates correct results. Data from the extensive instrumentation provides excellent insights into transient system operation.
- The five mass flow rate calculations can be used to record accurate values and, specifically, the refrigerant-side venturis can be used to obtain mass flow rates that are frequently within ± 2 of the mass flow rate reported by the Micro Motion coriolis-effect meter. However, the reader should realize that accurate venturi mass flow rates can only be obtained after proper venturi calibration.
- The test facility was shown to be capable of reliably generating the wide range of operating conditions required for transient testing.

4.2 Recommendations

Despite the accuracy of the results, a few recommendations concerning the test facility instrumentation are presented.

- The evaporator air-side outlet humidity probe should be moved from its current location (downstream of the duct heater) to the blower outlet 6" sheet metal pipe (see Figure 2.16). This will (a) ensure the air is mixed before being read by the sensor and (b) maintain the temperature at the sensor below the maximum recommended operating limit of 140 °F.
- Larger diameter copper tubing should be installed on the refrigerant-side venturi differential pressure transducers. The larger tubing will prevent the

surface tension of the refrigerant oil from affecting the transmission of pressure to the very sensitive differential pressure transducers.

APPENDIX

EES Energy Balance Program

```
{This program is used to calculate the condenser and evaporator air-side versus
refrigerant-side energy balances. In the process of determining the energy balance,
the program calculates all other test stand parameters such as: flow rates,
temperatures, and pressures.}

{Function that calculates temperature(C) given thermocouple voltage(mV)
obtained from IPS-90 tables in CRC Handbook of Chemistry and Physics}
Function TfV(V)
   If (V<0) Then
      c0:= 0
      c1:= 2.5949192E1
      c2:= -2.1316967E-1
      c3:= 7.9018692E-1
      c4:= 4.2527777E-1
      c5:= 1.3304473E-1
      c6:= 2.0241446E-2
      c7:= 1.2668171E-3
   Else
      c0:= 0
      c1:= 2.592800E1
      c2:= -7.602961E-1
      c3:= 4.637791E-2
      c4:= -2.165394E-3
      c5:= 6.048144E-5
      c6:= -7.293422E-7
      c7:=0
   EndIf
   TfV:=c0+c1*V+c2*V^2+c3*V^3+c4*V^4+c5*V^5+c6*V^6+c7*V^7
END

{Function that calculates thermocouple voltage(mV) given temperature (C)}
Function VfT(T)
   If (T<0) Then
      c0:= 0
      c1:= 3.8748106364E-2
      c2:= 4.4194434347E-5
      c3:= 1.1844323105E-7
      c4:= 2.0032973554E-8
      c5:= 9.0138019559E-10
      c6:= 2.2651156593E-11
```

```
        c7:= 3.6071154205E-13
        c8:= 3.8493939883E-15
        c9:= 2.8213521925E-17
        c10:= 1.4251594779E-19
        c11:= 4.8768662286E-22
        c12:= 1.0795539270E-24
        c13:= 1.3945027062E-27
        c14:= 7.9795153927E-31
    Else
        c0:= 0
        c1:= 3.8748106364E-2
        c2:= 3.3292227880E-5
        c3:= 2.0618243404E-7
        c4:= -2.1882256846E-9
        c5:= 1.0996880928E-11
        c6:= -3.0815758772E-14
        c7:= 4.5479135290E-17
        c8:= -2.7512901673E-20
        c9:= 0
        c10:= 0
        c11:= 0
        c12:= 0
        c13:= 0
        c14:= 0
    EndIf
    VfT:=c0+c1*T+c2*T^2+c3*T^3+c4*T^4+c5*T^5+c6*T^6+c7*T^7+c8*T^8+c9*T^9+
      c10*T^10+c11*T^11+c12*T^12+c13*T^13+c14*T^14
END

{Function that converts degrees C to F}
Function FfC(C)
    FfC=9/5*C+32
end

{Function that converts degrees F to C}
Function CfF(F)
    CfF=5/9*(F-32)
end



{BEGINNING OF MAIN  EES PROGRAM}
{Correct the barometer for temperature and gravity as per the users manual, p. 11}
Pt=Proom+Proom*((1+L*(Troom-Ts))/(1+M*(Troom-Tm))-1)  {inHg @ 32 F}
Ts=62 {F}
Tm=32 {F}
```

```
L=0.0000102 {in/in-F}
M=0.0001010 {in^3/in^3-F}

Pl=Pt+Pt*(980.616/980.665*(1-0.0026373*cos(2*phi)+0.0000059*(cos(2*phi))^2)-1)
      {inHg at 32 F}
phi=40.109 {Latitude of Urbana, Illinois in degrees}

{Calculate atmospheric pressure from corrected barometer reading. Conversion
factor is from CRC Handbook, 64th ed., p.F-314:  70.7262{psf/inHg @ 32
F}*1{psi}/144{psf}=0.491154 {psi/inHg @ 32 F}}
Patm=Pl*0.491154 {psia}

{Enter pressure transducer calibration slopes "m" below (from curve fit of
Pressure=m*Volts+b)}
m_Peri=20.038 {psig/V}
m_dPer=5.1463 {psid/V}
m_Pkri=20.38 {psig/V}
m_Pkro=121.07 {psig/V}
m_dPdv=1.0144 {mV/V}
m_Pcri=100.63 {psig/V}
m_dPcr=4.9448 {psid/V}
m_Plv=100.86 {psig/V}
m_dPlv=0.50393 {mV/V}
m_Peav=0.10833 {psig/V}
m_dPeav=0.065652 {psid/ma}
m_Pcav=0.10719 {psig/V}
m_dPcav=0.06841 {psid/ma}

{Calculate pressures from slope "m", daily offset value Vo, and atmospheric
pressure Patm}
Peri=m_Peri*(V_Peri-Vo_Peri)+Patm {psia}
dPer=m_dPer*(V_dPer-Vo_dPer) {psid}
Pkri=m_Pkri*(V_Pkri-Vo_Pkri)+Patm {psia}
Pkro=m_Pkro*(V_Pkro-Vo_Pkro)+Patm {psia}
dPdv=m_dPdv*(V_dPdv-Vo_dPdv)*1000/V_5V-0.0022797 {psid}
Pcri=m_Pcri*(V_Pcri-Vo_Pcri)+Patm {psia}
dPcr=m_dPcr*(V_dPcr-Vo_dPcr) {psid}
Plv=m_Plv*(V_Plv-Vo_Plv)+Patm {psia}
dPlv=m_dPlv*(V_dPlv-Vo_dPlv)*1000/V_5V-0.0013125 {psid}
Peav=m_Peav*(V_Peav-Vo_Peav)+Patm {psia}
dPeav=m_dPeav*(A_dPeav-Ao_dPeav) {psid}
Pcav=m_Pcav*(V_Pcav-Vo_Pcav)+Patm {psia}
dPcav=m_dPcav*(A_dPcav-Ao_dPcav) {psid}

{Calculate water bath temp & back out thermocouple voltage}
Tbath_F=164.96*V_Tmstr/V_5V+60.96 {F}
```

```
V_TCBath=VfT(CfF(Tbath_F)) {mV}

{Calculate thermocouple temperatures from logged voltages}
Teai=FfC(TfV(V_TCBath+V_Teai*1000)) {F}
Teao=FfC(TfV(V_TCBath+V_Teao*1000)) {F}
Teav=FfC(TfV(V_TCBath+V_Teav*1000)) {F}
Tcai=FfC(TfV(V_TCBath+V_Tcai*1000)) {F}
Tcao=FfC(TfV(V_TCBath+V_Tcao*1000)) {F}
Tcav=FfC(TfV(V_TCBath+V_Tcav*1000)) {F}
Teri=FfC(TfV(V_TCBath+V_Teri*1000)) {F}
Tero=FfC(TfV(V_TCBath+V_Tero*1000)) {F}
Tkri=FfC(TfV(V_TCBath+V_Tkri*1000)) {F}
Tkro=FfC(TfV(V_TCBath+V_Tkro*1000)) {F}
Tcri=FfC(TfV(V_TCBath+V_Tcri*1000)) {F}
Tcro=FfC(TfV(V_TCBath+V_Tcro*1000)) {F}
Tlv=FfC(TfV(V_TCBath+V_Tlv*1000)) {F}

{Calculate Micro Motion flow. Micro Motion checked by John Cioch & calibrated to
read 4.00mA at zero flow.}
m_Micro=25.0 {lbm/hr/ma}
mdot_Micro=m_Micro*(A_Micro-4.000) {lbm/hr}

{Calculate other variables in the loop}
Tdv=Tkro {F}
Pdv=Pkro {psia}
Pcro=Pcri-dPcr {psia}
Pero=Peri-dPer {psia}
Pcai=Patm {psia}
Pcao=Patm {psia}
Peai=Patm {psia}
Peao=Patm {psia}

{Calculate humidity ratios}
weai=HumRat(AirH2O,T=TRHeai,P=Peai,R=RHeai/100) {lbm H2O/lbm dry air}
weao=HumRat(AirH2O,T=TRHeao,P=Peao,R=RHeao/100) {lbm H2O/lbm dry air}
wca=HumRat(AirH2O,T=TRHcao,P=Pcao,R=RHcao/100) {lbm H2O/lbm dry air}

{Calculate enthalpies}
heri=Enthalpy(R134a,T=Tlv,P=Plv) {Btu/lbm}
hero=Enthalpy(R134a,T=Tero,P=Pero) {Btu/lbm}
hcri=Enthalpy(R134a,T=Tcri,P=Pcri) {Btu/lbm}
hcro=Enthalpy(R134a,T=Tcro,P=Pcro) {Btu/lbm}
hlv=Enthalpy(R134a,T=Tlv,P=Plv) {Btu/lbm}

heai=Enthalpy(Air,T=Teai)+weai*Enthalpy(Steam,T=Teai,x=1.0) {Btu/lbm dry air}
heao=Enthalpy(Air,T=Teao)+weao*Enthalpy(Steam,T=Teao,x=1.0) {Btu/lbm dry air}
```

```
hcai=Enthalpy(Air,T=Tcai)+wca*Enthalpy(Steam,T=Tcai,x=1.0) {Btu/lbm dry air}
hcao=Enthalpy(Air,T=Tcao)+wca*Enthalpy(Steam,T=Tcao,x=1.0) {Btu/lbm dry air}

{Calculate densities at venturi inlet and throat}
Rho_eav=1/Volume(AirH2O,T=Teav,P=Peav,w=weao) {lbm wet air/ft^3}
s1_eav=Entropy(AirH2O,T=Teav,P=Peav,w=weao) {Btu/lbm-hr}
s2_eav=s1_eav  {isentropic so s2=s1, solve for T2 below}
s2_eav=Entropy(AirH2O,T=Teav2,P=Peav-dPeav,w=weao) {Btu/lbm-hr}
Rho_eav2=1/Volume(AirH2O,T=Teav2,P=Peav-dPeav,w=weao) {lbm wet air/ft^3}
Rho_cav=1/Volume(AirH2O,T=Tcav,P=Pcav,w=wca) {lbm wet air/ft^3}
s1_cav=Entropy(AirH2O,T=Tcav,P=Pcav,w=wca)
s2_cav=s1_cav
s2_cav=Entropy(AirH2O,T=Tcav2,P=Pcav-dPcav,w=wca) {Btu/lbm-hr}
Rho_cav2=1/Volume(AirH2O,T=Tcav2,P=Pcav-dPcav,w=wca) {lbm wet air/ft^3}
Rho_dv=1/Volume(R134a,T=Tdv,P=Pdv) {lbm/ft^3}
s1_dv=Entropy(R134a,T=Tdv,P=Pdv)
s2_dv=s1_dv
s2_dv=Entropy(R134a,T=Tdv2,P=Pdv-dPdv) {Btu/lbm-hr}
Rho_dv2=1/Volume(R134a,T=Tdv2,P=Pdv-dPdv) {lbm/ft^3}
Rho_lv=1/Volume(R134a,T=Tlv,P=Plv) {lbm/ft^3}
s1_lv=Entropy(R134a,T=Tlv,P=Plv)
s2_lv=s1_lv
s2_lv=Entropy(R134a,T=Tlv2,P=Plv-dPlv) {Btu/lbm-hr}
Rho_lv2=1/Volume(R134a,T=Tlv2,P=Plv-dPlv) {lbm/ft^3}

{Venturi diameters and beta ratios}
D1eav=3.085 {in}
D1cav=6.123 {in}
D1dv=0.917 {in}
D1lv=0.720 {in}

deav=1.877 {in}
dcav=4.491 {in}
ddv=0.375 {in}
dlv=0.189 {in}

Beav=deav/D1eav
Bcav=dcav/D1cav
Bdv=ddv/D1dv
Blv=dlv/D1lv

{Venturi discharge coefficients}
Ceav=0.946 {From calibration}
Ccav=0.830 {From calibration}
Cdv=0.910 {From calibration}
Clv=0.954 {From calibration}
```

```
{Vapor venturi area expansion factors}
alpha_steel=6.7e-6 {in/in-F}
alpha_brass=1.0e-5 {in/in-F}
Fa_eav=(1+alpha_steel*(Teav-68))^2
Fa_cav=(1+alpha_steel*(Tcav-68))^2
Fa_dv=(1+alpha_brass*(Tdv-68))^2
Fa_lv=(1+alpha_brass*(Tlv-68))^2

{Calculate mass flows using conservation of mass and momentum equations}
meav=Ceav*Fa_eav*deav^2*pi/4*3600/12*sqrt((2*32.174*Rho_eav*dPeav)/
(Rho_eav/Rho_eav2-Beav^4)) {lbm/hr}
mcav=Ccav*Fa_cav*dcav^2*pi/4*3600/12*sqrt((2*32.174*Rho_cav*dPcav)/
(Rho_cav/Rho_cav2-Bcav^4)) {lbm/hr}
mdv=Cdv*Fa_dv*ddv^2*pi/4*3600/12*sqrt((2*32.174*Rho_dv*dPdv)/
(Rho_dv/Rho_dv2-Bdv^4)) {lbm/hr}
mlv=Clv*Fa_lv*dlv^2*pi/4*3600/12*sqrt((2*32.174*Rho_lv*dPlv)/
(Rho_lv/Rho_lv2-Blv^4)) {lbm/hr}

Qeav=meav/Rho_eav/60 {cfm}
Qcav=mcav/Rho_cav/60 {cfm}

{Calculate energy balances}
meav_dry=meav/(1+weao) {lbm dry air/hr}
hw=Enthalpy(Steam,T=Teao,x=0.0)
erht=mlv*(hero-hlv) {Btu/hr}
eaht=meav_dry*((heai-heao)-(weai-weao)*hw) {Btu/hr}
eEbal=(erht-eaht)/erht*100 {%}

erht_micro=mdot_Micro*(hero-hlv) {Btu/hr}
eEbal_micro=(erht_micro-eaht)/erht_micro*100 {%}

mcav_dry=mcav/(1+wca) {lbm dry air/hr}
crht=mlv*(hcri-hcro) {Btu/hr}
caht=mcav_dry*(hcao-hcai) {Btu/hr}
cEbal=(crht-caht)/crht*100 {%}

crht_micro=mdot_Micro*(hcri-hcro) {Btu/hr}
cEbal_micro=(crht_micro-caht)/crht_micro*100 {%}

{Compressor Information}
PulleyRatio=0.9963  {Compressor drive pulley ratio for Ford FS-10 compressor as
                     determined with strobe}
krpm=PulleyRatio*drpm {rpm}
```

ktorque=-1*dtorque/PulleyRatio {in-lb} {The -1 is to change the sign on the dtorque value. The dtorque value always logs negative because the torque is counter-clockwise}

{Oil Concentration Device, to be used later}
Dummy1=Toil {F}
Dummy2=TOF {micro sec}

BIBLIOGRAPHY

5167, I.S.O., 1980, *Measurement of Fluid Flow by Means of Orifice Plates, Nozzles and Venturi Tubes Inserted in Circular Cross-Section Conduits Running Full*, International Organization for Standardization.

ASME, 1971, *Fluid Meters*, The American Society of Mechanical Engineers, New York.

ASME, Research Committee on Fluid Meters, 1973, *Metering Performance Investigation and Substantiation of the "Universal Venturi Tube" (U.V.T.)*, The American Society of Mechanical Engineers Report # 73-WA/FM-3.

ASME, Research Committee on Fluid Meters, 1973, "Practical Guide to the Evaluation of the Metering Performance of Differential Producers," *ASME*, Ref. 180.21-5.

Bean, H.S., 1983, *Fluid Meters - Their Theory and Application*, ASME, New York.

Benedict, R.P., 1977, *Fundamentals of Temperature, Pressure, and Flow Measurements*, 2nd Edition, John Wiley & Sons, New York.

Benedict, R.P., 1963, "Some Comparisons Between Compressible and Incompressible Treatments of Compressible Fluids," *ASME*, Research Committee on Fluid Meters, Paper No. 63—WA-18.

Farell, C., V. Saxena, and Sadek Youssef, 1993, "Experiments on Turbulence Management Using Screens and Honeycombs," *ASME, Devices for Flow Measurement and Control*, Vol. FED, Vol. 159, pp. 1-10.

Halmi, D., 1974, *"C" Evaluation-Differences Between "Mathematical" and "Physical" Possibilities*, The American Society of Mechanical Engineers Report # 74-WA/FM-2.

Laws, E.M., and Andre Chesnoy, 1993, "The Design and Development of Flow Conditioning Devices," *ASME, Devices for Flow Measurement and Control*, Vol. FED-Vol. 159, pp. 11-17.

Michael, R.A., 1987, *Design of an Automotive Air Conditioning Test Stand for Screening and Transient Studies*, University of Illinois at Urbana-Champaign, M.S. Thesis.

Rivas, M.A., and Shapiro, A.H., 1954, "On the Theory of Discharge Coefficients for Reounded-Entrance Flowmeters and Venturis," *ASME*, Research Committee on Fluid Meters, Paper No. 54—A-98.

Weston, P., 1995, *Design and Construction of a Mobile Air Conditioning Test Facility*, University of Illinois at Urbana-Champaign, M.S. Thesis.